ALMA MATER STUDIORUM UNIVERSITY OF
BOLOGNA

SCHOOL OF ENGINEERING

Forlì Campus

SECOND CYCLE MASTER'S DEGREE in

AEROSPACE ENGINEERING

Class LM-20

GRADUATION THESIS in
AEROSPACE TECHNOLOGIES AND MATERIALS

NEGATIVE STIFFNESS STRUCTURES: AN ADDITIVELY MANUFACTURED DESIGN SOLUTION FOR AEROSPACE APPLICATIONS

Candidate:
Luca NERI

Supervisor:
Prof. Eng. Sara BAGASSI

Co-Supervisor:
Eng. Marzia CORSI

Academic Year 2020/2021

Declaration of Authorship

I, Luca NERI, declare that this thesis titled, "NEGATIVE STIFFNESS STRUCTURES: AN ADDITIVELY MANUFACTURED DESIGN SOLUTION FOR AEROSPACE APPLICATIONS" and the work presented in it are my own. I confirm that:

- This work was done wholly or mainly while in candidature for a research degree at this University.

- Where any part of this thesis has previously been submitted for a degree or any other qualification at this University or any other institution, this has been clearly stated.

- Where I have consulted the published work of others, this is always clearly attributed.

- Where I have quoted from the work of others, the source is always given. With the exception of such quotations, this thesis is entirely my own work.

- I have acknowledged all main sources of help.

- Where the thesis is based on work done by myself jointly with others, I have made clear exactly what was done by others and what I have contributed myself.

Signed:

_____

Date:

_____

ALMA MATER STUDIORUM UNIVERSITY OF BOLOGNA

Abstract

Aerospace Engineering

Master Thesis

NEGATIVE STIFFNESS STRUCTURES: AN ADDITIVELY MANUFACTURED DESIGN SOLUTION FOR AEROSPACE APPLICATIONS

by Luca NERI

The aim of this project is to investigate two damping structures based on negative stiffness behavior and realized by Additive Manufacturing Technology in the rubber like material Tango Gray. The first structure is based on the circular geometry by Wang et al. and Corsi et al. This structure is obtained by a circular repetition of an unit cell based on a curved beam plane geometry. When the curved beam is loaded the buckling instability phenomenon appears and the collapse of the structure reduces the force reaction: the fast change of configuration is called snap-through behaviour. If after buckling the force applied is removed the structure can remain in a different stable position: this is the bistability phenomenon. The second structure is a newly conceived toroidal design. It is obtained by a rotation about a vertical axis parallel to the symmetry axis of the unit cell and at a distance R from the unit cell symmetry axis. The first step of this project is to determine which parameters might influence the behaviour of both structures. The high number of possible configuration to study are analized with the DOE (Design of Experiment) method. In this way is possible to select a reduced number of samples to be analized and find which variation of the characteristic parameters is favourable. The structures selected are verified with the numerical software ANSYS with a FEA (Finite Elements Analysis): the 3-dimensional model takes into consideration both material properties and geometrical dimensions. The obtained results are fundamental to choose which structures are the best to be prototyped and experimentally tested in a quasistatic compression test. At this point the experimental results are compared with the numerical ones to validate the numerical model. In this way it is possible to use this generical model for any type of material and geometry. A possible application of this innovative structure in the aerospace sector could be the possibility to dissipate impact energy with this damping structures. In particular new spacecrafts projects need dampers to capture space debris and clean the most crowded orbits: the excess energy of the impact in a space rendez-vous between a small spacecraft and the collected orbital debris can be easily absorbed by Negative Stiffness Structures instead of accurate manouvres more expensive in terms of fuel consumption and computational power.

Contents

viii

List of Figures

List of Tables

List of Abbreviations

NSS   Negative Stiffness Structures
FEA   Finite Element Analysis
DOE   Design Of Experiment
LEO   Low Earth Orbit

xvii

List of Symbols

n	cell number	
t	beam thickness	[mm]
h	apex heigth	[mm]
Q	ratio h/t	
b	beam width	[mm]
Ri	inner radius	[mm]
R	radius	[mm]
θ	angle	[°]

Chapter 1

Introduction

Damping structures based on negative stiffness behaviour is a new field of research only recently investigated with a variety of configurations [1]. One of the most attractive direction is Negative Stiffness Structure produced by Additive Manufacturing that allows complex design and different materials with reduced time of production. These new stuctures can find applications in innovative aerospace projects as spacecrafts for space debris removal that need a system for reducing the excess of energy during the rendez-vouz operations.

1.1   Motivation and objectives

Low Earth Orbits operations are fundamental for the modern society because the greatest part of our technology is based on the satellites infrastructures and it is essential to guarantee that it works safely. The biggest danger for satellites orbiting in really crowed space regions it is generated by an impact with space debris. The debris are mainly composed by final launcher stages and inoperative satellites but a large quantity of small objects are generated also by impact fragmentation. To solve this problem different studies proposed solutions to reduce debris with different methods and technologies [2]. One of this project, developed by DeLuca et al. [3], is based on a spacecarrier orbiting around Earth that can carry small self-propulsed spacecrafts provided with a robotic arm to connect to debris. When the rendez-vous is concluded the module starts deorbiting the object with autonomous procedure. The most critical and dangerous phase is the rendez-vous: a really accurate navigation system requires high computational resources and even a small error could be cathastrophic. This is the reason why it is taken into consideration a damping system to absorb the excess impact energy and stabilize the robotic arm. The aim of this work is to validate a generic numerical model in order to simulate the behaviour of any damping system based on Negative Stiffness Structures and produced with Additive Manufacturing for aerospace applications.

1.2   Project main phases

The first part of the project consists in the design of the structures: the first one is a circular structure previously studied by Wang et al. [4] and Corsi et al. [5], the second one is a new toroidal structure obtained by the revolution of the unit cell desined by Wang et al. [6]. In each structures it is important to determine the geometric parameters that control the mechanical behaviour. Therefore, different values of each design parameter and parameters' combinations are selected in order to determine the behaviour of the structure. The Design of Experiment method allows to select, among all the parameters combinations, only a small number of samples

to be analyzed. In the second numerical phase the selected structures are analysed through FEA: the structures are first modelled with SolidWorks software and then tested in Ansys Mechanical. The obtained results show the relations between each geometry parameters and their behaviour. The last experimental phase consists in the selection of only 10 simulated structures (5 circular structures and 5 toroidal structures), the most promising to be prototyped with Additive Manufacturing photopolimer technology in a rubber like material. Then all the prototypes are tested in a quasi-static compression test and is determined the force-displacement relation and the bistability behaviour. In the end a comparison between the numerical results and the experimental test is performed to validate the numerical model that can be applied for different geometries and material.

Chapter 2

Theoretical background

2.1 Negative Stiffness Structures

Negative Stiffness Structures are a special branch of multi-stable mechanical meta-materials that require a decrease in the applied force to generate and increase in displacement. The mechanical characteristic is determined by the phenomenon of buckling and shows bistability, snap-through and negative stiffness behaviour [1].
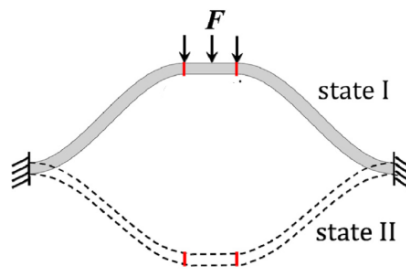
FIGURE 2.1: Buckling effect in a curved beam [7].

Buckling is a non linear phenomenom that appears when a loaded structure changes configuration from an equilibrium position to another one. This unpredictable deformation may appear also below the ultimate strength. If the deformation do not cause the complete collapse of the structure the load that causes the buckling can be redistributed through the deformed part. In the past without numerical simulation was difficult to predict buckling and only simple cases were possible to solve. The selected geometry is similar to the behaviour of a curved beam (see Fig2.1) fixed to the ends with fixed hinges. When the curved beam is subjected to a vertical load it will face an increase of force reaction and deforms until it reaches a critical value, then buckling appears, the beam moves to another equilibrium position and the force reaction decreases to a minimum value. The rapid shift of equilbrium position is called snap-through (see Fig2.2).
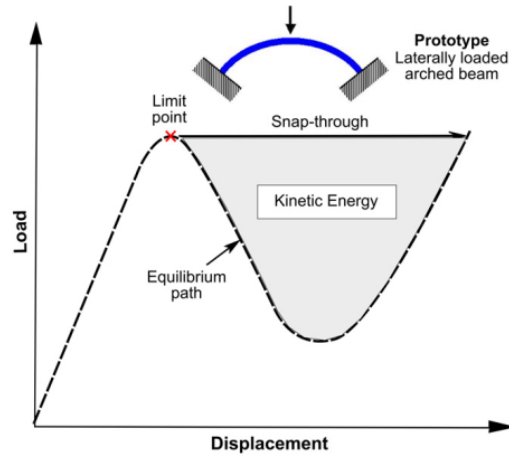
FIGURE 2.2: Snap-through behaviour [1].

If the new position is a stable configuration (see Fig2.3) the structure remains deformed, instead if it is unstable (see Fig2.4), when the load is removed it comes back to the initial configuration. The existance of two equilibrium positions characterizes bi-stable structures. The self-recovering and bi-stability are particularly usefull for designing damping structures and energy dissipative mechanism [7].
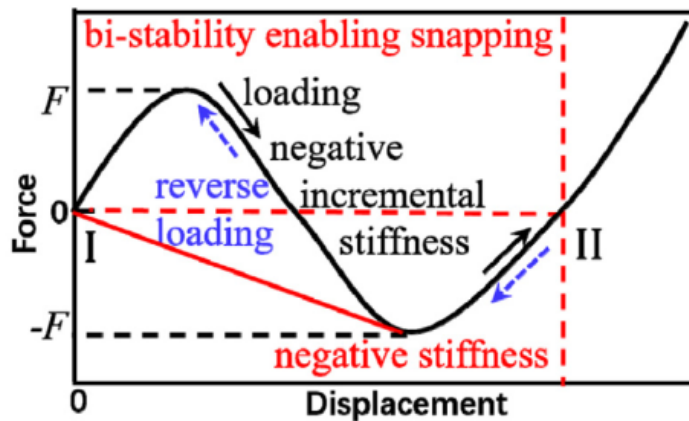
FIGURE 2.3: Negative stiffness behaviour [7].
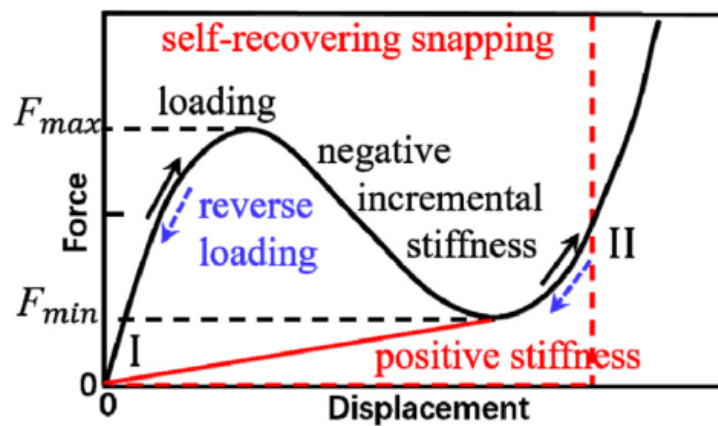
FIGURE 2.4: Positive stiffness behaviour [7].

2.2 Additive Manufacturing

Additive Manufacturing is process of joining materials to make parts from 3D model data, usually layer upon layer, as opposed to subtractive manufacturing and formative manufacturing methodologies (ISO/ASTM 52900) [8]. This method is particularly usefull for rapid prototyping or rapid tooling since it needs less time of production than traditional methods [9]. The advantages of this technology are the possibility to design almost every geometry without limitation due to the machining, to reduce cost and time for prototyping, low cost for facilities and expert hand-skilled technicians are not necessary thanks to the easy interface of the machines. The disadvantages are the non uniform mechanical property due to the layer-by-layer deposition, the low accuracy compared to traditional methods and not competitiveness for mass production. The principal additive technology methods are based on vat photopolymerization, material extrusion, material jetting, binder jetting, powder bed fusion, direct energy deposition and sheet lamination (see Tab2.1).

TABLE 2.1: Additive technology.

Technology	Process	Phase Change	Material
Vat Photopolymerization	Stereolithography	Laser	Plastic
	Digital Light Processing	Projector	Plastic
	Continuos Digital Light Processing	LED and Oxygen	Plastic
Material Jetting	Material Jetting	UV Light	Plastic
	Nano Particle Jetting	Heat	Metal
	Drop on Demand	Milled	wax
Binder Jetting	Binder Jetting	Bonding Agent	Gypsum, Sand, Metal
Powder Bed Fusion	Multi Jet Fusion	Agent and Energy	Plastic
	Selective Laser Sintering	Laser	Plastic
	Selective Laser Melting	Laser	Metal
	Electron Beam Melting	Electron Beam	Metal
Direct Energy Deposition	Laser Enginerring Net Shape	Laser	Metal
	Electron Beam Additive Manufacturing	Electron Beam	Metal
Sheet Lamination	Lamineted Object Manufacturing		Composite, Paper

One of the Additive Manufacturing machines available in the laboratory of the university is based on material jetting and it will be described in a dedicated section. Material jetting is a process in which liquid droplets of model material and support material are selectively deposited layer upon layer and the photopolymerization is

obtained with a UV lamp. The support material can be removed mechanically or with solvent and the part is ready to use without post machining.

2.3   Finite Element Analysis

Structural problems can be described with differential equations and boundary conditions. In some case it is possible to solve analitically the problem but usually due to complexity of the structure the solution is found with numerical model [10]. In these case is possible to obtain approximated solutions if the loading conditions and the material properties are exactly known. FEA (Finite Elements Analysis) is a numerical procedure for solving the problem: instead of solving the differential equations, the body is reduced to a finite number of elements joined at their boundary. In this way the problem is solved in a matrix formulation with the force method or the displacement method.

In the force method they are considered equilibrium equations, compatibility and stress-strain-temperature relationships. The structure is composed by simple element (bars, beams,etc.) in which the force-displacement relationships are known. The internal force are applied on the elements joints. In matrix formulation $R = [R_1...R_m]$ is the generalized force applied on the structure, $S = [S_1...S_g]$ is the internal force and b_g is a rectangular matrix of dimension $g * m$. So the internal and the applied force are related by $S = bR$. In a statically determined structure, the b_g elements are determined from equilibrium conditions. In case of indetermined structure the internal forces must satisfy compatibility conditions.

2.3.1   Curve fitting

The solution with FEA requires the exact knowledge of the loading and material property. For this reason it is necessary to know the stress-strain curves. The curve fitting procedure is a matemathical procedure to set the parameters of a model function in such a way that the fitted stress-strain curve is as close as possible to the measured values [11]. The best procedure to represent the real behaviour of the material is to use different loading mode: uniaxial, biaxial and shear test data. The curve fitting for hyperelastic material models follows some phases. First, the stress-strain curves need to be checked and corrected: the initial point should be zero stress and zero strain. Second, the material model and an error criterion have to be selected for the fitting: this choice should be the one that generates the curve closer to the measured data. The curve that fits the material of this project is the Yeoh 2nd order model (see next page) [11]. Yeoh model was developed 1993 for hyperelastic material, it is based on a series expansion truncated after the first three terms and depending only on the first strain invariant.

The strain energy definition is:

$$W = \sum_{i=1}^{n} C_i * (I_1 - 3)^i$$

I_1: first deviatoric strain invariant
C_i: material constants
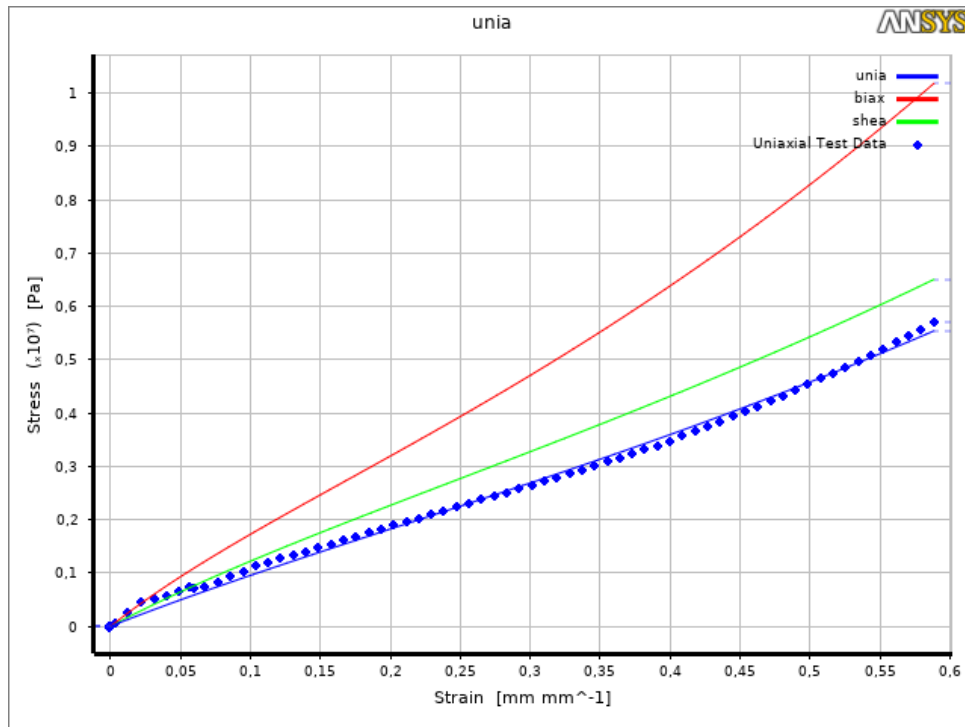
FIGURE 2.5: Yeoh 2nd order curve fitting.

2.4 Design of Experiment

The Design of Experiment is a statistical method to plan the experimental test phase in order to obtain relevant results. The method is based on the analysis of the problem-cause-solution [12] (see Fig2.6).
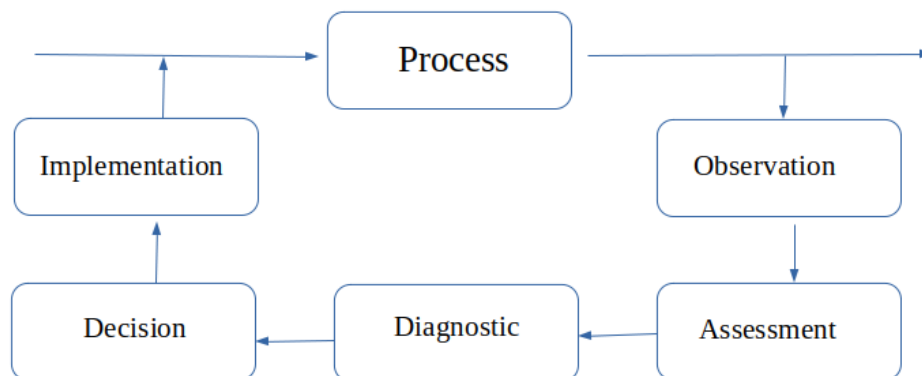
FIGURE 2.6: DOE process scheme.

The DOE method is particularly usefull in the definition of the control parameters and their combinations that influence the behaviour of the system and improve the desired phenomenon with the minimum cost and time. The first step is to define the experimental result we are interested in and the factors (the characteristic parameters taken into consideration), that could influence the result. Then certain amount of tests are set with variation of the levels (the values taken into consideration for each parameter). The experimental process offers a statistical interpretation

of the reality: the variability of the data, test on the hypothesis, evaluation of the experimental error, the influence of factors, interaction of effects, variance of the effects and the discover of a mathematical model of the system. During the experimental phase it is possible to change one variable at a time but the interaction of effects disappears. For this reason it is more effective to change more factors in each test (full factorial). This procedure can generate a great number of combinations to be evaluated. In order to reduce cost and time only some combinations are selected by a random method or by previous knowledge of the problem. The obtained results can be interpolated to obtain the response in all the points not studied.

Chapter 3

Design

3.1 3D model

The first step of the project is to design the structures for the prototyping and test phase. The chosen structures are a circular geometry derived by previous studies of Wang et al. [6] and Corsi et al. [5] and a new toroidal structure obtained with the revolution around a vertical axis of the unit cell of the circular geometry. The design of the circular structure and the toroidal structure is performed with SOLID-WORKS software, a 3D CAD available for students in the University. Thanks to the parametrization of characteristic dimensions it is easy to change the structures and to obtain all the geometries necessary for the DOE method. The experimental method allows to define the best structures that show negative stiffness behaviour and bistability with the lowest possible number of prototypes and reduce cost and time for the production and test.

3.1.1 Circular structure

The circular structure is the one studied by Wang et al. [6] and Corsi et al. [5] but, due to the different material and printing technology it is necessary to verify all the geometric relations previously discovered that define the behaviour of the structure. The structure consists of two layers and each layer is formed by a circular repetition of unit cell (see Fig3.1). According to the previous studies the number of layers is equal to the number of buckling phase and the number of cells changes the total force reaction (see Fig3.2). Another parameter is the *Qratio* defined as h/t where t is the beam thickness and h the apex height. This ratio influences the bistability behaviour when it increases. Some geometric limitations are present in the choice of h and t (see Fig3.3). The radius R is the external dimension of the structure and it is constant in order to reduce the number of parameters. On the other side the ratio of the inner radius R_i and the beam width b controls the snap-through behaviour. Another effect to take into consideration is the θ angle that depends on the number of elements in a layer: this parameter changes the curvature of the element and probably the distribution of forces.
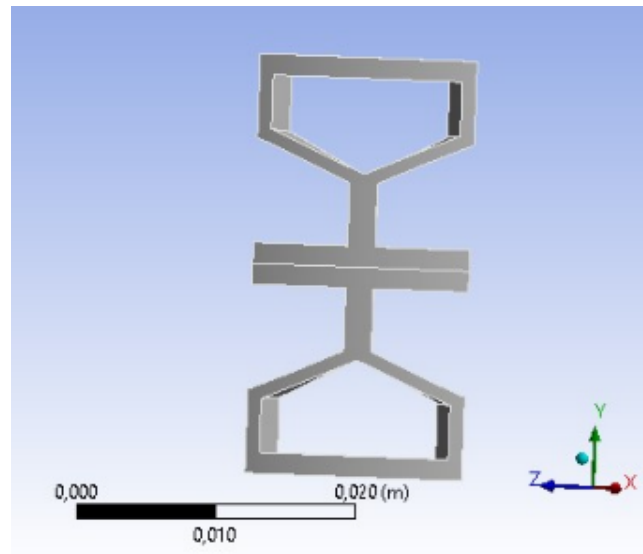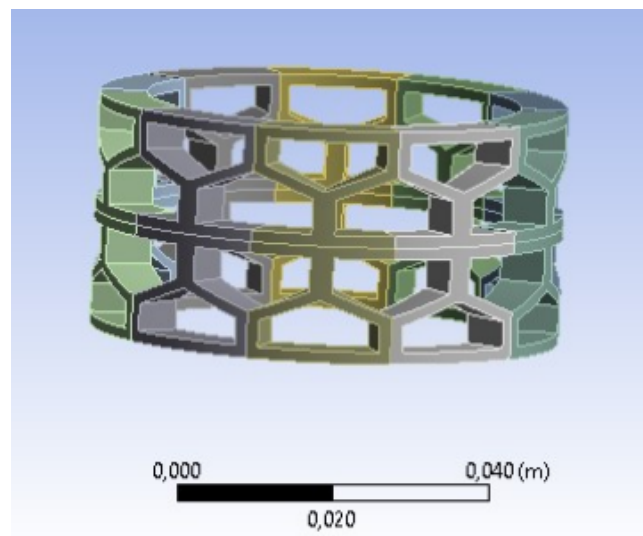
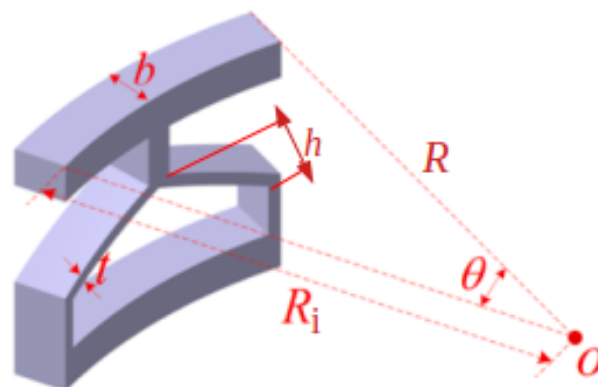FIGURE 3.1: One cell Circular structure.

FIGURE 3.2: Circular structure.

FIGURE 3.3: Characteristic dimensions of the Circular structure.

3.1.2 DOE for Circular structure

The combination of all the 4 parameters and levels (see Tab3.1) obtained with the Design of Experiment, generates 128 possible combinations for the circular structure (see Tab3.2), but taking into consideration the structures studied by Corsi et al. [5] and the analysis of the $b/R_i ratio$ the total possible combinations are reduced to 14 (see Tab3.3).

TABLE 3.1: Factors and levels for Circular structure.

Factor	Level
t	t_1=1.0 mm
	t_2=1.5 mm
n	n_1=9
	n_2=10
	n_3=12
	n_4=15
h	h_1=3.0 mm
	h_2=4.0 mm
	h_3=4.5 mm
	h_4=6.0 mm
b	b_1=5.0 mm
	b_2=6.0 mm
	b_3=7.0 mm
	b_4=10.0 mm

TABLE 3.2: DOE for Circular structure.

	t_1				t_2			
n_1	h_1b_1	h_1b_2	h_1b_3	h_1b_4	h_1b_1	h_1b_2	h_1b_3	h_1b_4
	h_2b_1	h_2b_2	h_2b_3	h_2b_4	h_2b_1	h_2b_2	h_2b_3	h_2b_4
	h_3b_1	h_3b_2	h_3b_3	h_3b_4	h_3b_1	h_3b_2	h_3b_3	h_3b_4
	h_4b_1	h_4b_2	h_4b_3	h_4b_4	h_4b_1	h_4b_2	h_4b_3	h_4b_4
n_2	h_1b_1	h_1b_2	h_1b_3	h_1b_4	h_1b_1	h_1b_2	h_1b_3	h_1b_4
	h_2b_1	h_2b_2	h_2b_3	h_2b_4	h_2b_1	h_2b_2	h_2b_3	h_2b_4
	h_3b_1	h_3b_2	h_3b_3	h_3b_4	h_3b_1	h_3b_2	h_3b_3	h_3b_4
	h_4b_1	h_4b_2	h_4b_3	h_4b_4	h_4b_1	h_4b_2	h_4b_3	h_4b_4
n_3	h_1b_1	h_1b_2	h_1b_3	h_1b_4	h_1b_1	h_1b_2	h_1b_3	h_1b_4
	h_2b_1	h_2b_2	h_2b_3	h_2b_4	h_2b_1	h_2b_2	h_2b_3	h_2b_4
	h_3b_1	h_3b_2	h_3b_3	h_3b_4	h_3b_1	h_3b_2	h_3b_3	h_3b_4
	h_4b_1	h_4b_2	h_4b_3	h_4b_4	h_4b_1	h_4b_2	h_4b_3	h_4b_4
n_4	h_1b_1	h_1b_2	h_1b_3	h_1b_4	h_1b_1	h_1b_2	h_1b_3	h_1b_4
	h_2b_1	h_2b_2	h_2b_3	h_2b_4	h_2b_1	h_2b_2	h_2b_3	h_2b_4
	h_3b_1	h_3b_2	h_3b_3	h_3b_4	h_3b_1	h_3b_2	h_3b_3	h_3b_4
	h_4b_1	h_4b_2	h_4b_3	h_4b_4	h_4b_1	h_4b_2	h_4b_3	h_4b_4

TABLE 3.3: Characteristic dimensions of the Circular structures.

	Cells number [n]	Beam thickness [t][mm]	Apex height [h][mm]	Q ratio [h/t]	Beam width [b][mm]	Inner radius [Ri][mm]	b/Ri ratio
A	10	1.5	3.0	2	5.0	25.0	0.20
B	9	1.5	3.0	2	5.0	25.0	0.20
C	10	1.0	4.0	4	5.0	25.0	0.20
D	9	1.5	4.5	3	5.0	25.0	0.20
E	12	1.0	1.0	1	5.0	25.0	0.20
F	10	1.5	3.0	2	6.0	24.0	0.25
G	10	1.5	4.5	3	6.0	24.0	0.25
H	10	1.5	6.0	4	5.0	25.0	0.20
I	10	1.5	4.5	3	7.0	23.0	0.30
K	15	1.0	3.0	3	5.0	25.0	0.20
L	10	1.5	3.0	2	10.0	20.0	0.50
M	10	1.0	3.0	3	6.0	24.0	0.25
N	10	1.0	3.0	3	7.0	23.0	0.30
O	10	1.0	4.0	4	6.0	24.0	0.25

3.1.3   Toroidal structure

The toroidal structure (see Fig3.4) is obtained by the rotation of the unit cell (see Fig3.5) desined by Wang et al. [4] around a central axis parallel to the symmetry axis and placed at a distance R (see Fig3.6). The apex height h and the beam thickness t are supposed to have the same effect on the bistability as in the circular structure. In this case it is necessary to investigate the effect of the radius R that could influence both the force reaction and the snap-through behaviour. In the design phase it is important to remember the prototyping technique selected: material jetting uses a support material in order to fill concave geometries and empty spaces to avoid the collapse of the structure. This is the reason why a set of holes are present on the top and in the bottom of the structure: the holes allow to remove mechanically and with water the support material.
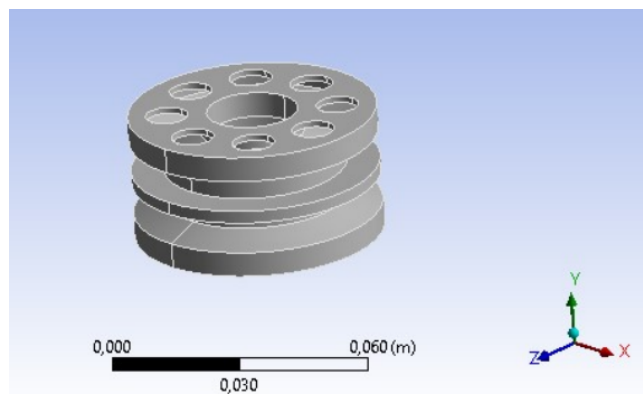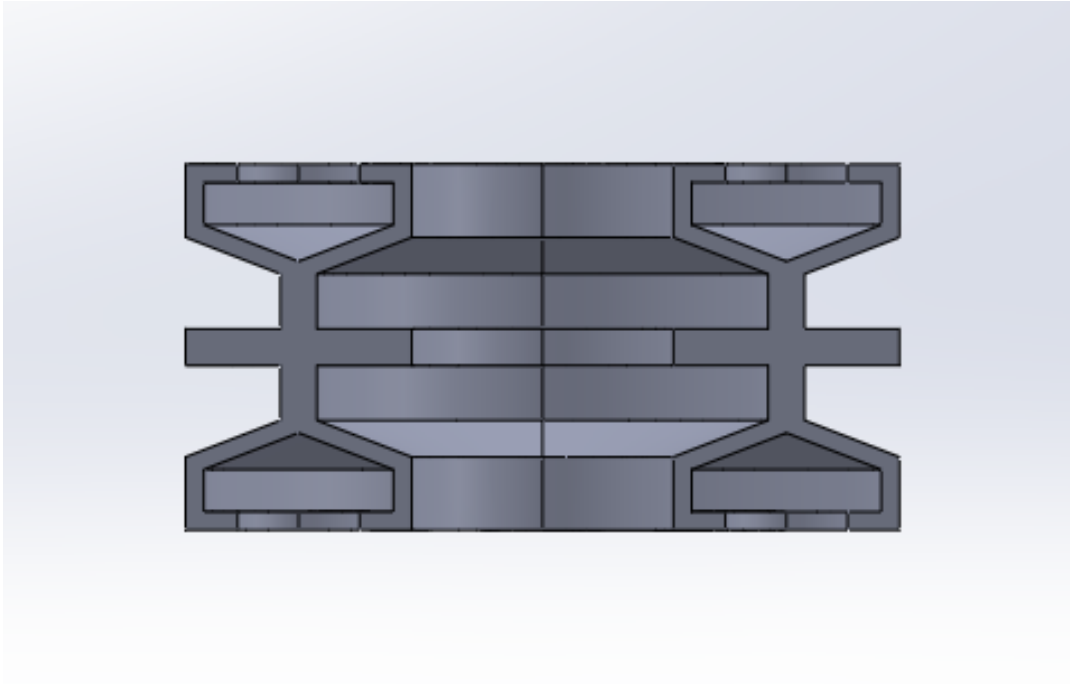

FIGURE 3.4: Toroidal structure.
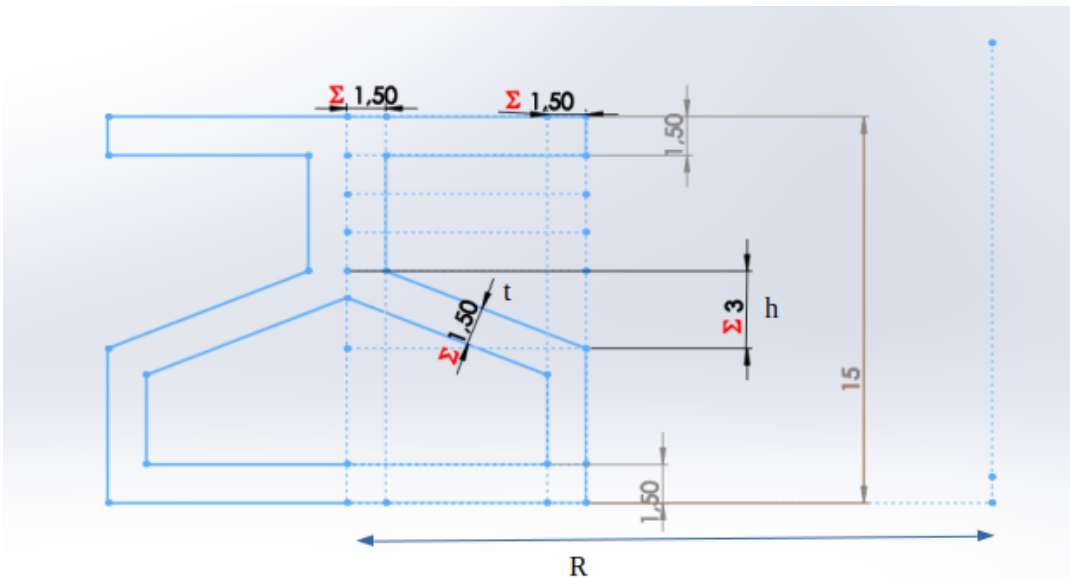
FIGURE 3.5: Section of the Toroidal structure.

FIGURE 3.6: Characteristic dimensions of the Toroidal structure.

3.1.4 DOE for Toroidal structure

The Design of Experiment considers in the toroidal structure 3 factors and a number of levels for each factor (see Tab3.4) to generate 12 possible combinations (see Tab3.5) but the DOE analysis allows to select only 5 experiments that take into consideration the main parameters variation (see Tab3.6).

TABLE 3.4: Factors and levels for Toroidal structure.

Factor	Level
t	t_1=1.0 mm
	t_2=1.5 mm
h	h_1=3.0 mm
	h_2=4.0 mm
	h_3=4.5 mm
R	R_1=20.0 mm
	R_2=25.0 mm

TABLE 3.5: DOE for Toroidal structure.

	R_1		R_2	
h_1	t_1	t_2	t_1	t_2
h_2	t_1	t_2	t_1	t_2
h_3	t_1	t_2	t_1	t_2

TABLE 3.6: Characteristic dimensions of the Toroidal structure.

	Beam thickness [t][mm]	Apex height [h][mm]	Q ratio [h/t]	Radius [R][mm]
torA	1.5	3.0	2	20.0
torB	1.5	3.0	2	25.0
torC	1.0	4.0	4	20.0
torD	1.5	4.5	3	20.0
torE	1.0	3.0	3	20.0

Chapter 4

Numerical analysis

4.1 Analysis setting

ANSYS is a commercial software avaiable for academic use that allows to generate a mesh of the body and to simulate mechanical analysis. The mesh and elements type are completely controllable by the user and different mechanical analysis are avaiable. It is possible to choose the mathematical solver and all the boundary conditions of the problem. The transient analysis works with load and boundary conditions that change over time so is the correct choice to evaluete the behaviour of the structure when the beam collapse and the buckling phenomenon appears. In addition to that a quasi static solution is the slowest possible: it means that the deformation is so slow that inertial effect are negligible and semplify the non linear problem in a linear system function of the stiffness matrix.
Dynamic equation of motion in matrix form:

$$f(t) = M * x''(t) + B * x'(t) + K * x(t)$$

$f(t)$ = force vector
M = mass matrix
K = stiffness matrix
$x(t)$ = displacement vector

Another important setting for a proper analysis is the mesh definition (see Fig4.1 and Fig4.2): the patch independent mesh second order method and tetrahedrons elements generate refined mesh close to corners and larger when possible. In the mechanical APDL [13], by a code command, is set a SOLID272 (see Fig4.3) to model mesh for axisymmetric solid structures. It is defined by four nodes on the master plane, and nodes created automatically in the circumferential direction based on the four master plane nodes. The total number of nodes depends on the number of nodal planes. Each node has three degrees of freedom: translations in the nodal x, y and z directions. The element allows a triangle as the degenerated shape on the base plane to simulate irregular areas. The element has plasticity, hyperelasticity, stress stiffening, large deflection, and large strain capabilities. It also has mixed-formulation capability for simulating deformations of nearly incompressible elastoplastic materials, and nearly and fully incompressible hyperelastic materials. In the compression phase some faces get in contact and to prevent penetration is set a frictionless contact with pure penalty property: the faces can slip but physical body can't penetrate.
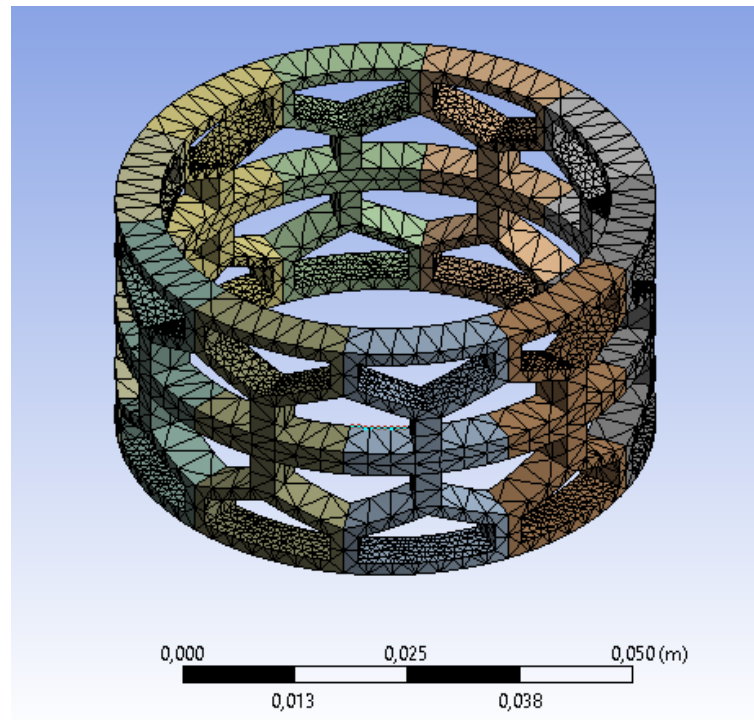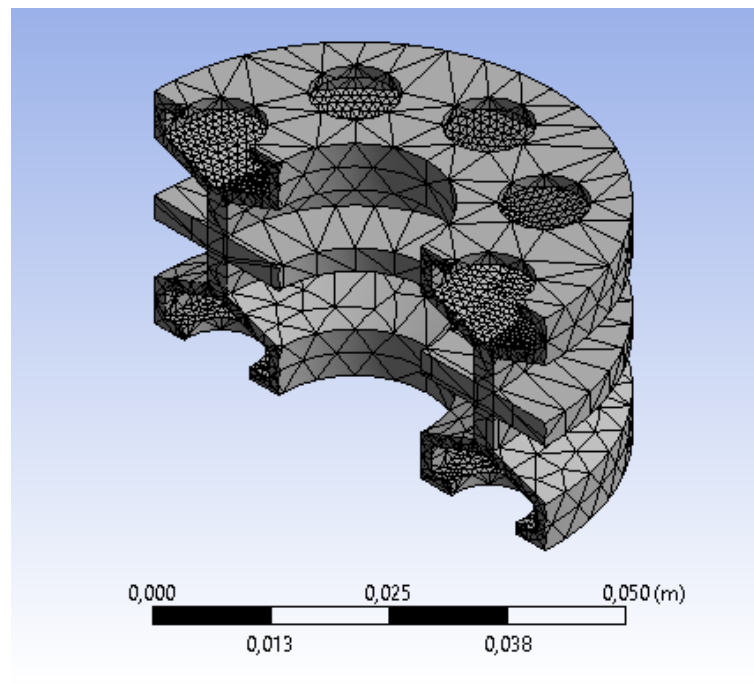
FIGURE 4.1: Mesh Circular structure.

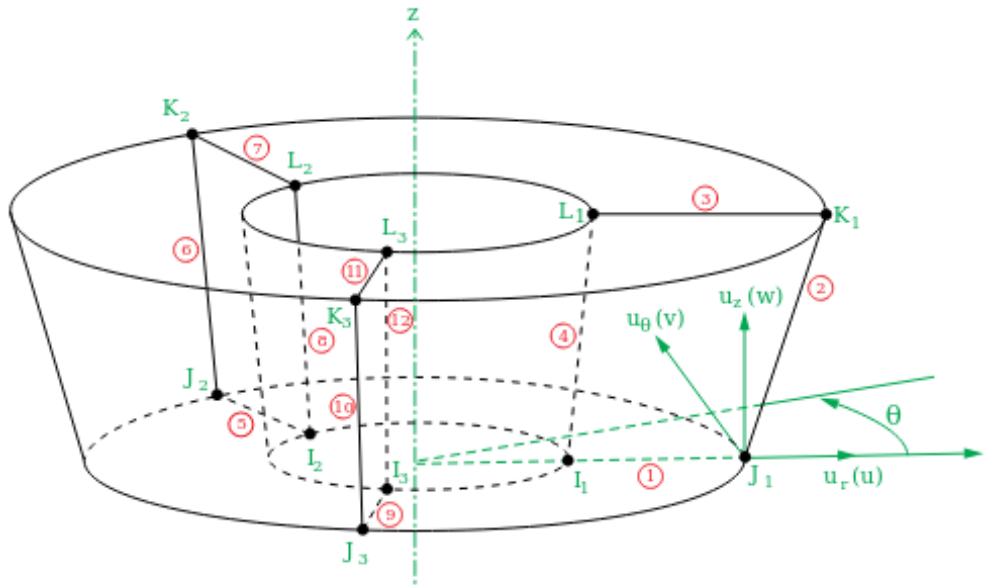

FIGURE 4.2: Mesh Toroidal structure section.

FIGURE 4.3: Mesh element definition SOLID272

4.2 Numerical result

The results analysis show the negative stiffness behaviour and the bistability. The circular structure is previously simulated only with a single unit cell, with more restricted boundary conditions, in order to analize the bistability because when the complete structure is evalueted the phenomenon disappears. The toroidal structure is analyzed only in the complete structure. The displacement plot (see Appendix) shows the compression of the structure over time. At time 1 second the compression ends and the structure is relaxed: if a bistable configuration appears the deformation can not reach zero. The equivalent Von Mises stress (see Appendix) shows if the structure reaches the ultimate strength and failure. The force reaction plot (see Appendix) show the negative stiffness behaviour in particular is evident the snap-through due to the buckling effect and the bistability when decreasing negative force values are obtained.

4.2.1 Circular structure plot analysis

In the numerical analysis of single cell is evident that only 3 structures are bistable: C, I, and O. The bistability in C and O is strongly related with the *Qratio* equal to 4, the main geometric parameter that influences this behaviour. On the other side, the structure I is bistable even if the *Qratio* is equal 3 thanks to the higher $b/R_i ratio$. This parameter influences the force oscillation between the high peak and the low peak in the force plot. The structure H fails because both the single cell and the entire structure exceed the ultimate strength. For this reason the result of structure H is not taken into consideration in the following analysis. All the other structures show the snap-through behaviour related to the buckling effect. A general overwiev of circular structure (see Fig4.4) shows results in agreement with the hypothesis made in previous studies on this geometry by Wang et al. [4].
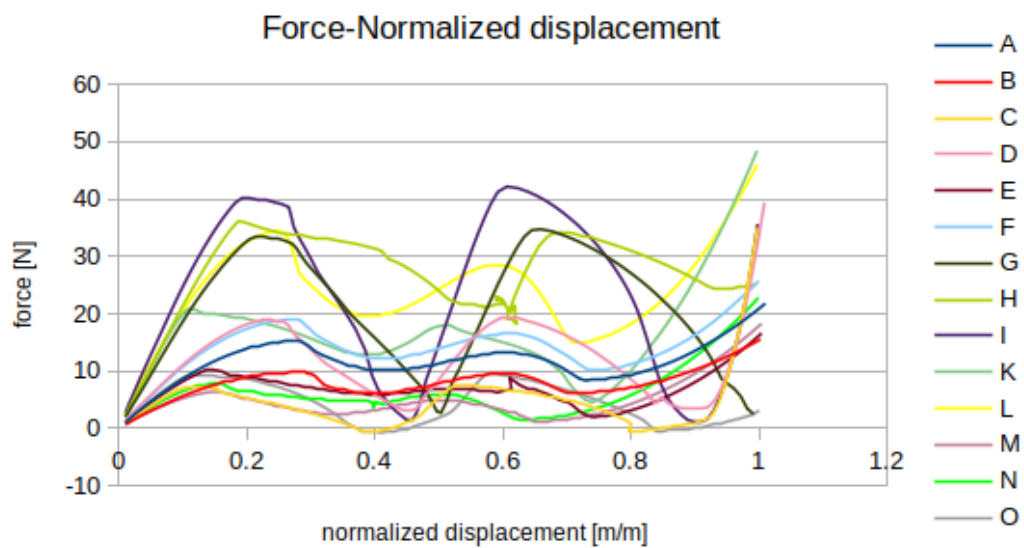
FIGURE 4.4: Circular structures force results.

The following force reaction plots (see next pages) show the characteristic dimensions variation that influence the structure behaviour and allow to make assumptions on the property of this particular NSS. For a better visualization each parameter variation is taken into consideration alone to compare the structures reaction and the displacement is normalized with the maximum displacement value.

The variation of cell number in every layer is considered in structures A, B, E, K (see Fig4.5). The result shows a relation between the number of cells and the force reaction. In particular if the structures A-B and E-K are compared, in which the only parameter variation is limited to n, the force reaction increases with an higher number of cells.

TABLE 4.1: Cell number on structure A-B and E-K.

	A	B	E	K
Cell number	10	9	12	15
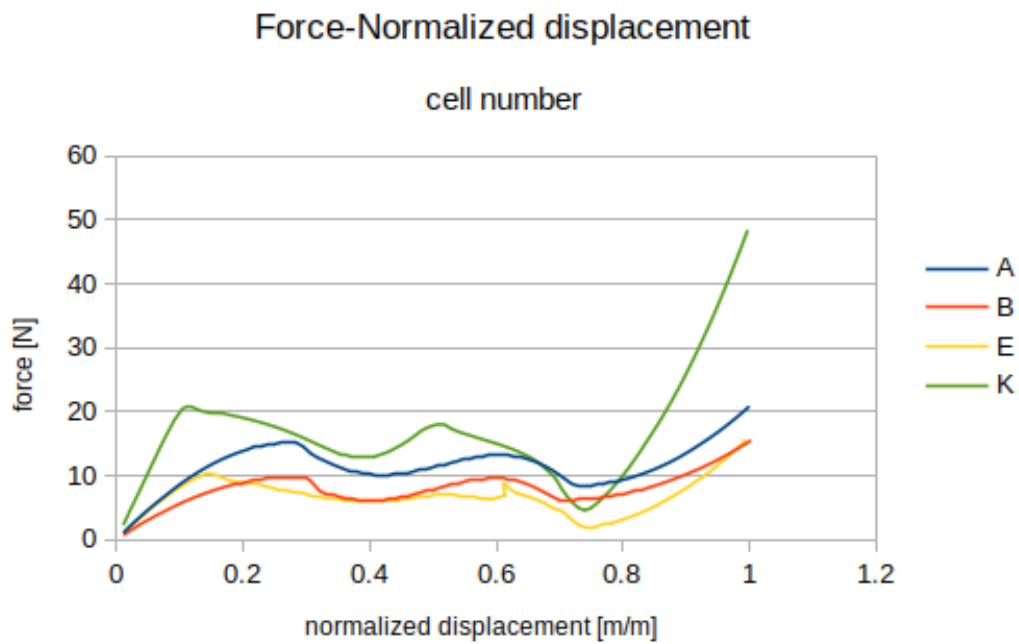
FIGURE 4.5: Cell number on structure A-B and E-K.

The θ angle variation is linked to the number of unit cell in a layer and the constant external dimension of *R*. The behaviour is analized in structures E-K (see Fig4.6). The external radius is constant for all the structures to reduce variables. This assumption can change the distribution of the total force in the 3 directions x, y, z due to the different curvature of each cell, because to fit more cells in the same circumference they should be smaller. If the force out of plane are too big some instability could appear in the structure.

TABLE 4.2: Cell number and theta on structure E-K.

	E	K
θ angle	30°	24°
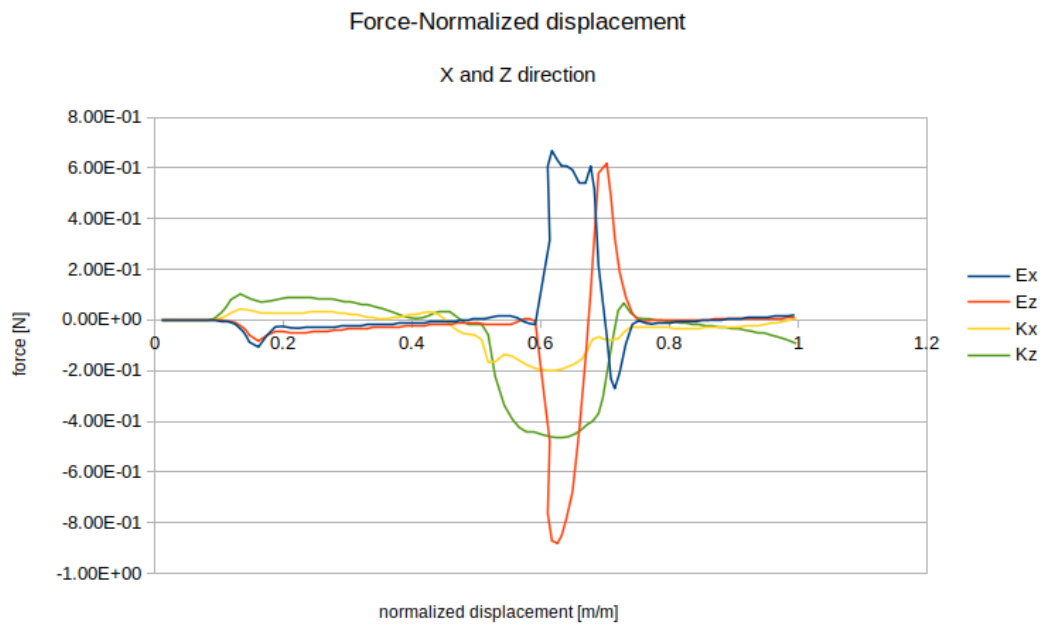
FIGURE 4.6: Cell number and theta on structure E-K.

The beam thickness *t* variation is studied in the structures F-M (see Fig4.7). This parameter controls the stiffness of the structure because is one of the two dimensions of the beam section. In this case an increase of *t* produces an higher force reaction before the buckling effect appears.

TABLE 4.3: Beam thickness on structure F-M.

	F	M
Beam thickness [mm]	1.5	1.0
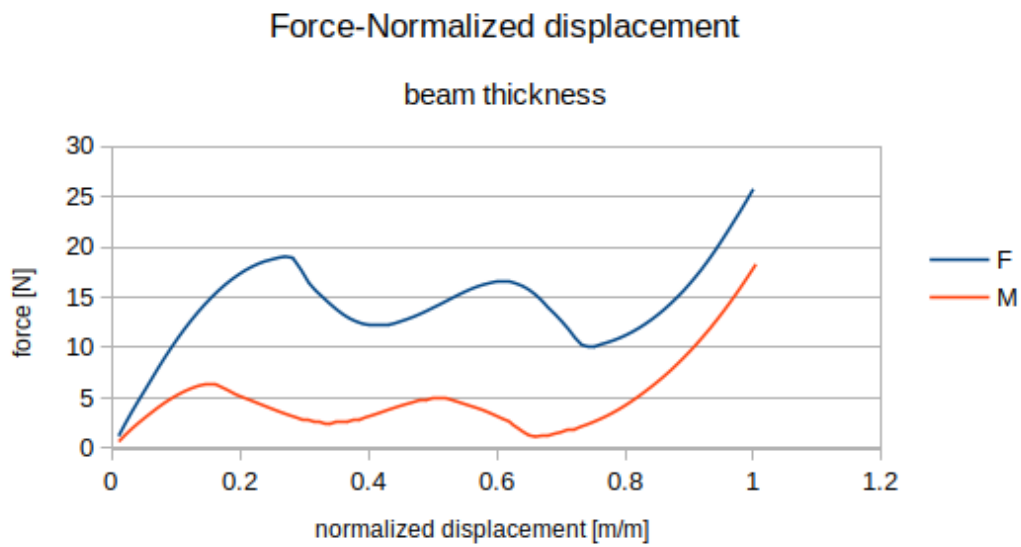
FIGURE 4.7: Beam thickness on structure F-M.

The apex height h defines the length and the inclination of the beam because the total height of the cell is geometrically fixed in order to have all the structures of the same dimensions. In the structures B-D and F-G (see Fig4.8) is evident that an higher h increases the inclination of the curve and produces a stronger snap-through behaviour.

TABLE 4.4: Apex height on structure B-D, F-G.

	B	D	F	G
Apex height [mm]	3.0	4.5	3.0	4.5
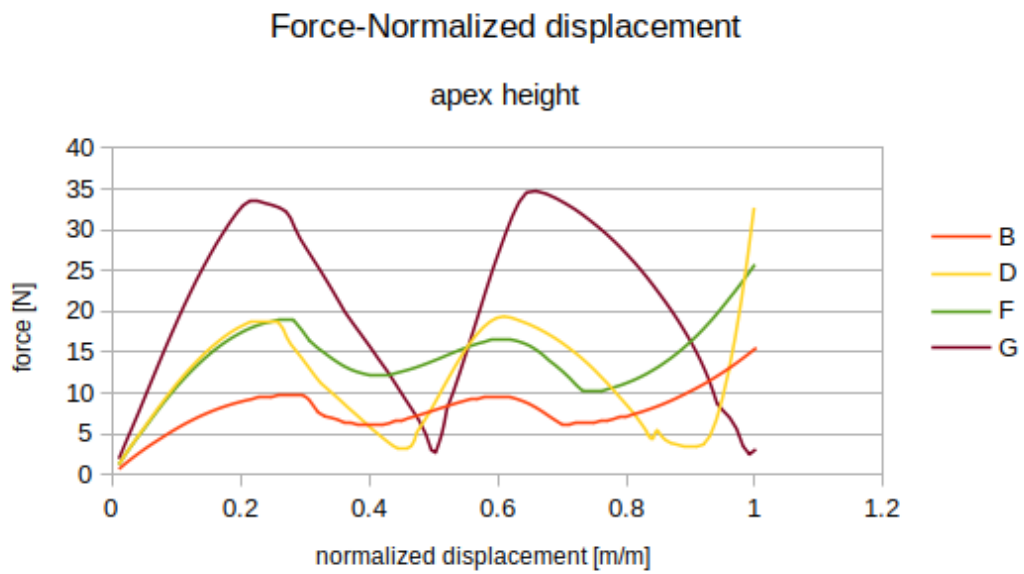
FIGURE 4.8: Apex height on structure B-D, F-G.

The structures A-C (see Fig4.9) are compared to show the variation effect of the *Qratio*. In this case, to obtain the variation of Q both the parameters t and h are changed. The plot shows that an higher value of Q equal to 4, produces negative force decremental and bistability should appear in structure C in accordance to the result from the single cell analysis.

TABLE 4.5: Q ratio on structure A-C.

	A	C
Q ratio	2	4
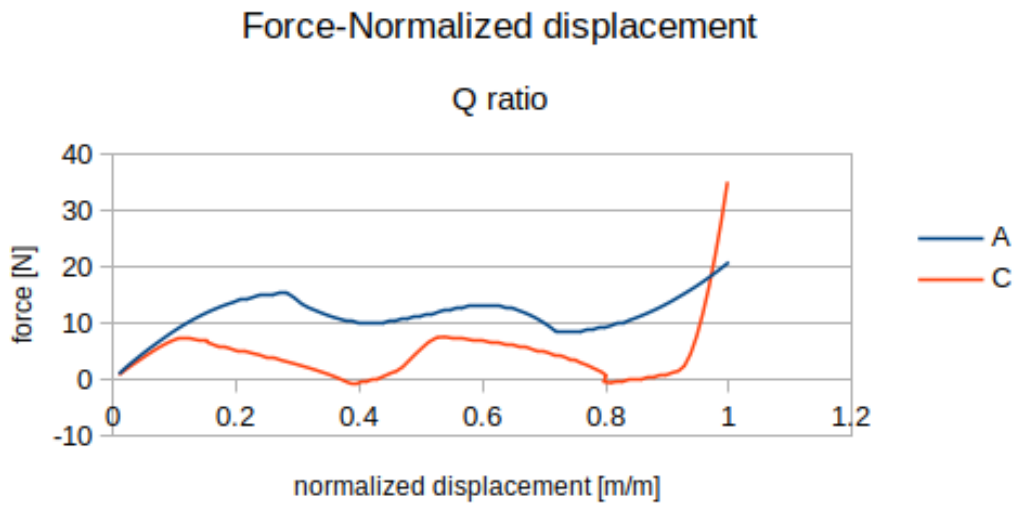
FIGURE 4.9: Q ratio on structure A-C.

In the analysis of the $b/R_i ratio$ it is avaiable (see Fig4.10) the highest number of structures to compare. As previously mentioned, the external radius is constant, so if the beam width b increases, the inner radius R_i decreases of the same amount. This geometry constrain produces a reduction of the cell section in the radial direction: the external face is larger than the internal face of the cell. In this way, thanks to the higher value of b is possible to imagine the structure made of two concentric circular structures with the same number of elements but with different cell dimensions. This phenomenon produces a higher force reaction of the structure.

TABLE 4.6: b/Ri ratio on structure A-F, G-I, A-L, M-N, C-O.

	A	C	F	G	I	L	M	N	O
b/Ri ratio	0.20	0.20	0.25	0.25	0.30	0.50	0.25	0.30	0.25
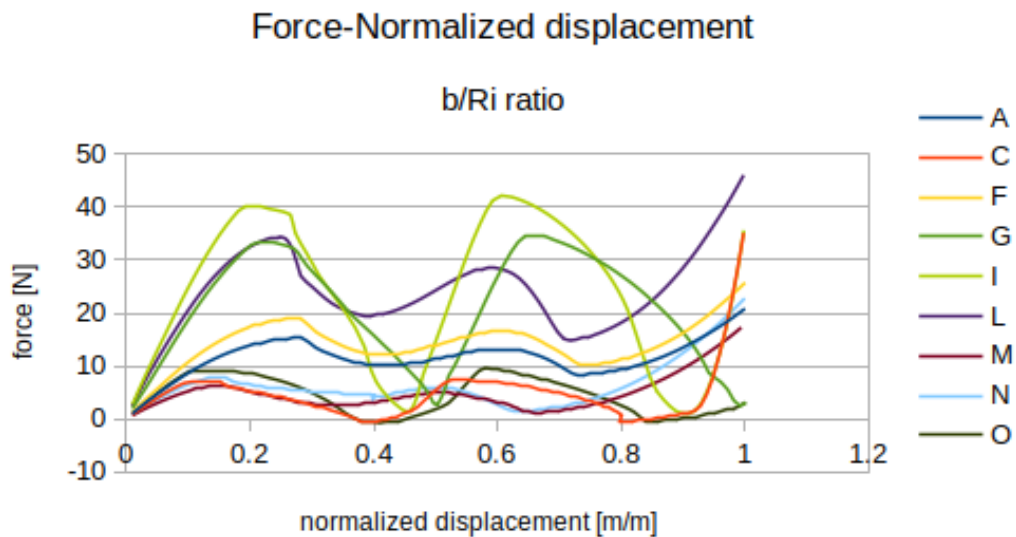
FIGURE 4.10: b/Ri ratio on structure A-F, G-I, A-L, M-N, C-O.

4.2.2 Toroidal structure plot analysis

The following force reaction plot (see Fig4.11) shows the characteristic dimension variations taken into cosideration that influence the structure behaviour. The displacement is normalized with the maximum displacement value. The negative stiffness behaviour is evident only in geometries torC and Dtor but the bistability is not present in the complete structure as for the circular structure. In torC it is possible to suppose that the *Qratio* has the same effect as in the circular structure so a value equal to 4 could generate bistability. The effect of *t* visible in torA-torE, is an increase of force reaction because as in the circular structure, it is the main dimension of the beam section of the unit cell and control the beam stiffness. In structures torA-torD and torC-torE is analyzed the effect of apex height *h*. Even if the curves of torA and torE are almost plane with no evident presence of negative stiffness behaviour, the fact that torC and torD are NSS and the only variation in parameter is *h*, it is possible to suppose that the apex height controls the snap-through behaviour as in the circular structure. The increase of the radius *R* in torA-torB is an evident increase of the force reaction due to a bigger circumferance generated by the radius: this is explainable because in a longer circumference is possible to extrude more unit cell with zero beam width during the revolution around the vertical axis when the toroid is generated.

TABLE 4.7: Toroidal structures force results.

	torA	torB	torC	torD	torE
Q ratio	2	2	4	3	3
Beam thickness [mm]	1.5	1.5	1.0	1.5	1.0
Apex height [mm]	3.0	3.0	4.0	4.5	3.0
Radius [mm]	20.0	25.0	20.0	20.0	20.0
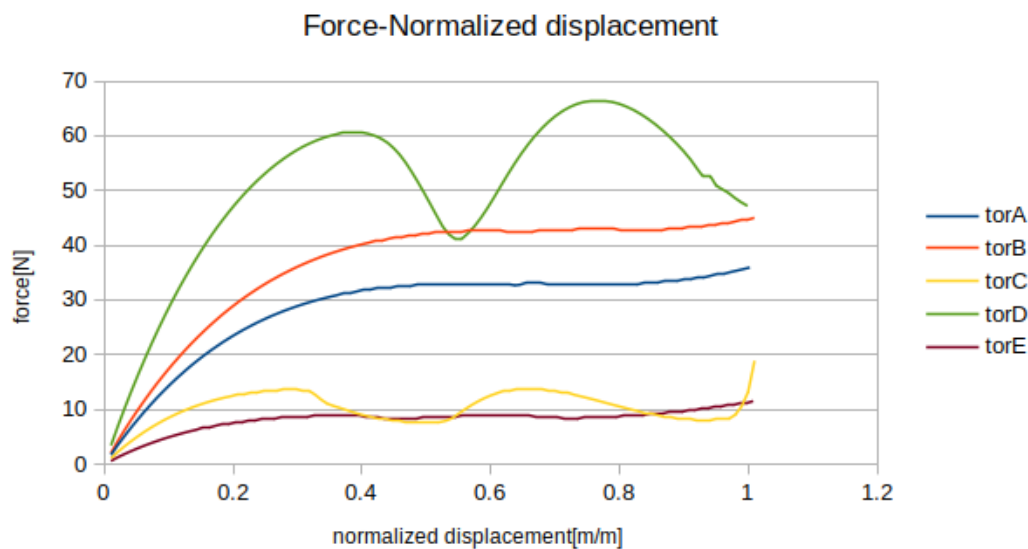
FIGURE 4.11: Toroidal structures force results.

Chapter 5

Experimental analysis

After the numerical analysis and the discussion on simulation results the experimental phase is necessary to validate the model. The prototyping is conducted for 5 circular structures and 5 toroidal structures with 3 repetitions in a quasi-static compression test following the ASTM D695 [14] standard.

5.1 Object30 V5 Prime

Object30 V5 Prime is the photopolymeric manufacturing device by Stratasys avaiable in the University Laboratory. In this machine is possible to choose different material but for this project it is selected the TangoGray model material. The photopolymeric resin is stored in a cartridge and by a vacuum pump it is transfered to the print head. The print head (see Fig5.1) heats the resin up to 70 °C and deposits it on a tray. Then a UV lamp activates the chemical reaction and a roller compacts the layer. The print head jets at the same time the resin model and the support material. The support material is needed to keep the model in position under the roller pressure in particular for concave geometries [15].

ID	Description	ID	Description
1	Y axis	6	Roller
2	X axis	7	Photopolymer
3	Build tray	8	Flexible material
4	Print heads	9	Color Rigid material
5	UV lamps	10	Support material
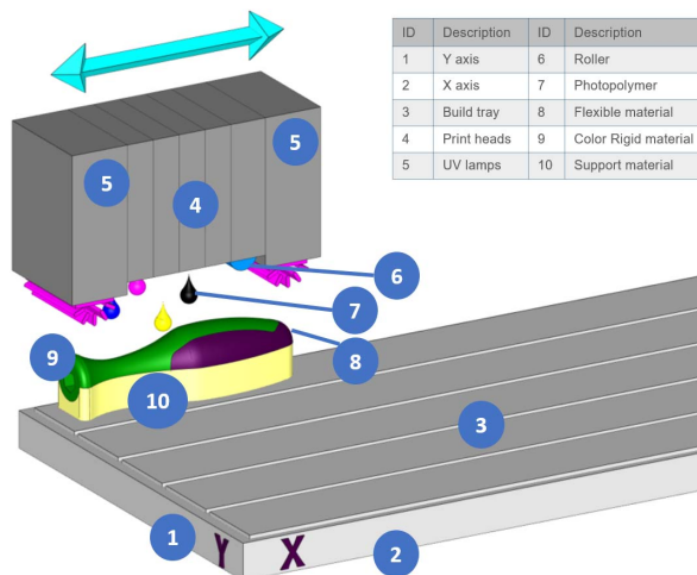
FIGURE 5.1: Print head and tray [15].

5.2   Model material

TangoGray is a rubber like material produced by Stratasys [16] particularly indicated to simulate soft-touch coatings, non-slip surfaces, overmolding grips, shoe soles and other applications requiring flexible characteristics [17]. In the following table the main properties are included (see Tab5.1).

TABLE 5.1: TangoGray FLX950 material property.

	ASTM	Metric
Tensile Strength	D-412	3-5 MPa
Elongation at Break	D-412	45-55%
Compressive Set	D-395	0.5-1.5%
Shore Hardness (A)	D-2240	73-77 Scale A
Tensile Tear Resistance	D-624	8-12 Kg/cm
Polymerized Density	D-792	1.16-1.17 g/cm^3

5.3   Prototypes

In Additive Manufacturing it is important to take into cosideration the printing direction [18] because it can affect the mechanical properties: Additive Manufacturing produces orthotropic structures due to the layer upon layer deposition method. Due to the symmetry axis in the circular structure and in the toroidal structure the direction is not relevant on the XY plane of the tray. External environment as humidity and temperature can influence the behaviour of the photopolymeric resin and should be manteined in the correct range suggested by the producer. Another fact to take into consideration is to print the same copy of a product without waiting between each manufacturing, because the products printed in series are dimensionally more similar to each other [19].
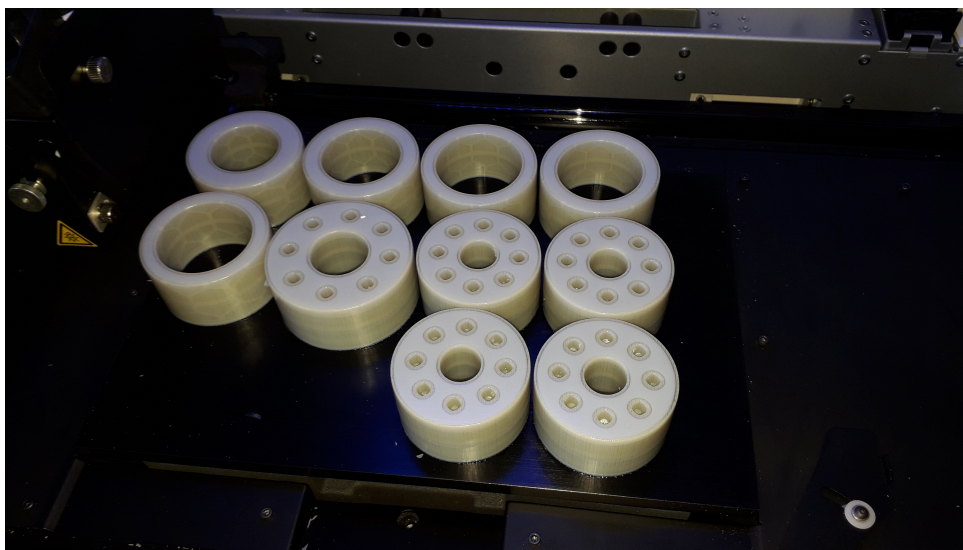
FIGURE 5.2: Additively Manufactured structures.

The selected structures to prototype are chosen in accordance to the simulation analysis results: the circular structures C, I and O show bistability, a relevant characteristic of NSS and in structures D and L is evident the effect of the beam width b, a parameter not studied by Corsi et al. [5]. All the toroidal structures are printed.
In order to obtain a suffcient number of experiments each component is printed 3 times. The structures on the tray are oriented by GRABCAD print software to save space and time. In the printer software is possible to select the finishing surface in matte and the support material in FullCure705 with standard density. The matte surface is obtained with the application of support in all the faces of the body and it appears opaque. In addition to that the matte surface increases the accuracy of the printer and it is possible to obtain lower tollerance values. The support density is essential to prevent deformation during the compacting phase by the roller because TangoGray material is not rigid enough without strong support. The print software estimates a time of production of 17 hours and 21 minutes with a material consumption of 653g of model and 929g of support but the real values are different. The mass of each structure is also evalueted with SOLIDWORKS and the polymerized density from the data sheet of the material. The first and the secon batch took 15h 30m. The last print tray took 16h 15m because an additional sacrifical structure was realized to set the testing facility and not damage the testing structures. The second print batch was done the day after the first print at the same time of the day and the last one after 3 days in the same room condition at 24°C and 67% of humidity.

TABLE 5.2: Structures mass and time.

	SOLIDWORKS [g]	Batch1 [g]	Batch2 [g]	Batch3 [g]
C	9.53	9.53	9.61	9.51 - 9.50
D	10.83	10.84	10.93	10.80
I	14.93	14.83	14.98	14.86
L	20.44	20.56	20.42	20.50
O	11.22	11.07	11.18	11.17
torA	29.19	29.51	29.31	29.45
torB	37.03	37.52	37.32	37.23
torC	24.05	24.51	24.47	24.45
torD	28.44	28.64	28.67	28.69
torE	24.41	25.07	24.98	24.97

The structures produced with PolyJet need a post processing cleaning phase to remove the support material: first mechanical cleaning with plastic tools and then water cleaning with high and low pressure water jet. During the design phase is important to take into cosideration the removal of support material: the holes in the toroidal structure allow to clean inside.
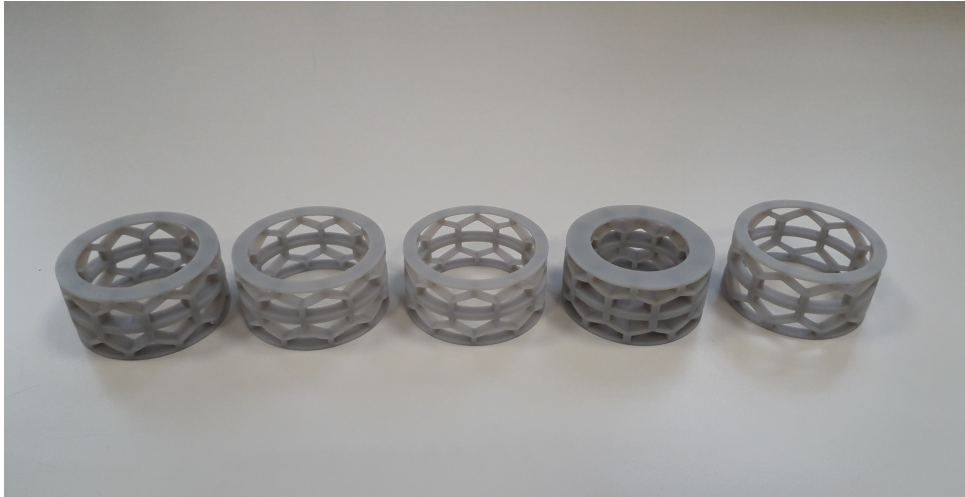
FIGURE 5.3: Circular structures.
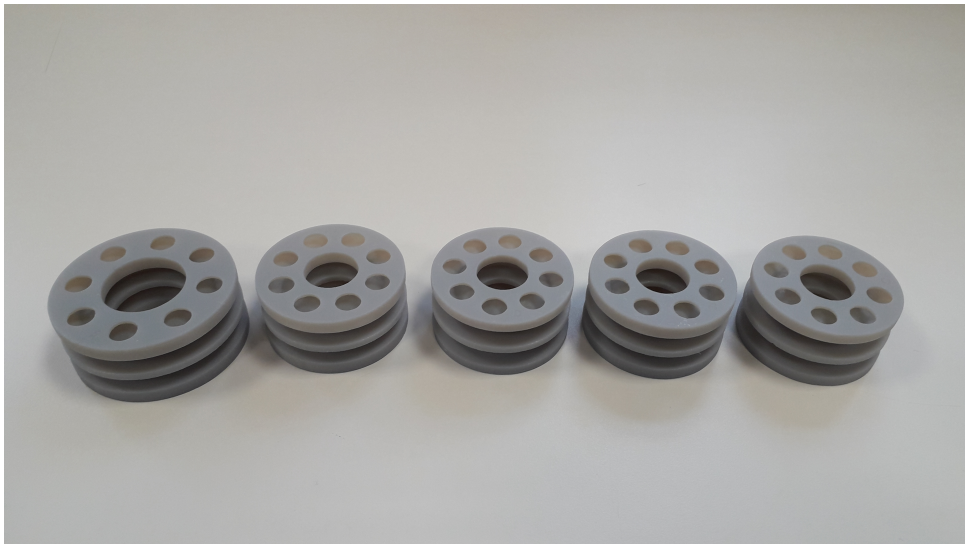
FIGURE 5.4: Toroidal structures.

A qualitatively analysis shows a rubber like behaviour of the material and some superficial defects are visible by eyes on the external surface. A possible origin of these defects can be a partial occlusion of the resin jets or contamination by solid particles present inside the printer.

5.4 Quasi-static compression test

The mechanical quasi static compression test conducted in the University facilities is based on the ASTM D695 [14] standard. The load cell was set at 200N with a sample rate of 1000Hz. The tested structures were not subjected to the conditioning procedure for the required time in the standard temperature and humidity condition and the test was conducted at a lower temperature without controlling the humidity in the laboratory. For each structure only three components (instead of five) are tested for a preliminary analysis to further investigation. The compression phase ends when the sensor measures a constant incremental of the force.

5.4.1 Circular structure

In the following pictures is shown the compression phase of the circular structure C1 (see Fig5.5). During the test all the samples of the circular structure I and L failed and none of the structures show bistability in the unloading phase (see Tab5.3). The collapsing phase due to buckiling shows asimmetry in the two layers: after a first global deformation one layer starts a more rapid collapsing phase then the other layer and in some cases few cells collapse even faster (local asimmetry). The differences in the deformation is generated by the non homogeneous material and defects in the prototyping. In the following plots is possible to see the characteristic behaviour of NSS in all the circular structures tested.

TABLE 5.3: Deformation of the tested Circular structures.

	Initial height [mm]	Final height [mm]
C1	29.43	29.31
D1	29.46	29.41
I1	29.68	failed
L1	29.73	failed
O1	29.38	29.06
C2	29.57	29.37
D2	29.72	29.59
I2	29.46	failed
L2	29.44	failed
O2	29.46	29.33
C3	29.40	29.13
D3	29.41	29.37
I3	29.82	failed
L3	29.37	failed
O3	29.73	29.14
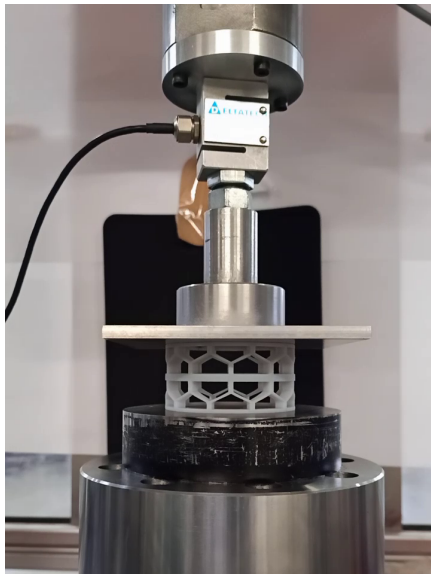
(A) Phase 1.
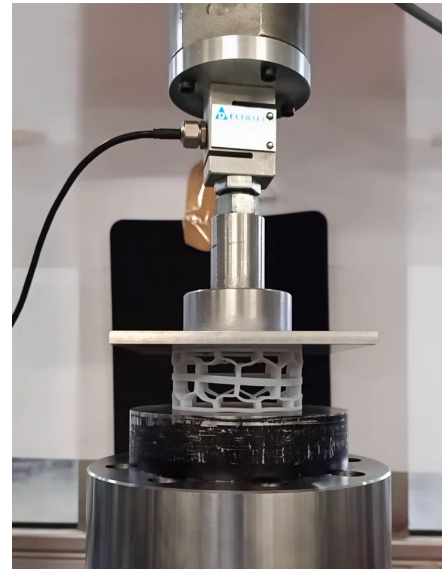
(B) Phase 2.
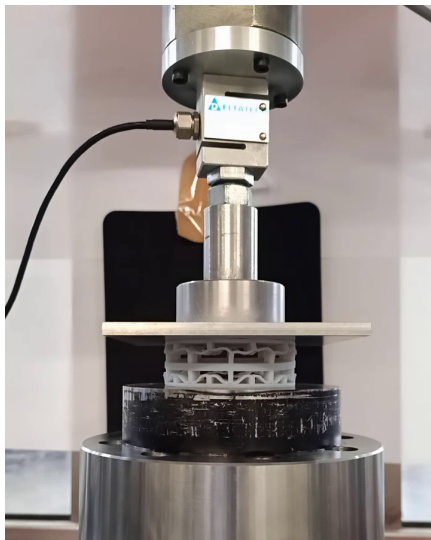
(C) Phase 3.
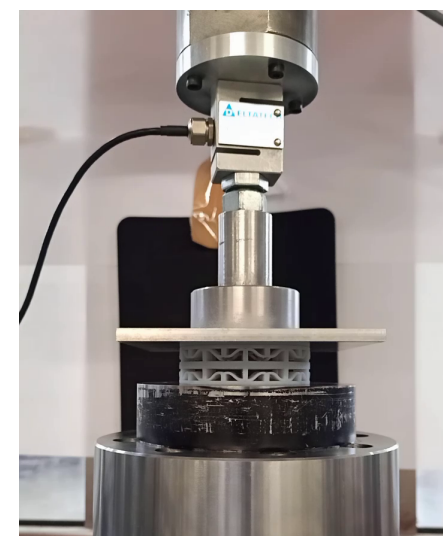
(D) Phase 4.

FIGURE 5.5: Compression phase Circular structure C1.
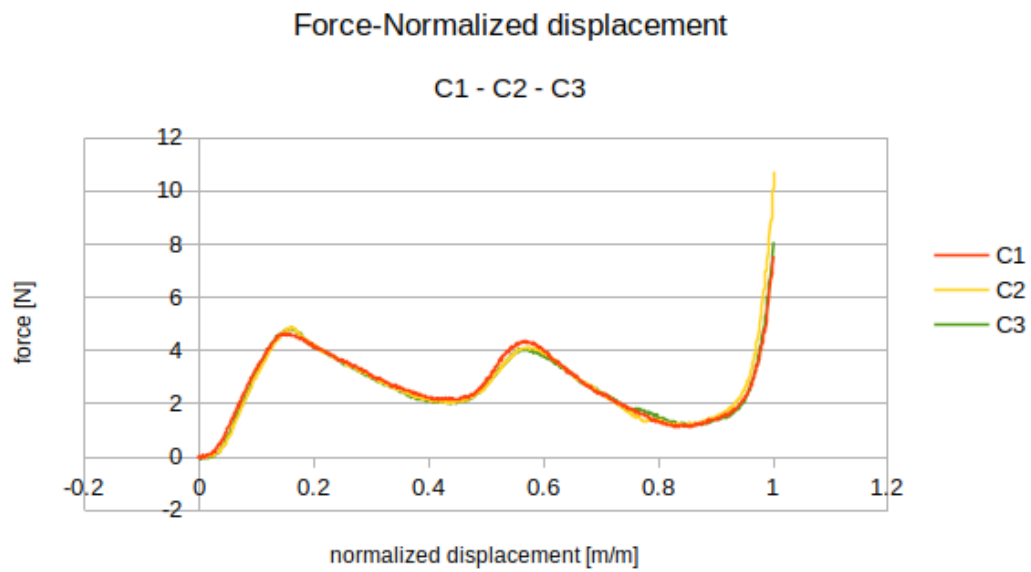
FIGURE 5.6: Experimental force reaction structure C.
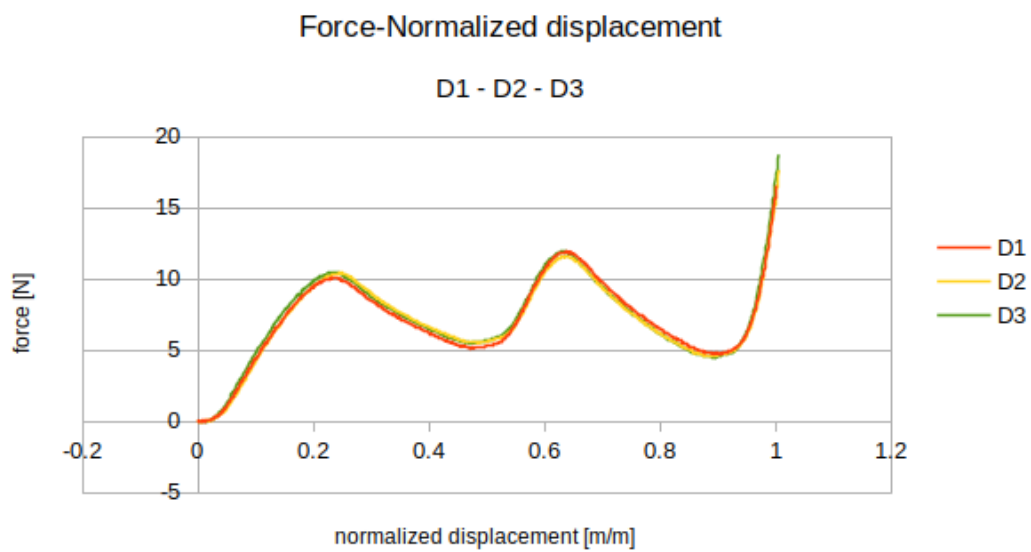
FIGURE 5.7: Experimental force reaction structure D.

Force-Normalized displacement

I1 - I2 - I3
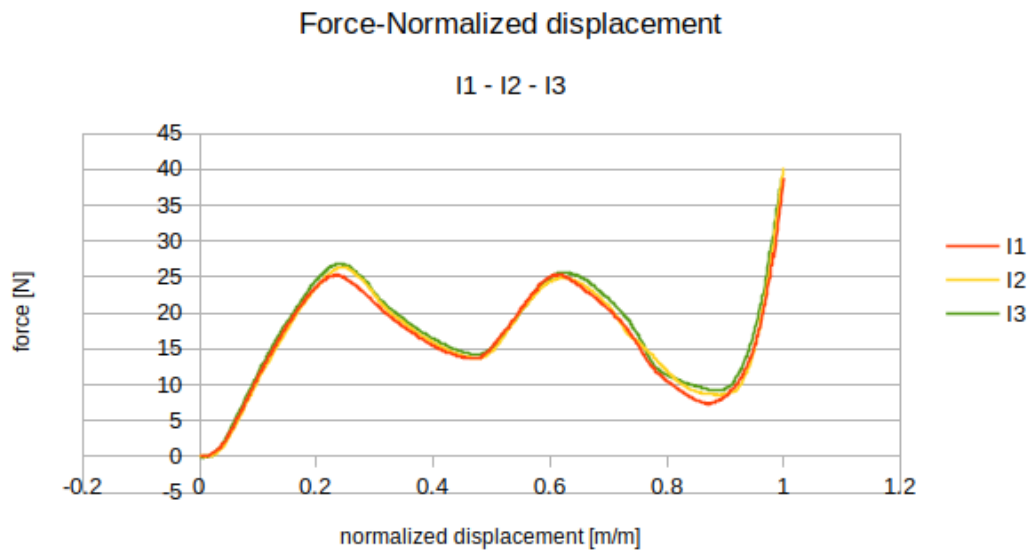
FIGURE 5.8: Experimental force reaction structure I.

Force-Normalized displacement

L1 - L2 - L3
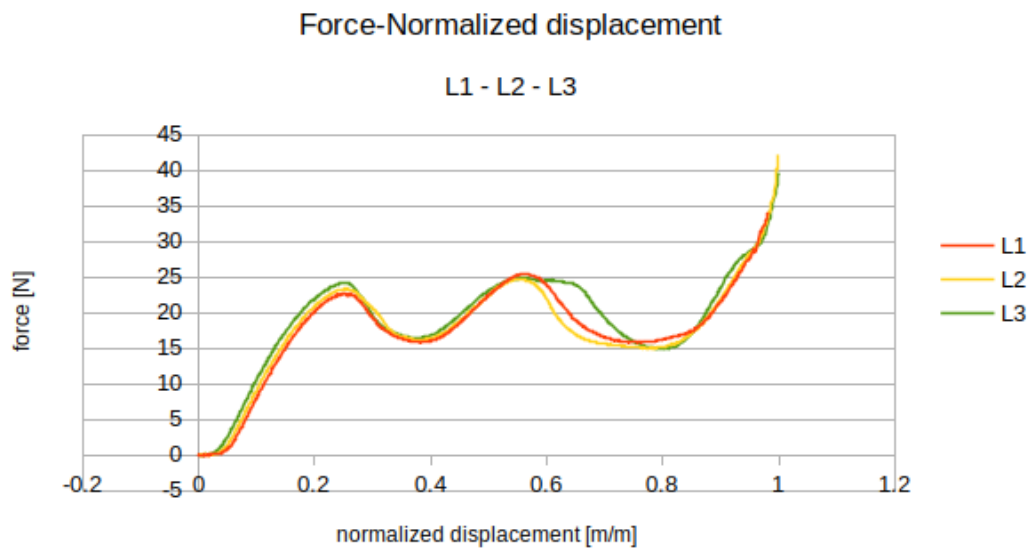
FIGURE 5.9: Experimental force reaction structure L.
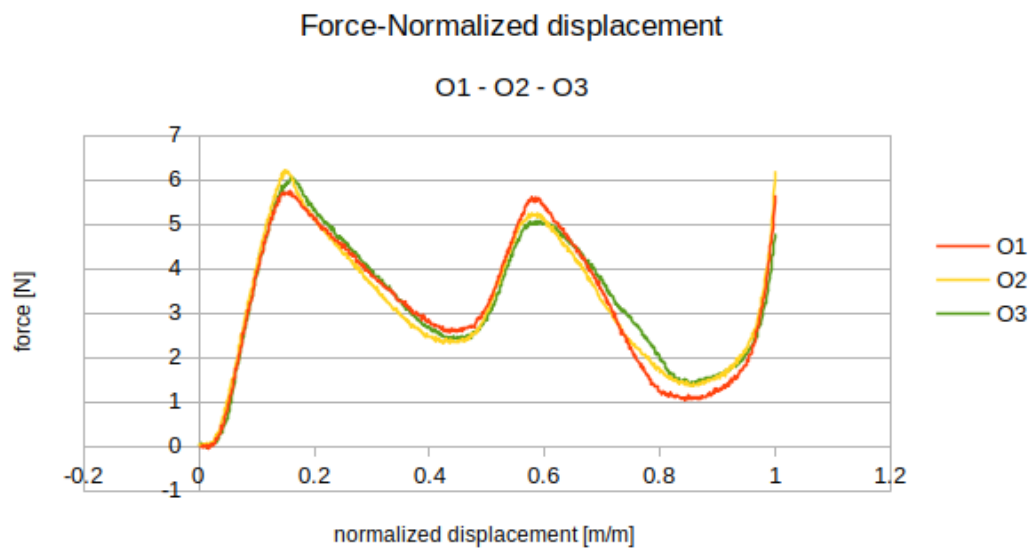
FIGURE 5.10: Experimental force reaction structure O.

5.4.2 Toroidal structure

During the test none of the toroidal structures failed but only the structure torC shows negative stiffness behaviour (see fig5.13). The bistability phenomenon is not evident in none of the structures. In the other toroidal structures initially the force increases then the plot becomes flat until the final compression phase when the structures is completely collapsed. The flat region is probably originated by the buckling phenomenon without the negative stiffness behaviour. After the compression phase the final height is lower in all the structures due to the low temperature in the laboratory: the TangoGray mechanical properties are related to the temperature.

TABLE 5.4: Deformation of the tested Toroidal structures.

	Initial height [mm]	Final height [mm]
torA1	29.39	29.31
torB1	29.10	28.55
torC1	28.98	27.88
torD1	29.30	28.24
torE1	29.03	26.87
torA2	29.27	28.71
torB2	29.21	27.80
torC2	29.05	27.64
torD2	29.38	28.36
torE2	29.08	26.53
torA3	29.61	28.05
torB3	29.12	28.46
torC3	29.36	ND
torD3	29.29	ND
torE3	29.35	27.11
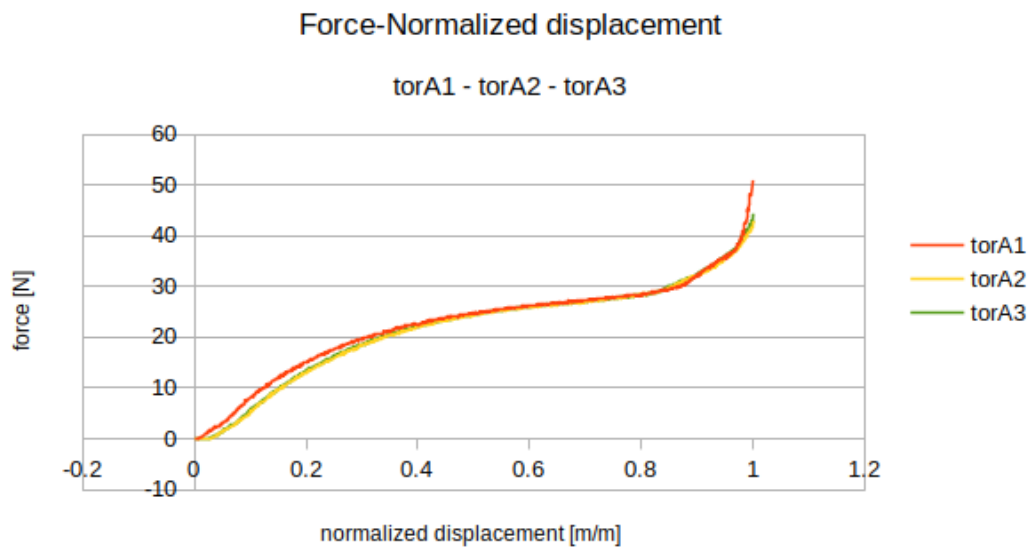
FIGURE 5.11: Experimental force reaction structure torA.
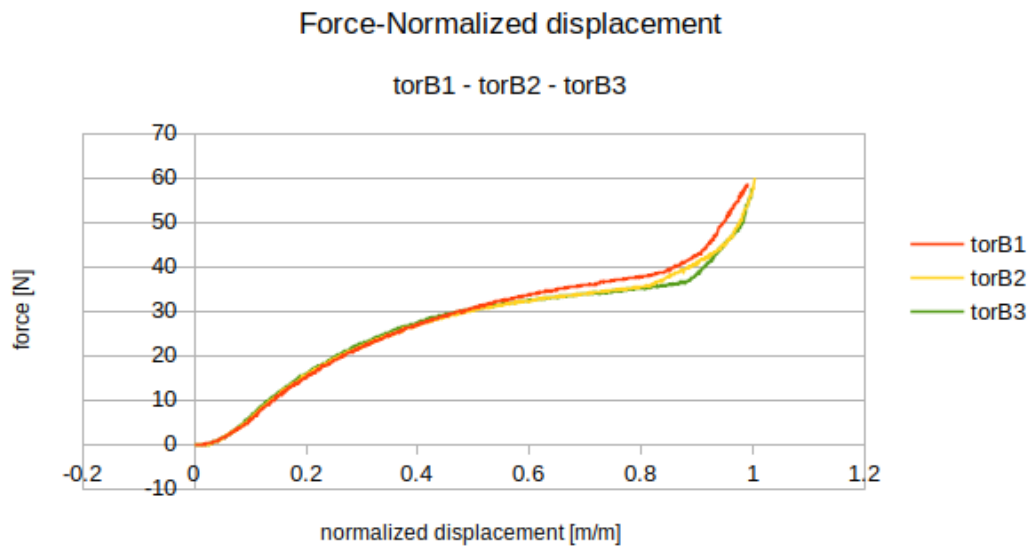
FIGURE 5.12: Experimental force reaction structure torB.
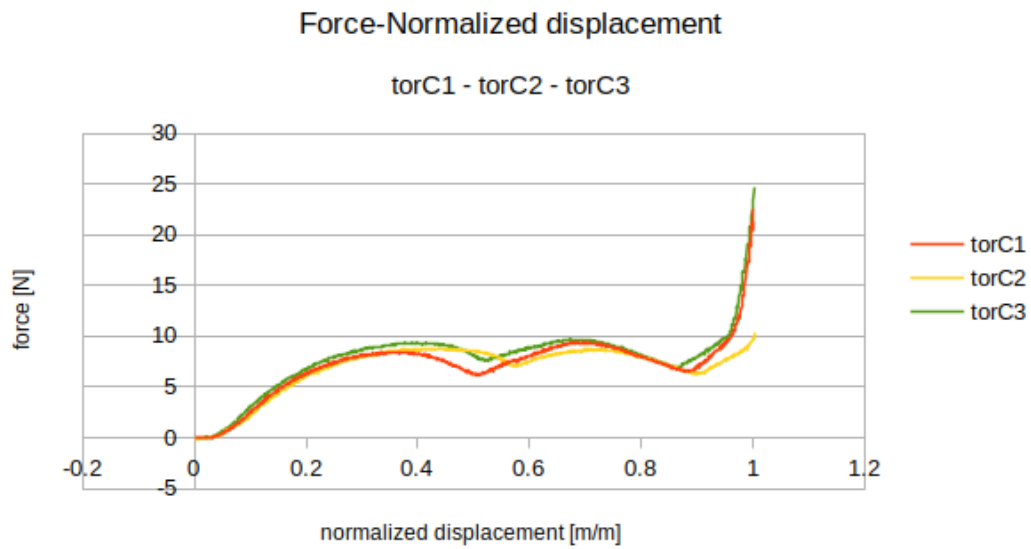
FIGURE 5.13: Experimental force reaction structure torC.

Force-Normalized displacement

torD1 - torD2 - torD3
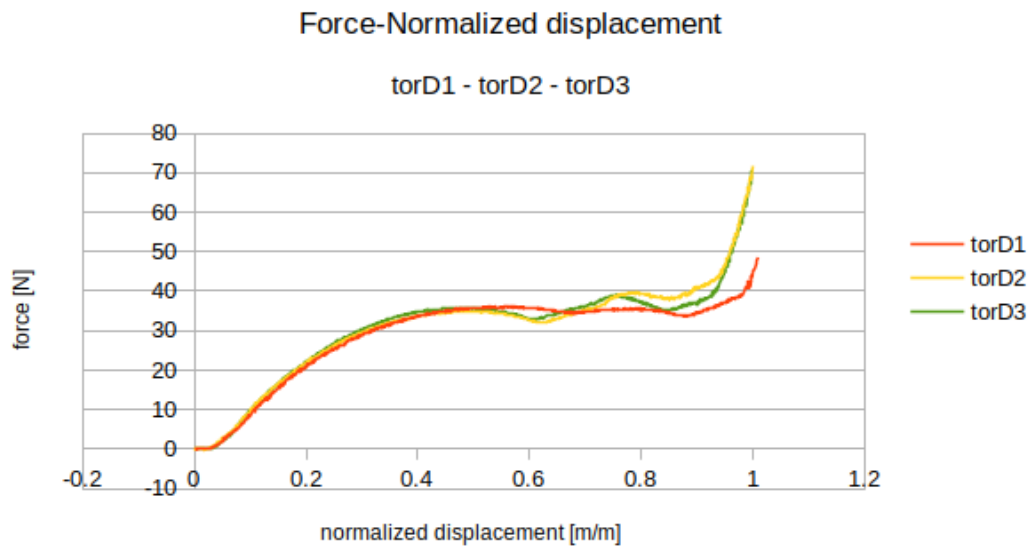
FIGURE 5.14: Experimental force reaction structure torD.

Force-Normalized displacement

torE1 - torE2 - torE3
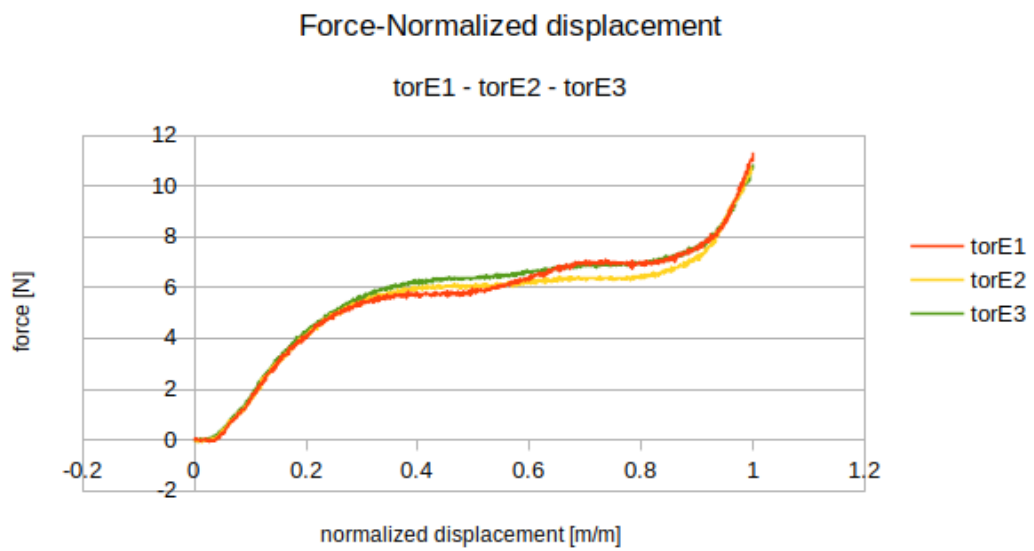
FIGURE 5.15: Experimental force reaction structure torE.

Chapter 6

Results

The comparison of the numerical results and experimental test results is the core of this project because it allows to verify if the assumptions and the design method are correct. In order to compare the three repetition test and the simulated behaviour in the plot the displacement is normalized with the maximum displacement of each structure. In order to have an estimation of the experimental results the standard deviation is calculated as required from the ASTM D695 [14].

$$s = \sqrt{\frac{\sum_{i=1}^{n}(X - \tilde{X})^2}{(n-1)}}$$

s = standard deviation
X = value of single observation
n = number of observations
$\tilde{X}$ = arithmetic mean of the set of observations.

6.1 Circular structure

In all the 5 circular structures tested the three repetitions show comparable force in the high peak and in the low peak (see plots in the next page). In addition to that the calculation of the standard deviation produces small values in every tested structures (see Tab6.1): this means that the prototyping phase produced samples with the same characteristics. If the experimental results are compared with the numerical simulation is evident that the peaks appear almost at the same value of displacement but with different force. In particular the simulated force is higher in the peak and lower in the minimum value. This means that the buckling phenomenon is correctly simulated but the snap-through shows a very different behaviour in all the structures. The difference in the peak force in the numerical simulation and in the average value of the test ranges from 33.1% to 44.7% (see Tab6.1).

TABLE 6.1: Maximum standard deviation Circular structure.

	C	D	I	L	O
Standard deviation	0.90	0.71	3.29	3.59	1.42

TABLE 6.2: Maximum force variation Circular structure.

	C	D	I	L	O
Maximum force variation	33.8%	44.7%	34.1%	33.1%	38.1%

Force-Normalized displacement

C - test average
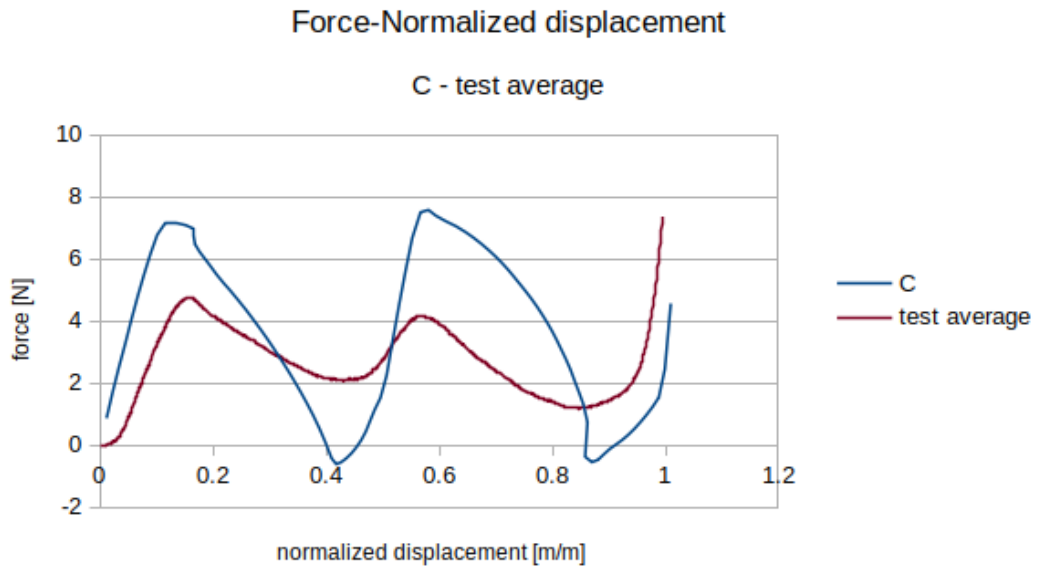
FIGURE 6.1: Numerical and experimental force reaction structure C.

Force-Normalized displacement

D - test average
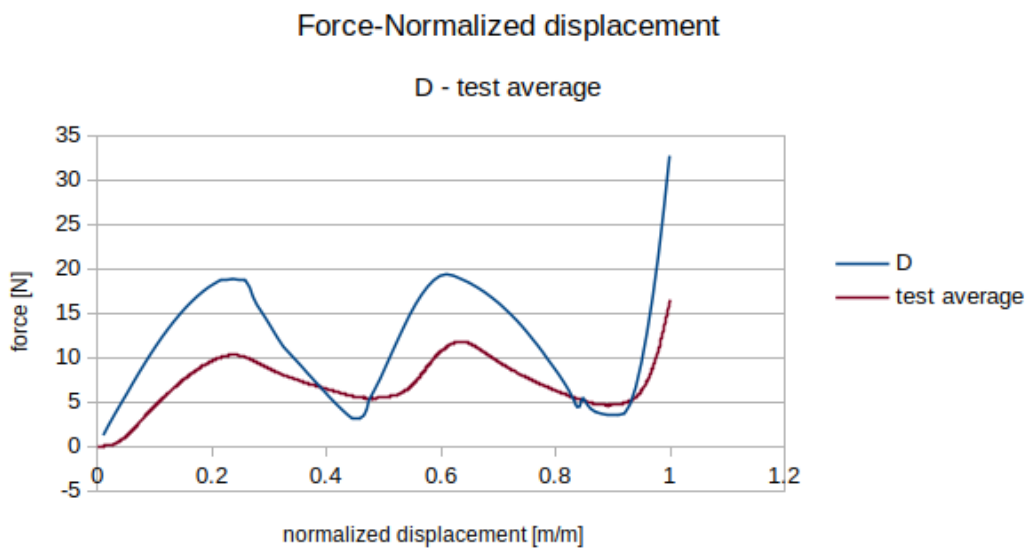
FIGURE 6.2: Numerical and experimental force reaction structure D.
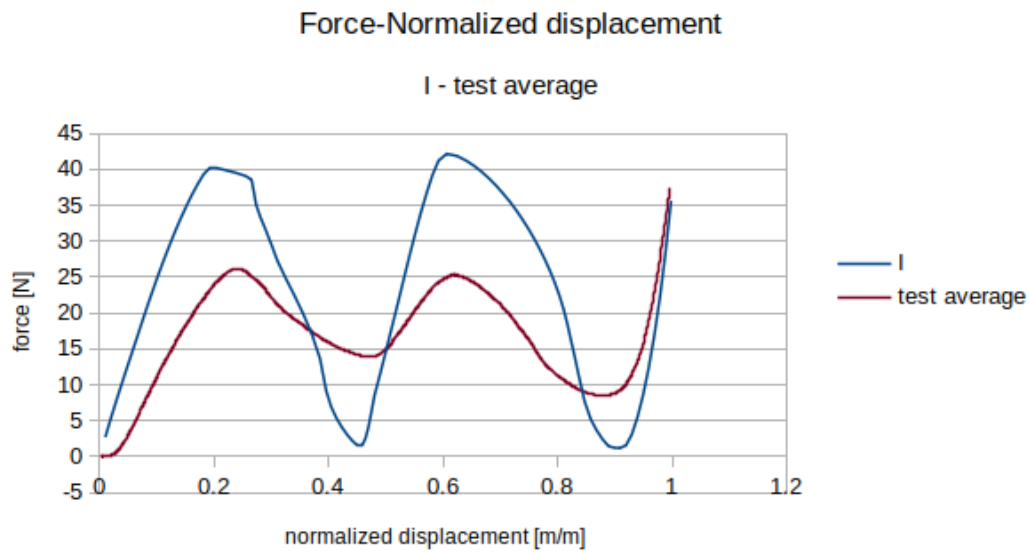
FIGURE 6.3: Numerical and experimental force reaction structure I.
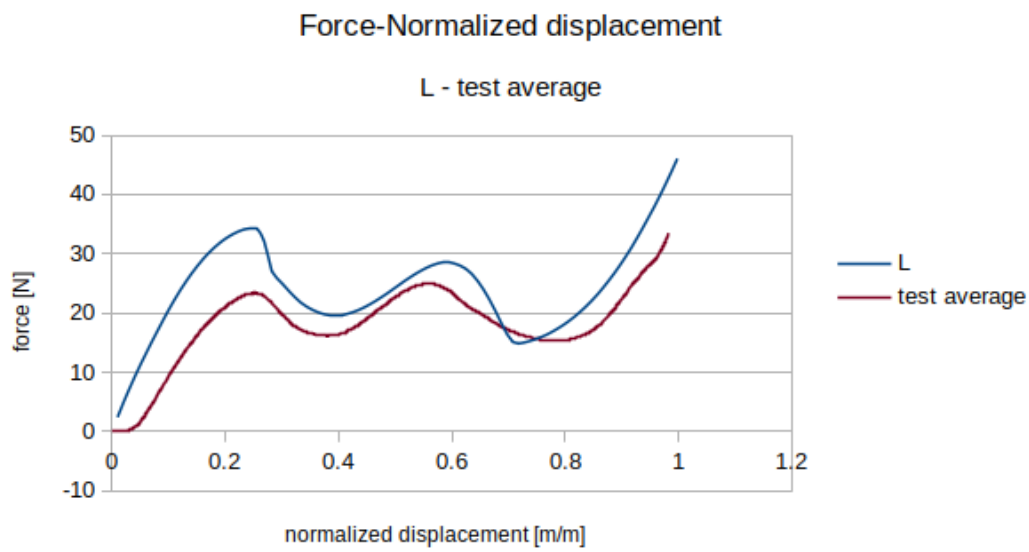
FIGURE 6.4: Numerical and experimental force reaction structure L.

Force-Normalized displacement

O - test average
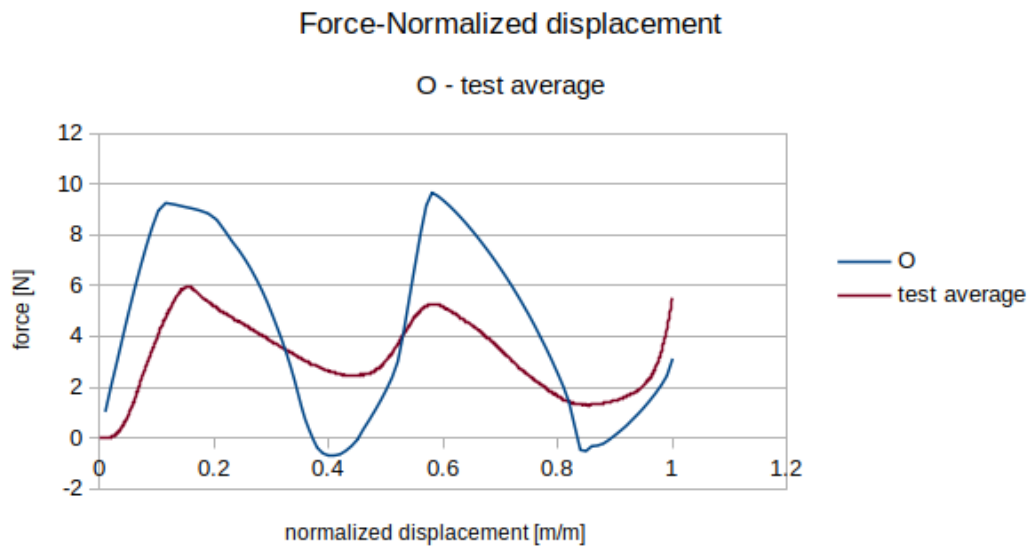
FIGURE 6.5: Numerical and experimental force reaction structure O.

6.2 Toroidal structure

The structures torA, torB and torE show a similar trend in the force-displacement plot but the obtained force value is lower. The simulated structure torD (see Fig6.9) shows negative stiffness behaviour but in the experimental test results the force plot is flat. Only in the structure torC (see Fig6.8) it is possible to see the negative stiffness behaviour in the experimental test result. The standard deviation (see Tab6.3) shows small results in all the samples tested: this means that the prototyping phase produced samples with the same characteristics. The difference in the maximum force in the numerical simulation and in the average value of the test ranges from 21.8% to 42.8% (see Tab6.4).

TABLE 6.3: Maximum standard deviation Toroidal structure.

	torA	torB	torC	torD	torE
Standard deviation	4.39	4.82	1.18	3.68	0.41

TABLE 6.4: Maximum force variation Toroidal structure.

	torA	torB	torC	torD	torE
Maximum force variation	21.8%	28.5%	42.8%	41.6%	33.3%

Force-Normalized displacement

torA - test average
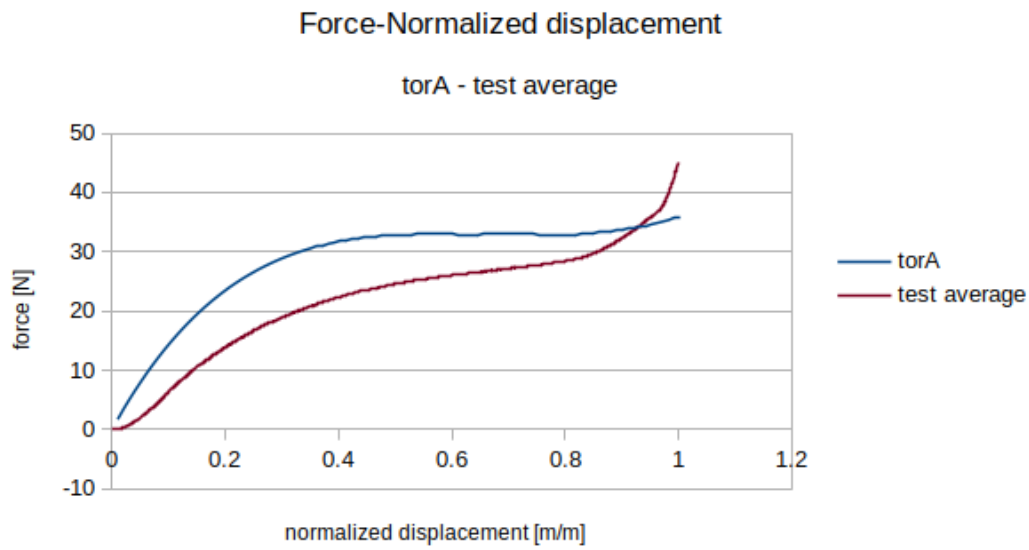
FIGURE 6.6: Numerical and experimental force reaction structure torA.

Force-Normalized displacement

torB - test average
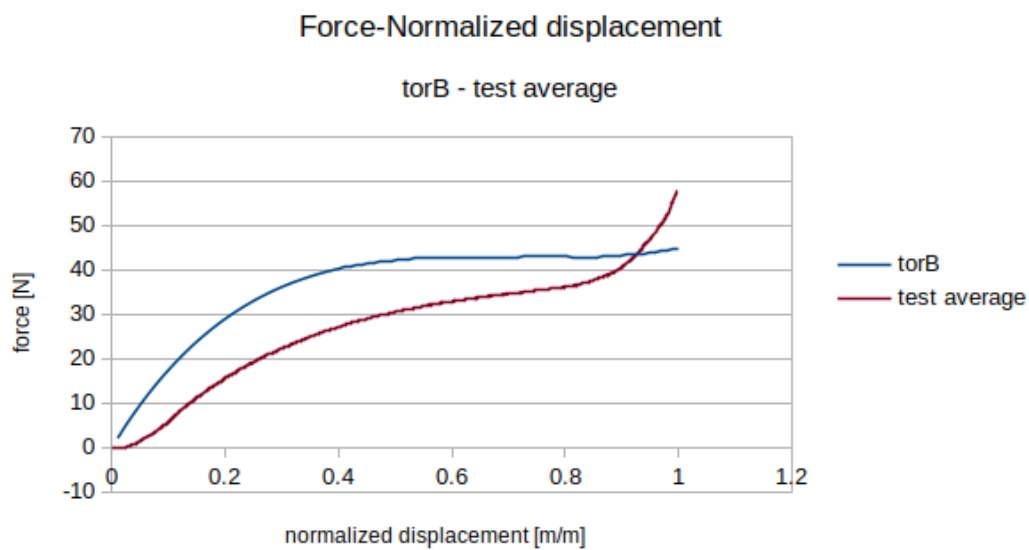
FIGURE 6.7: Numerical and experimental force reaction structure torB.

Force-Normalized displacement

torC - test average
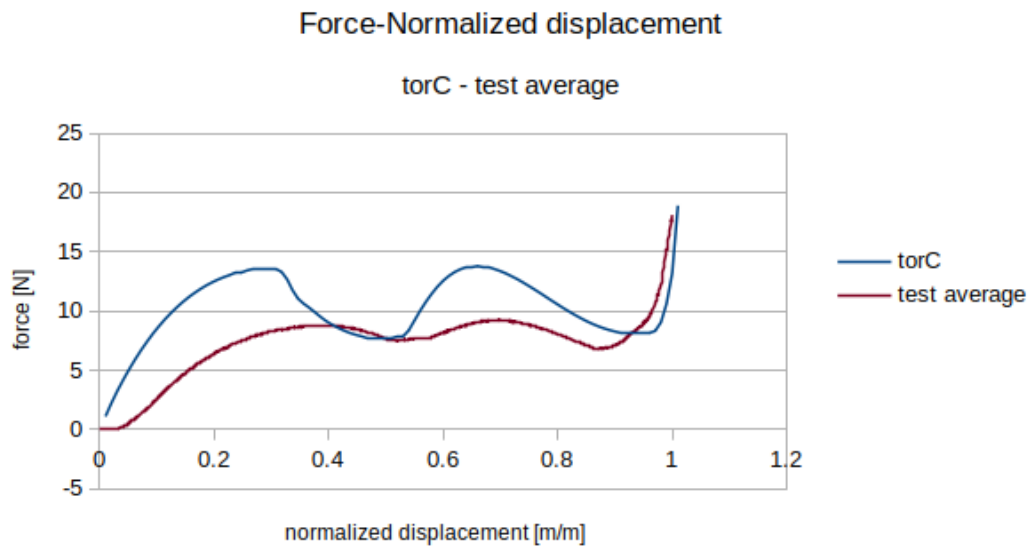
FIGURE 6.8: Numerical and experimental force reaction structure torC.

Force-Normalized displacement

torD - test average
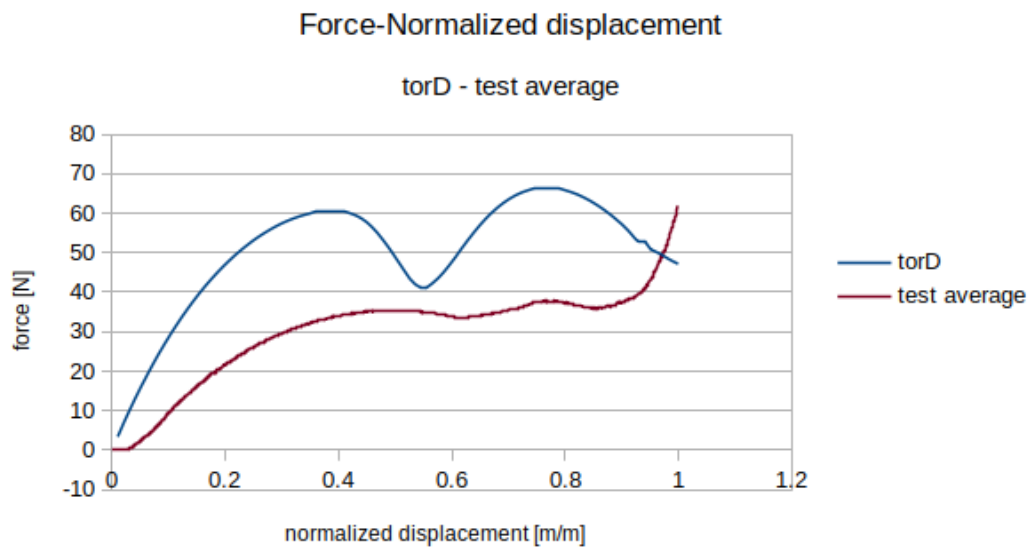
FIGURE 6.9: Numerical and experimental force reaction structure torD.

Force-Normalized displacement

torE - test average
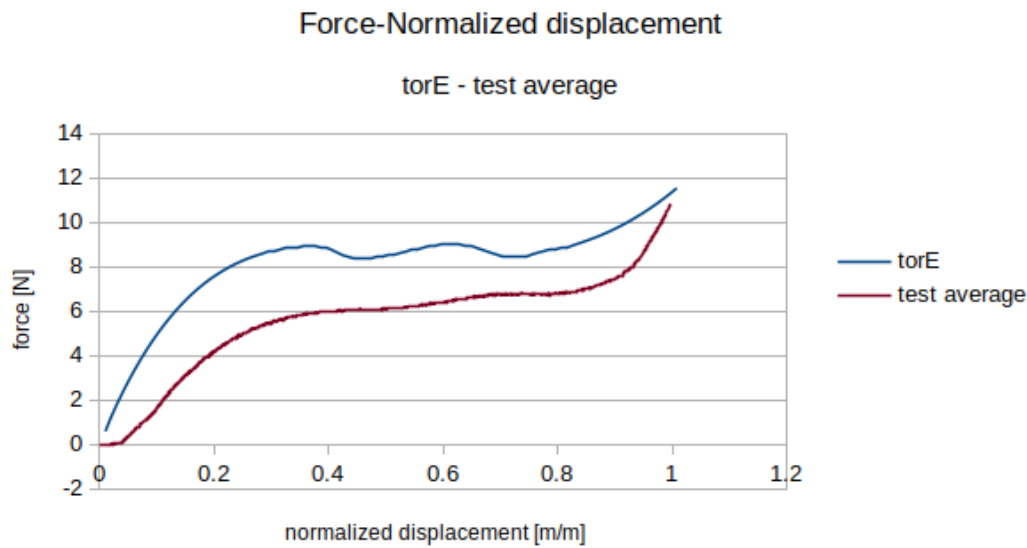
FIGURE 6.10: Numerical and experimental force reaction structure torE.

6.3 Discussion

The test repetition plots are almost coincident, this means that all the samples show the same mechanical property and the prototyping phase was conducted in the correct environment.

In all the circular structure plots the buckling phenomenon is correctly simulated because it appears at the same displacement value of the test. In the toroidal structure it is evident the negative stiffness behaviour with the characteristic peaks only in one structure.

The numerical solution of the force reaction is different from the test result. This difference in the force reaction is not negligible and there are several possible explanations. First of all it is possible that the numerical model is not correct or the material curve fitting not well approximated: a complete revise of the simulation analysis is necessary but not affordable due to time. Second, the problem could be related to the testing method because conducted in different condition from the standard protocol and in particular the temperature can influence the material properties.

Merit index

In order to have a standard method to compare the results obtained in the test it is chosen a normalization introduced by Corsi et al. [5] because the conventional index of merit for bulk structures is not applicable. This normalization takes into consideration the weight of the structure: an high merit index indicates a more efficient structure. The relative strength is evaluated with the load applied on the structure at the 50% of the displacement divided by the weight of the structure.

$$Merit\ index = \frac{Load\ at\ 50\%\ of\ the\ displacement}{Weight}$$

The circular structures I and L and the toroidal structure torD are the best in terms of weight because the merit index is high.

TABLE 6.5: Merit index Circular structures.

	Numerical	Sample1	Sample2	Sample3
C	24.00	31.16	28.62	28.59
D	85.21	49.55	52.94	53.51
I	122.74	104.14	101.54	102.00
L	122.66	112.12	113.36	115.85
O	17.27	32.48	29.98	29.58

TABLE 6.6: Merit index Toroidal structures.

	Numerical	Sample1	Sample2	Sample3
torA	114.71	85.76	86.03	85.62
torB	116.11	84.31	82.02	83.73
torC	32.79	26.03	35.09	33.66
torD	170.32	126.56	124.15	126.68
torE	35.50	23.86	24.37	26.04

Chapter 7

Case study

7.1 Orbital debris

Since the very first space missions during the last century, humanity continues to send material in space and in the last 40 years it 's reached a mass rate in orbit of 145 metric tons annually [3]. The main space debris are 4600 intact objects and 1000 active spacecrafts. This big number of abandoned material is very dangerous for space activities because is out of control. In addition to that the major part orbits in very crowded region very important for new mission and also for the International Space Station. Another big problem are the debris produced by impact between object as the accidental collision among Iridium 33 and Cosmos 2251 in 2009 or the Chinese anti-satellite missile test in 2007. These debris in LEO orbits travel at 10 km/s and even a 10 cm body is a projectile that can cause a serius damage to active spacecraft. The accidentally collision of debris can increase exponentially the number of the objects (Kessler syndrome) and so the number of catastrophic collisions.
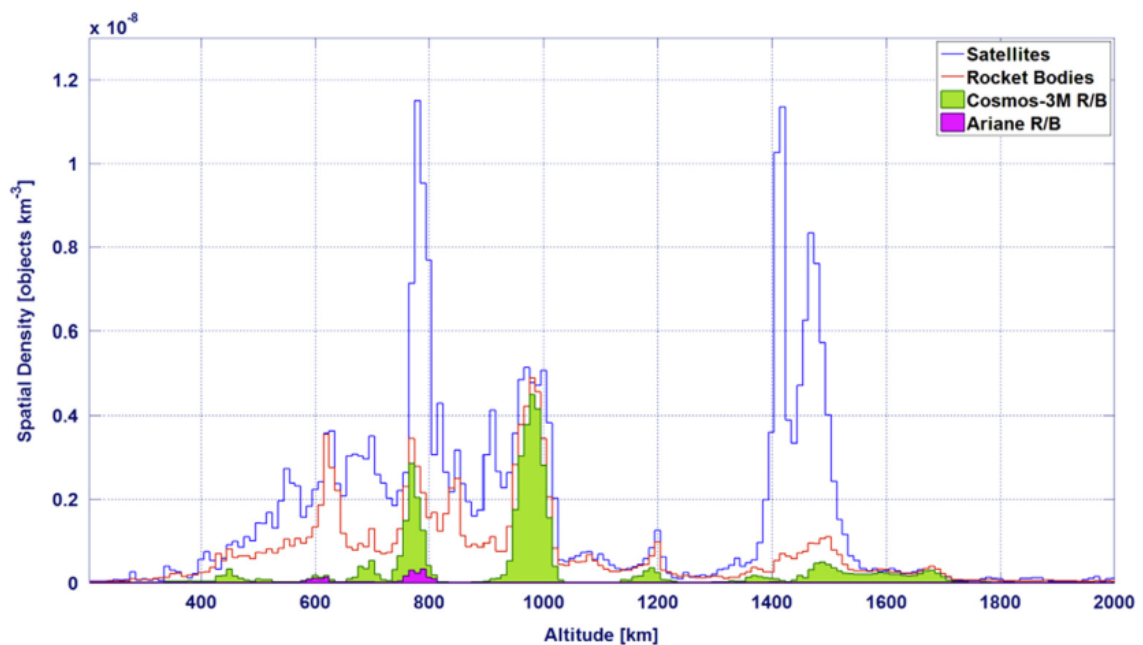
FIGURE 7.1: Space debris distribution [3].

7.2   Solution

Due to the current critical situation it is not sufficent to avoid to generate new debris but it is needed a removing strategy for the abandoned bodies. In this direction there are several studied techniques [2] based on different methods. One of this strategy is designed in Italy by university collaboration by DeLuca e al. [3]. An unmanned spacecraft should transport in the desired orbit a module provided of navigation and propulsion system. This module will be attached with a robotic arm to the debris and with an adesive system fixed. At this point the hybrid propulsion system should deorbit the debris and the carrier moves to the next debris with another propulsion module. The evaluation of the effectivity of removing several big debris each year appears a good solution for reducing the probability of dangerous impact.
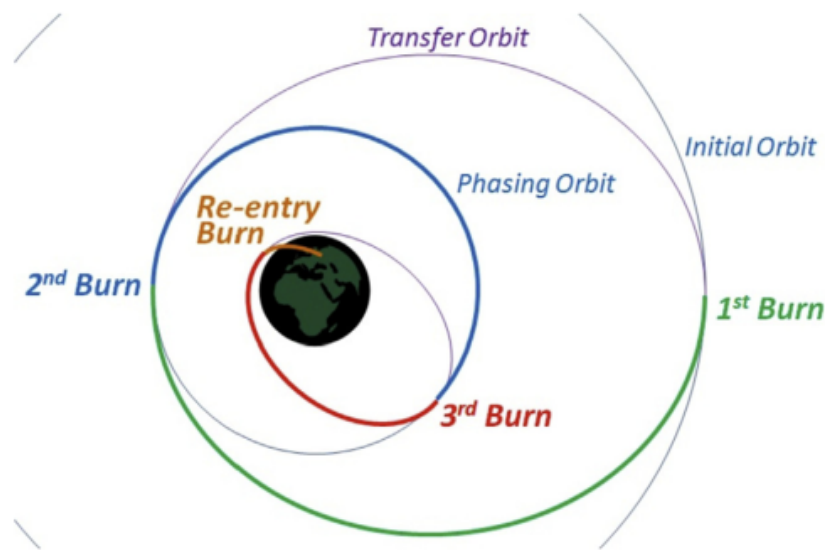
FIGURE 7.2: Debris disposal strategy scheme [3].

7.3 Application of NSS

During the adhesion phase it is important to reduce impact forces and to dissipate the relative velocity and oscillations between the debris and the deorbiting vehicle after contact. For this task the researcher proposed a damping joint made of elastomeric material whose deformation determines internal energy dissipation. An elastomeric device could be based on negative stiffness technology, in particular one based on the geometry studied in this thesis and produced with Additive Manufacturing process. The rubber like material studied in this project is not certificated for aerospace application: as it would not satisfy the vacuum conditions requirements. In addition to that, in high temperature gradient and with low temperature the mechanical properties of TangoGray change and it becomes more brittle. In order to solve this problem it is possible to select another material for the Additive Manufacturing such as metal or composite material. The selection of a different material can be usefull also to obtain a different force reaction of the structure: a stiffer material can increase the force needed to obtain buckling and so absorb more energy.
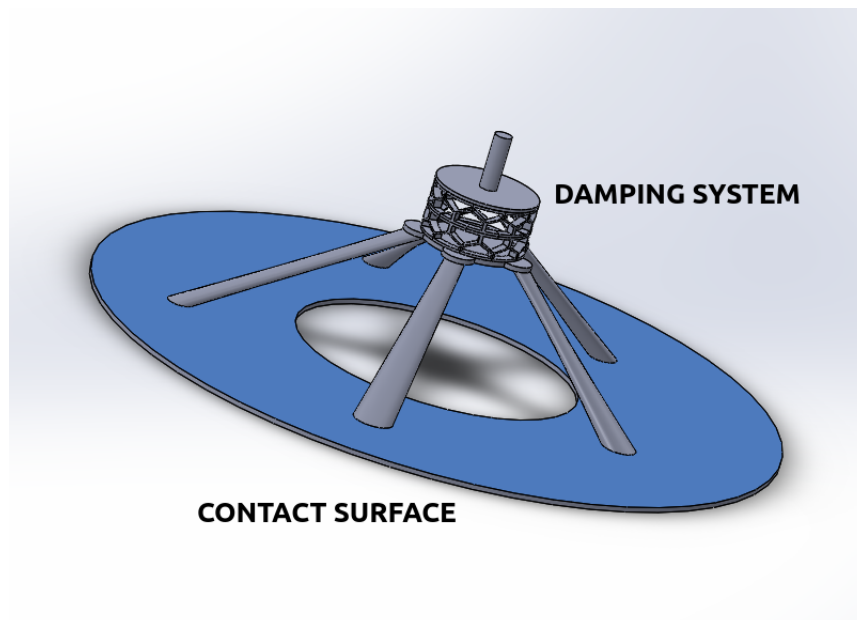
FIGURE 7.3: Capture method and damping joint.

Chapter 8

Conclusion

The aim of this project is to set a correct numerical model to simulate the behaviour of an innovative NSS damping system realized with additive manufacturing for a space debris removal mission. The study of the problem started from the analysis of previously studied negative stiffnes circular structure and the elementary negative stiffness curved beams to learn how is possible to control the properties of this structure such as bistability and snap-trough. The acquired knowledge allowed to create a toroidal structure derived from the same elementary element. When the characteristic parameters of the two geometries are defined is possible to apply the DOE and simulate the mechanical behaviour of the structure. The circular structures produced with a different rubber like material allow to verify the behaviour of the selected parameters with the previous studies by Wang. The analysis of the toroidal structure confirms that some parameters are fondamental to control the negative stiffness behaviour as the *Qratio*. The experimental phase is focused on the prototyping of 5 circular structures and 5 toroidal structures in order to verify the numerical simulations. The calculated numerical results are compared with the quasi static compression test results of the prototypes produced with Additive Manufacturing in the rubber like material.

8.1 Study limitations

The structure of this project follows a logical process from the analysis of the problem, the formulation of hypothesis with numerical and experimental verification to the final results applicable in an engineering structural problem. The simulation model is based on previous knowledge of the buckling problem and skills acquired during the initial phase of the project. Respect to the experimental nominal conditions the temperature was below 20°C and it changed during the test. In addition to that the conditioning phase was not performed.

8.2 Future studies

In next studies will be necessary to verify this project with two different methods. The first method is to apply the numerical model in a new project with different structures and materials and compare the experimental results. In this case the differences in the results of this project are supposed to be linked with an error in the numerical analysis. The second method is the experimental validation of this project: in this case it is necessary to prototype the same structures with the same material following the standard method and compare the new experimental results with the simulation.

When the experimental and numerical results will be comparable it is possible to consider this project as a tool for the study of Negative Stiffness Structures.

Appendix A

Simulation plots

Color	Red	Green	Blue
Direction	X	Y	Z

A.0.1 Circular structure
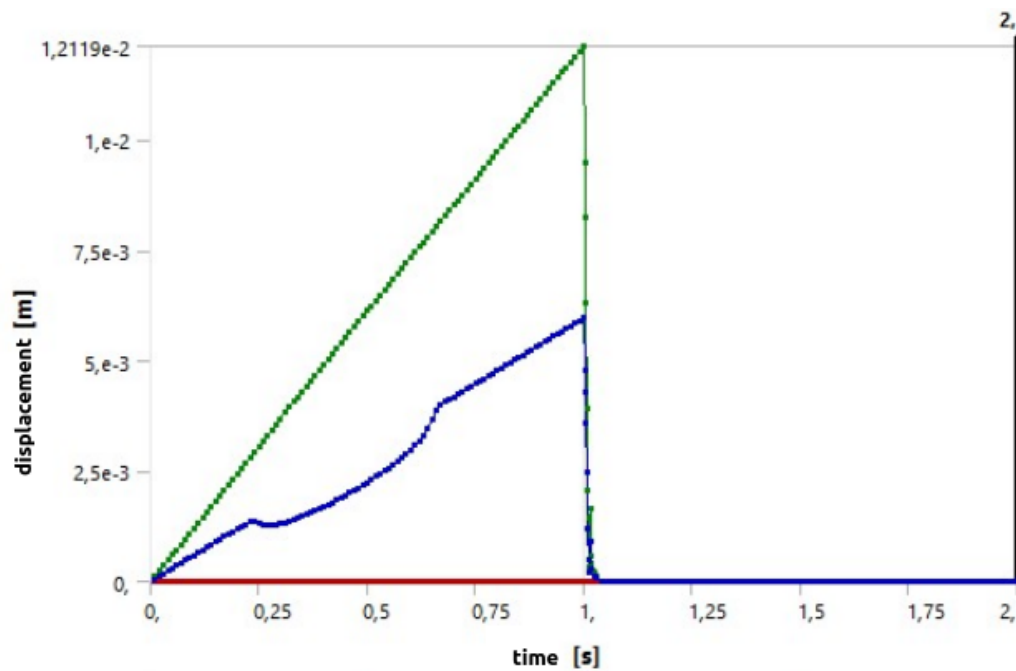
FIGURE A.1: Displacement one element structure A.
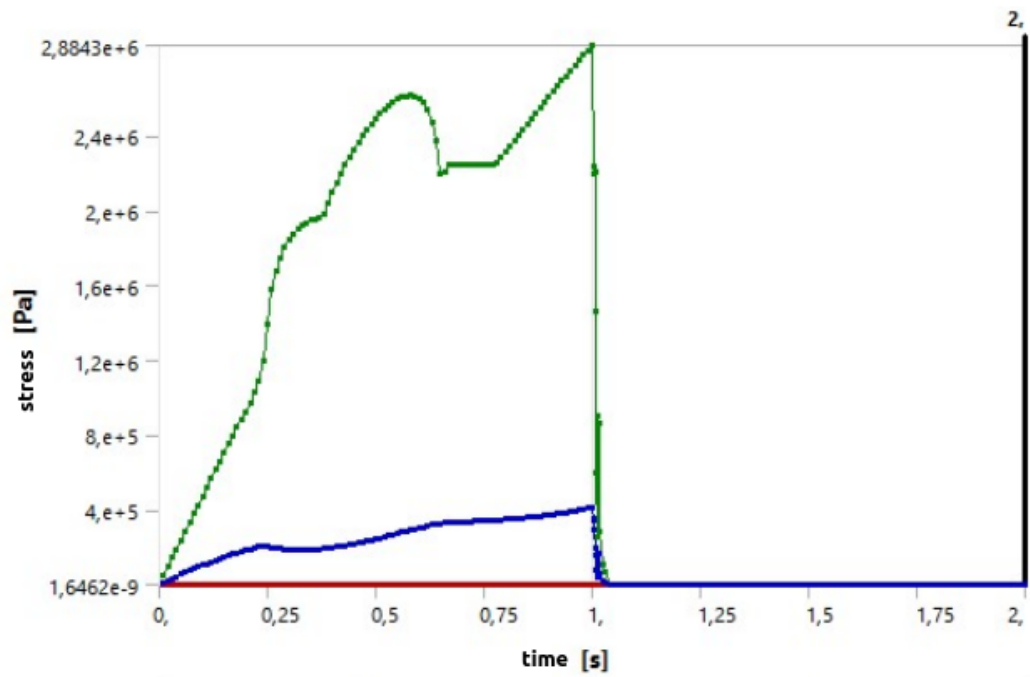
FIGURE A.2: Equivalent stress one element structure A.
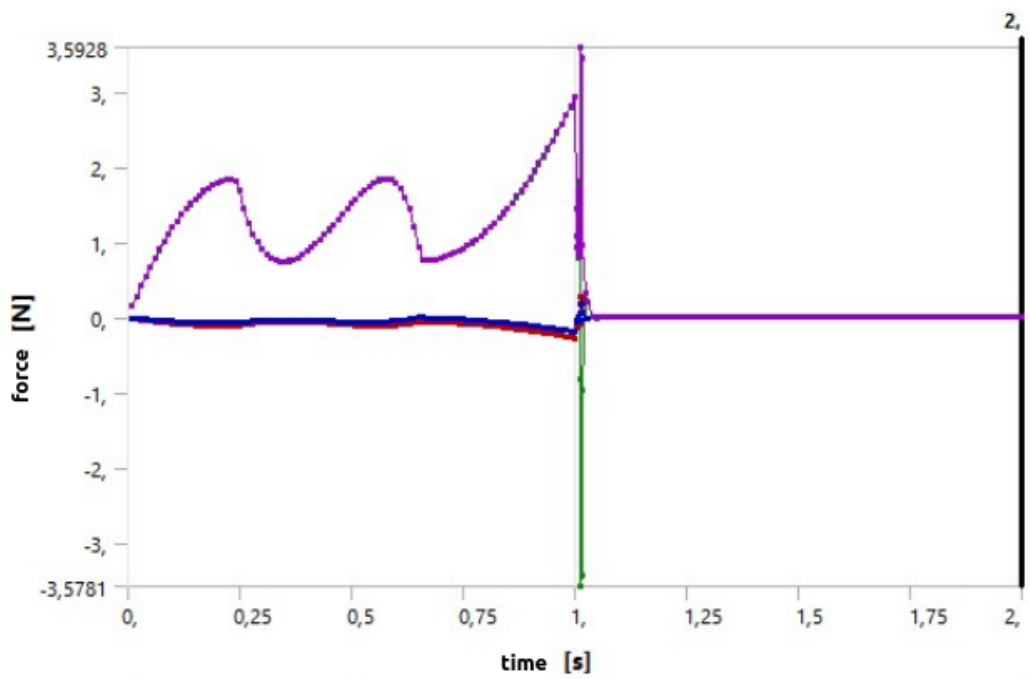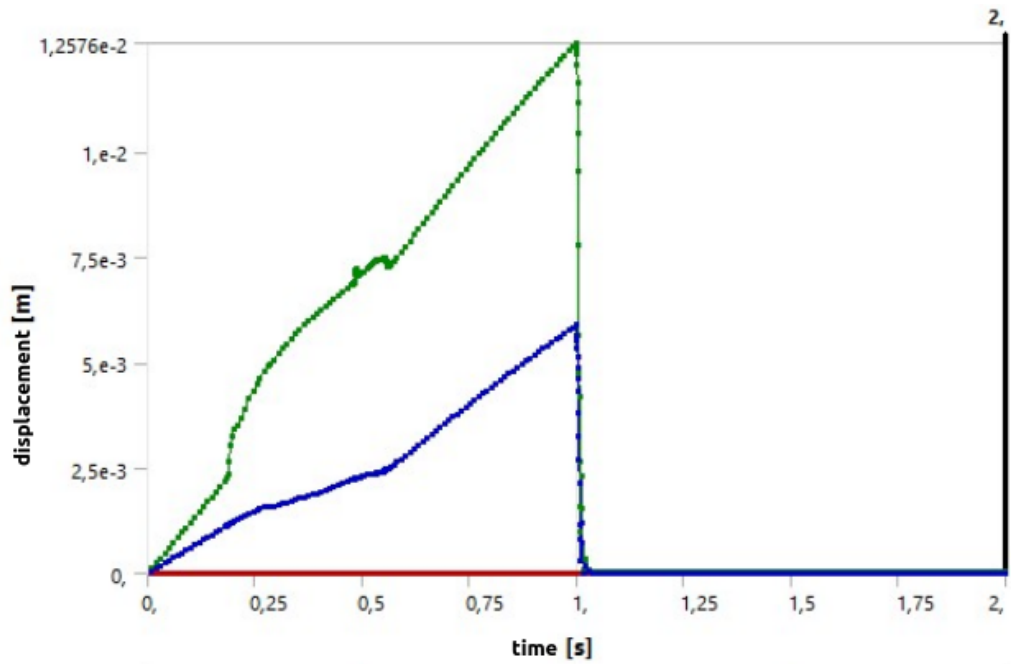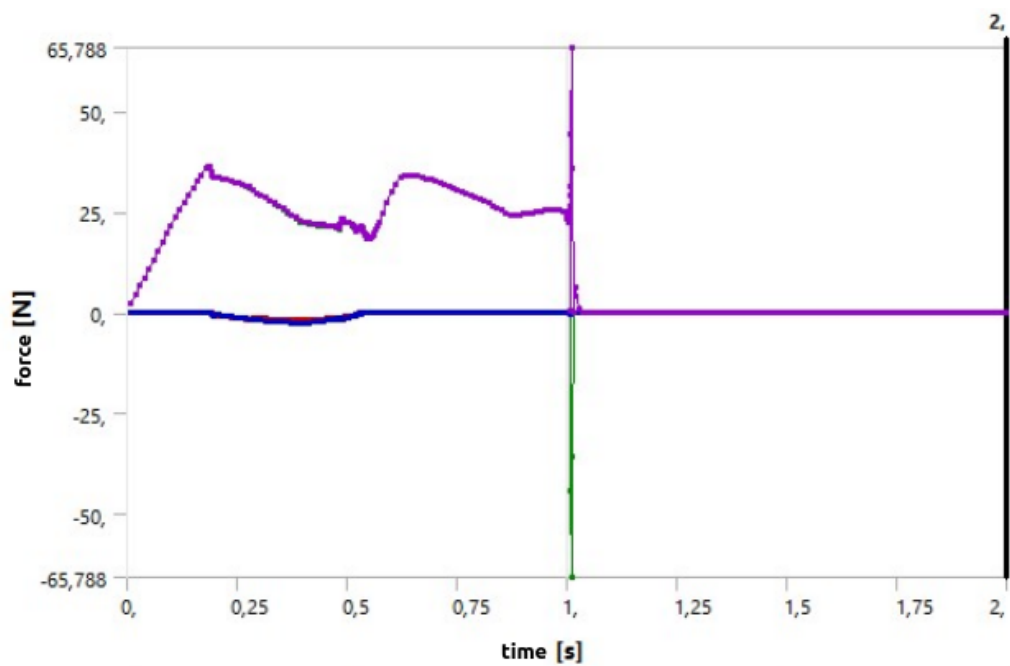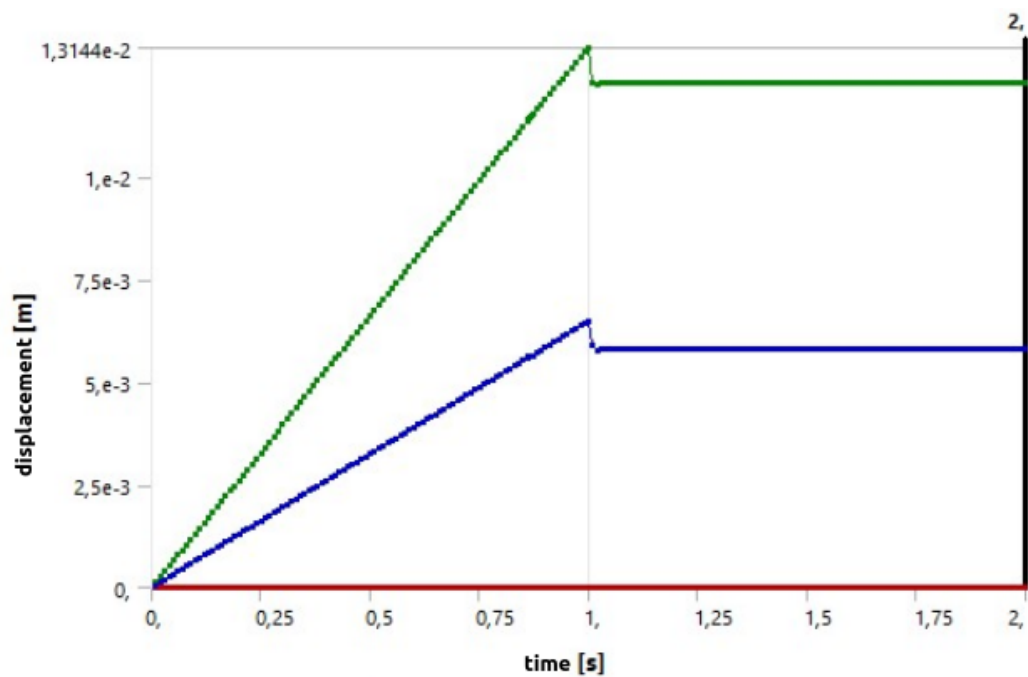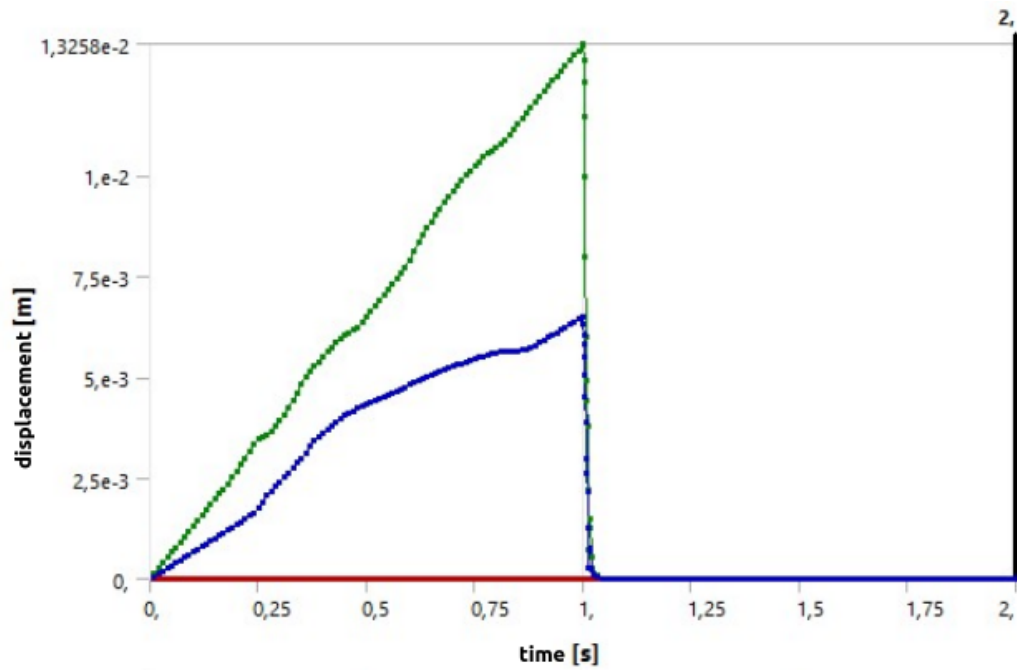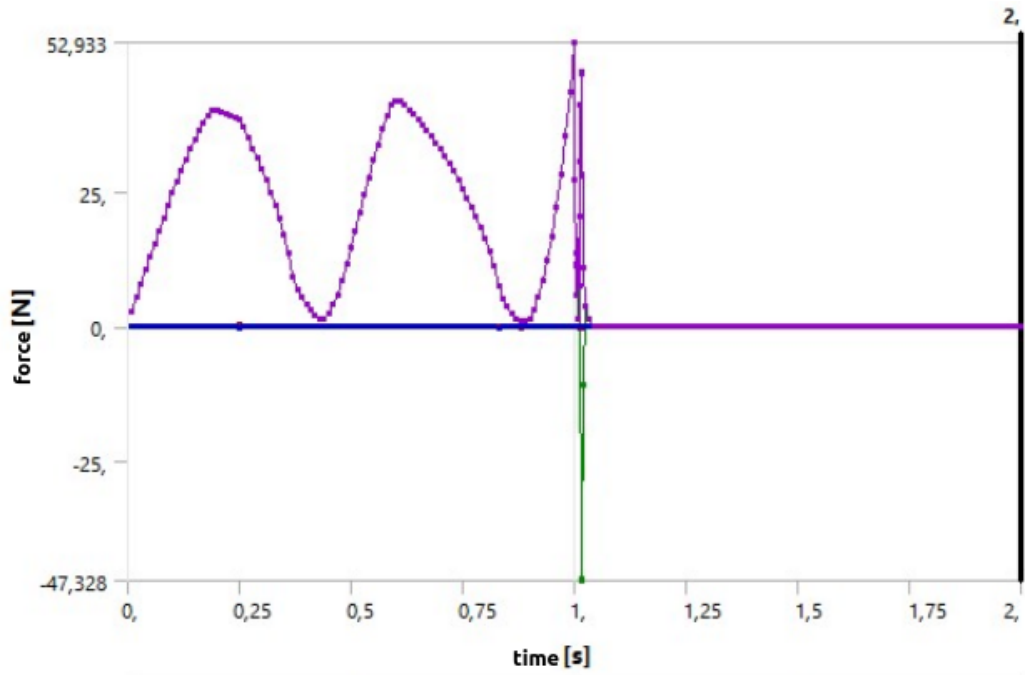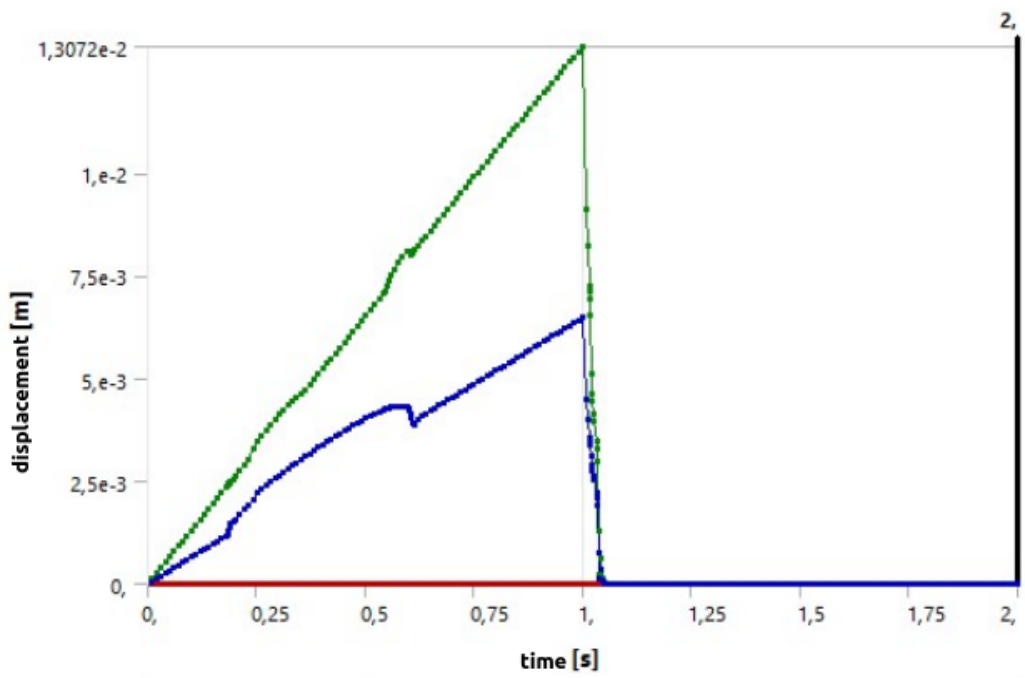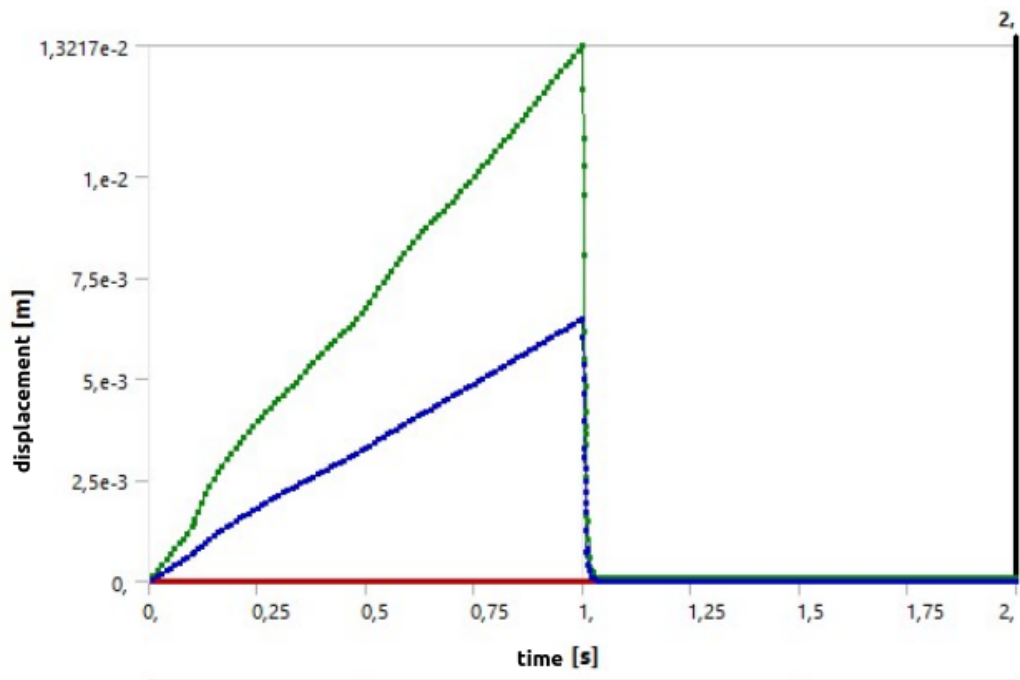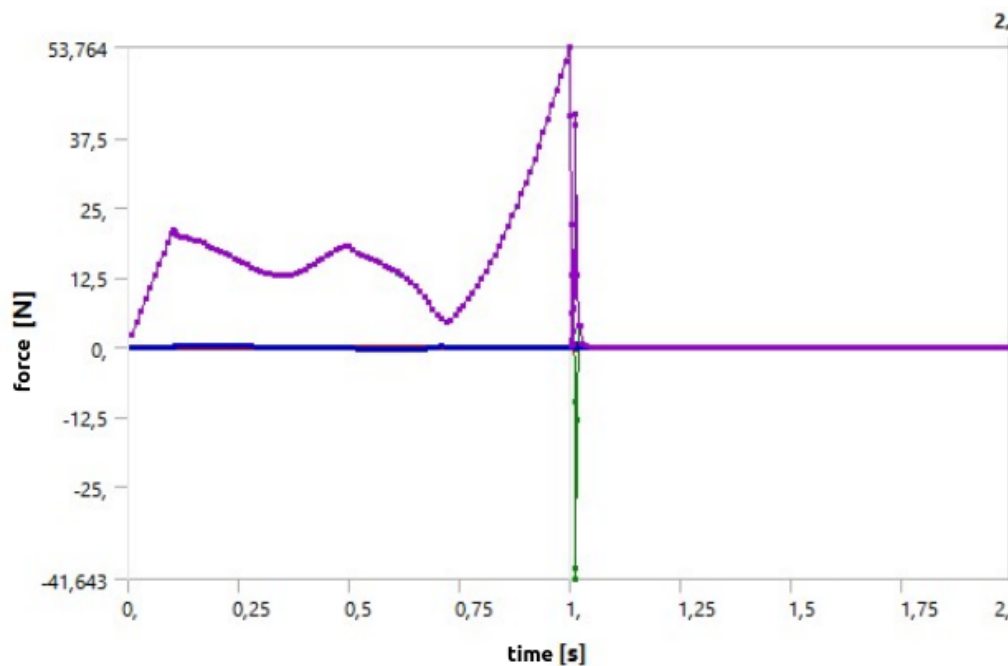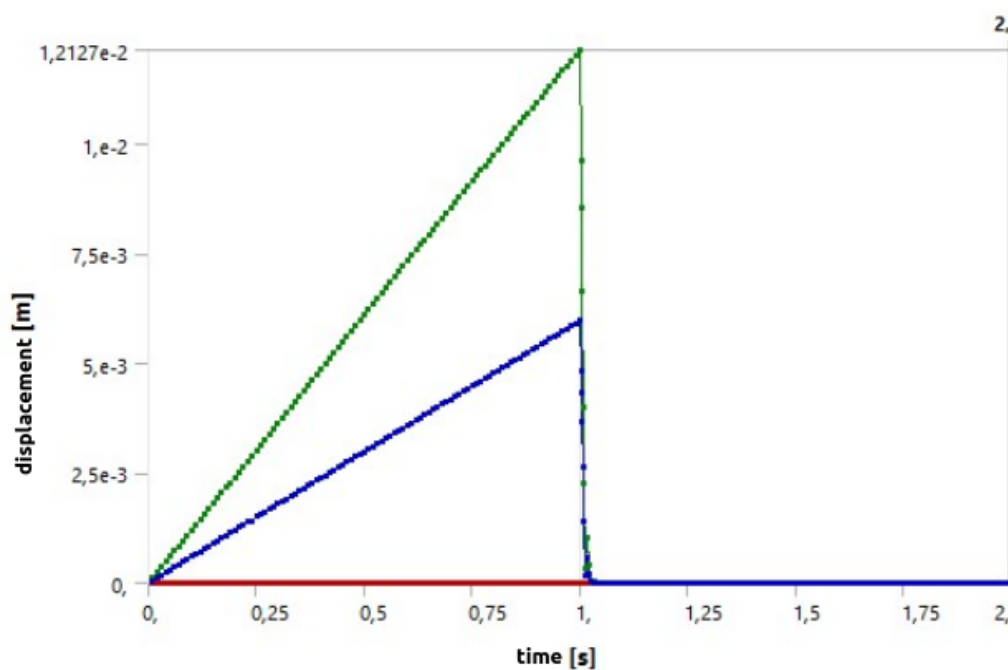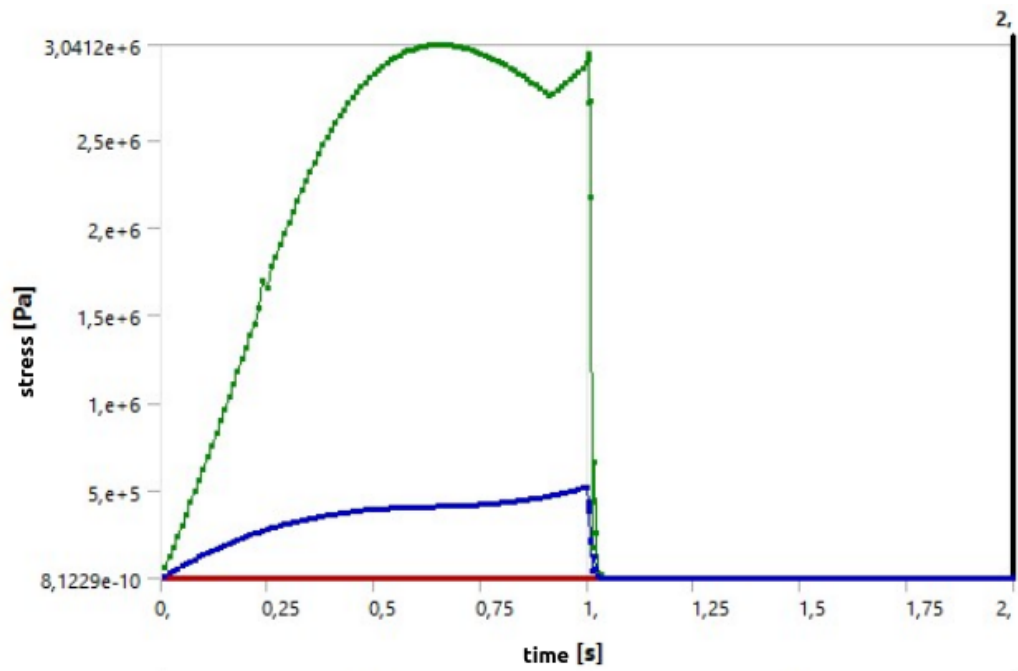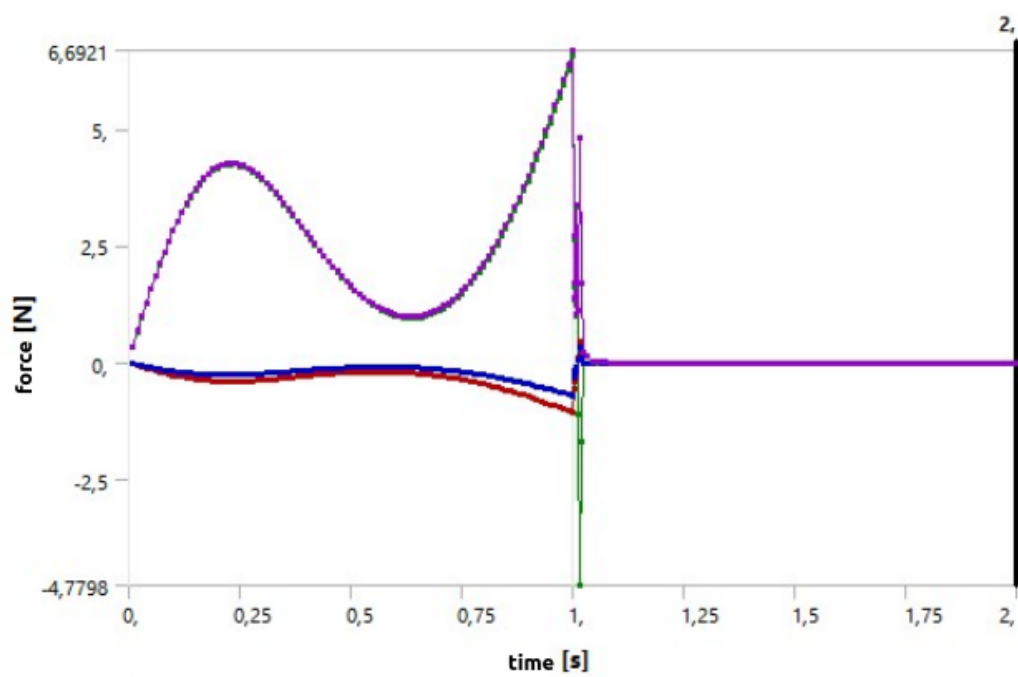

FIGURE A.3: Force reaction one element structure A.
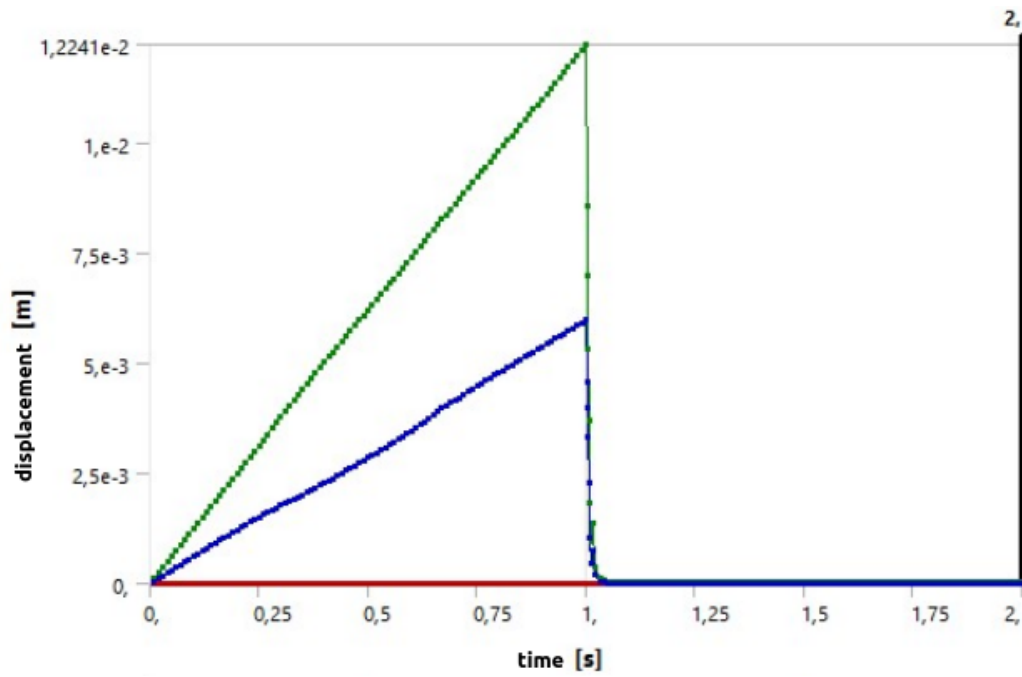
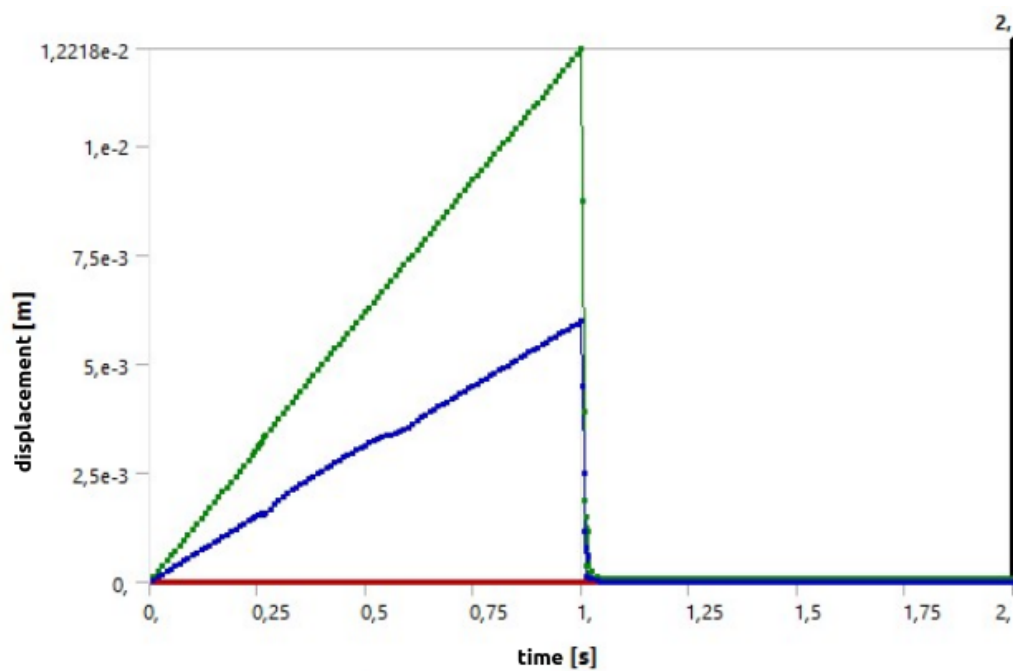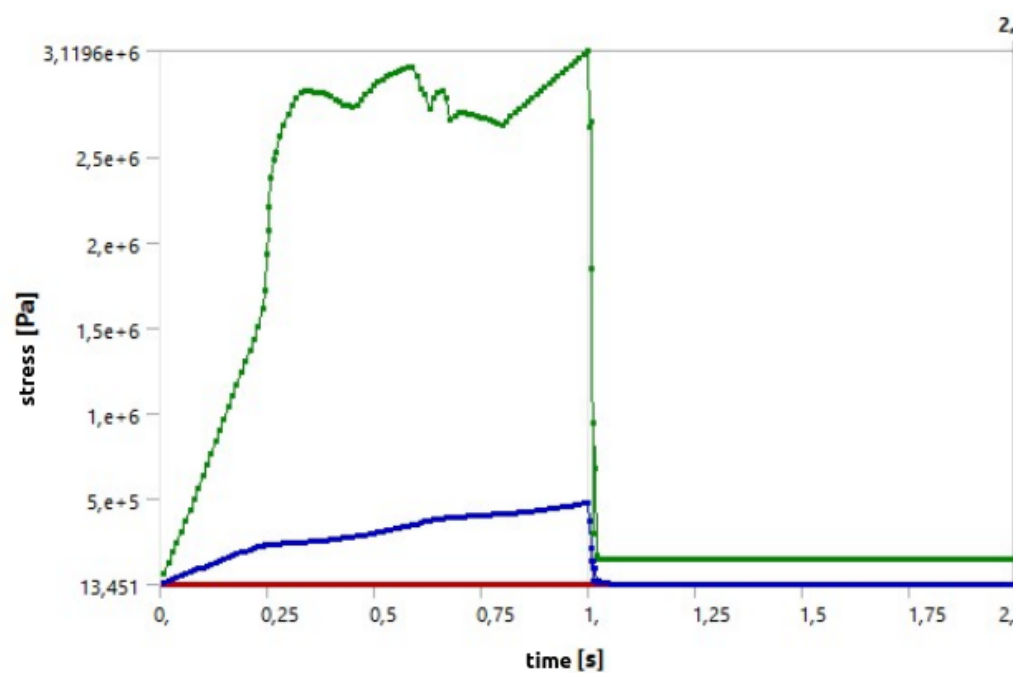FIGURE A.4: Displacement structure A.
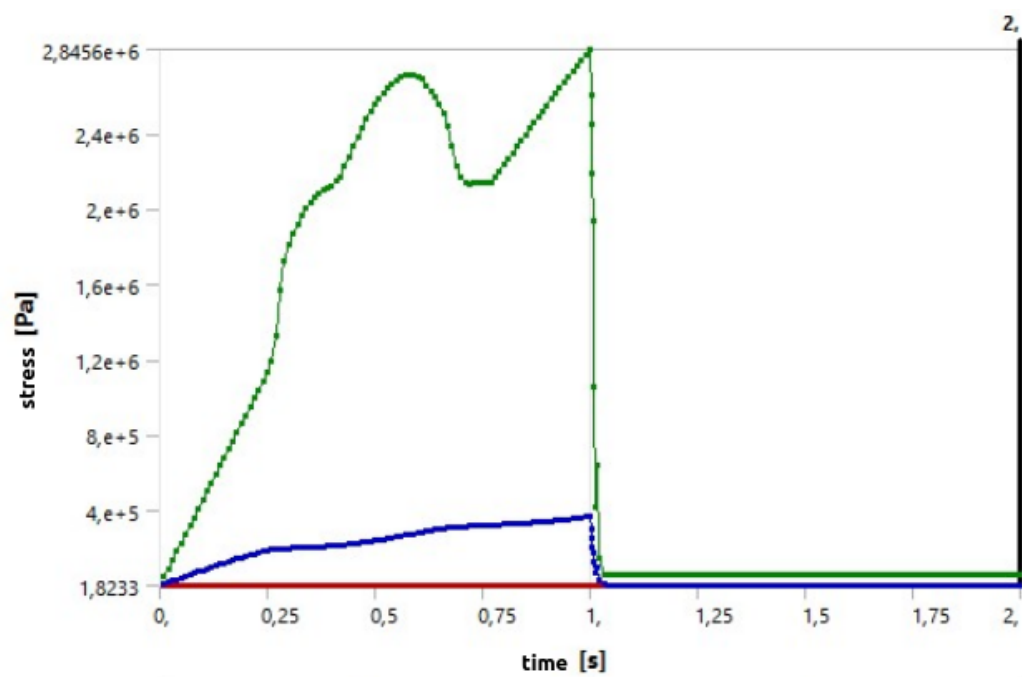
FIGURE A.5: Equivalent stress structure A.
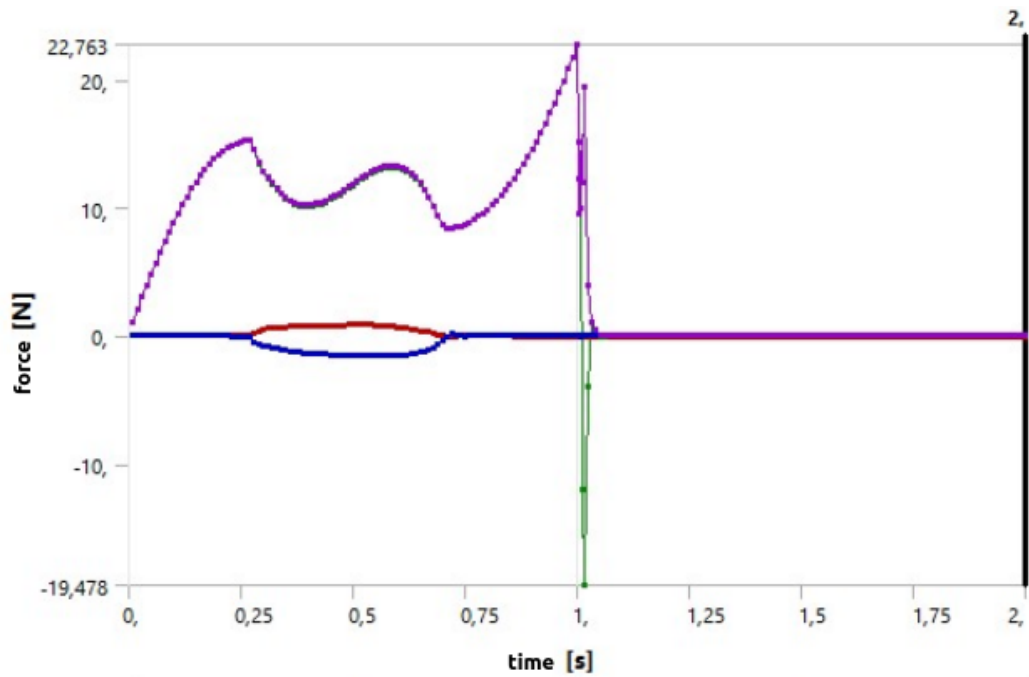
FIGURE A.6: Force reaction structure A.
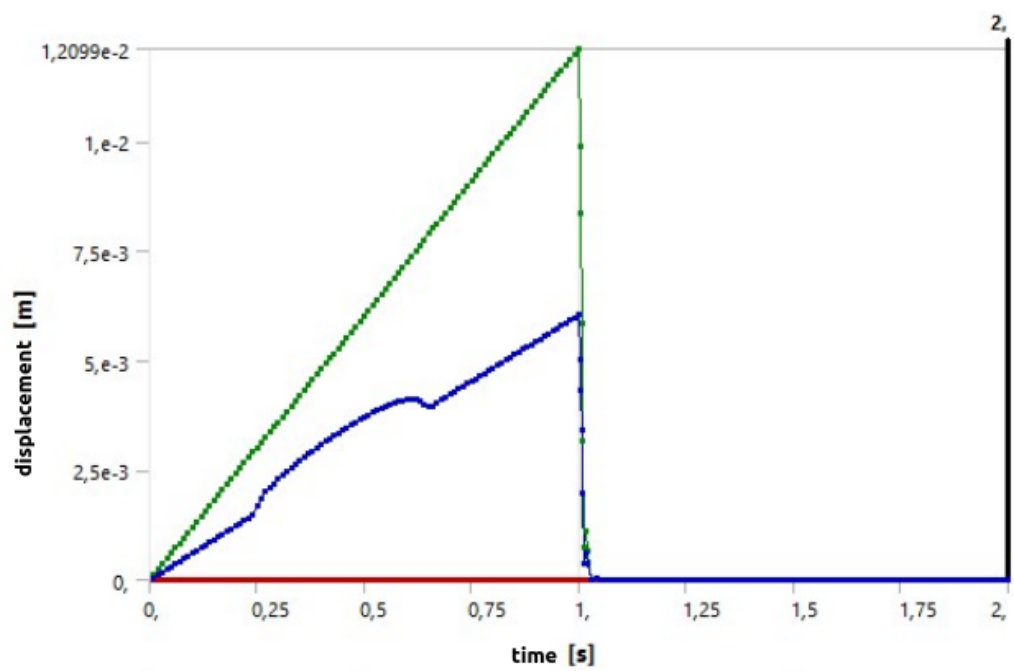
FIGURE A.7: Displacement one element structure B.
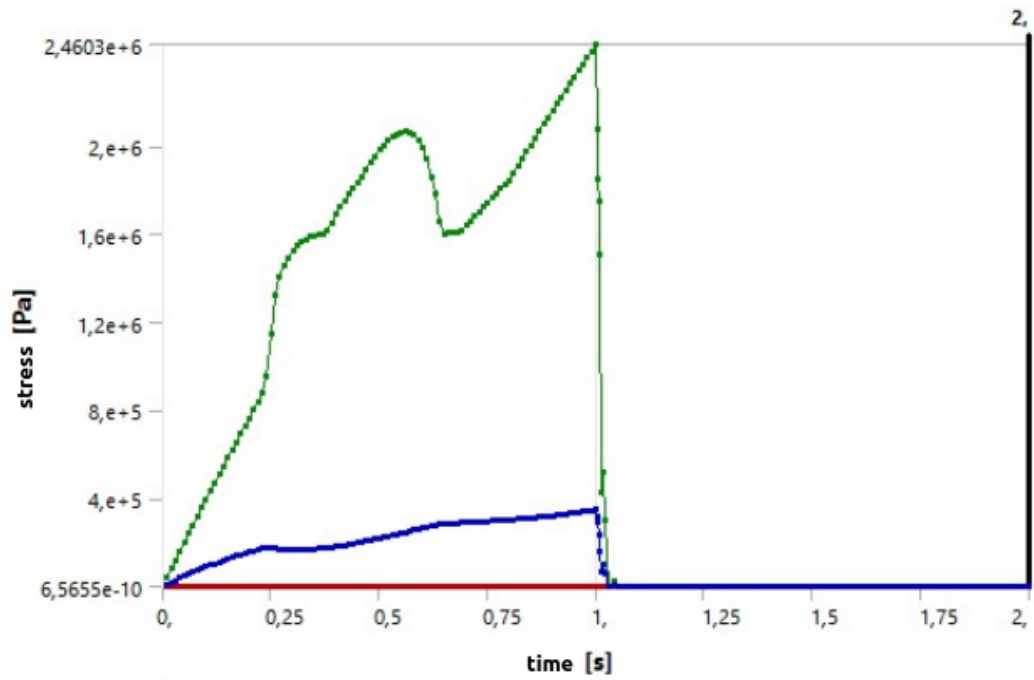
FIGURE A.8: Equivalent stress one element structure B.
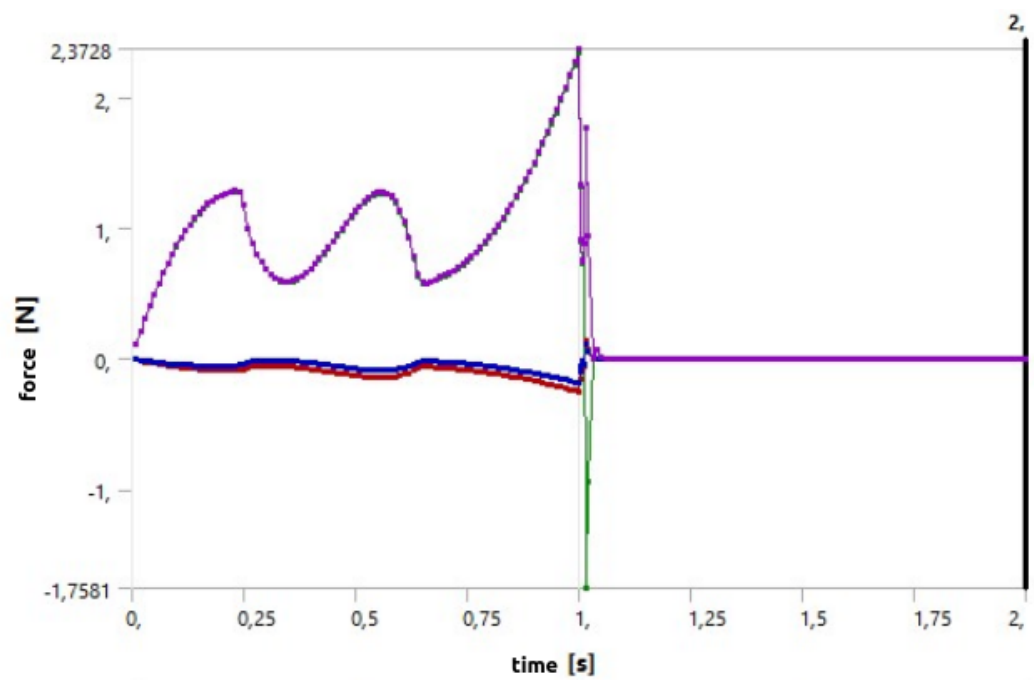
FIGURE A.9: Force reaction one element structure B.
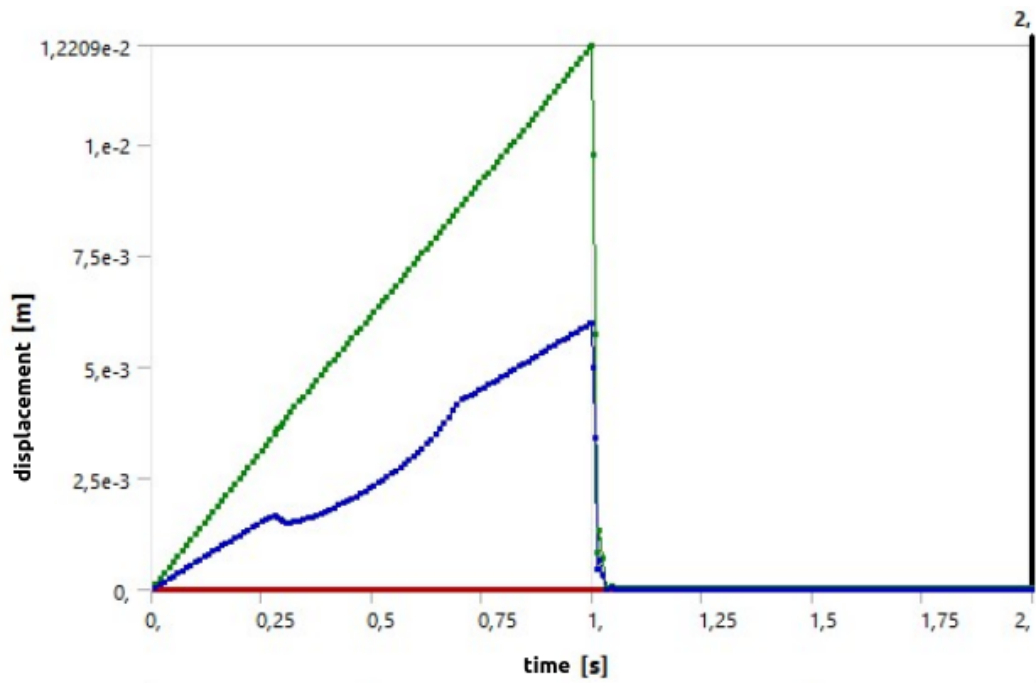
FIGURE A.10: Displacement structure B.
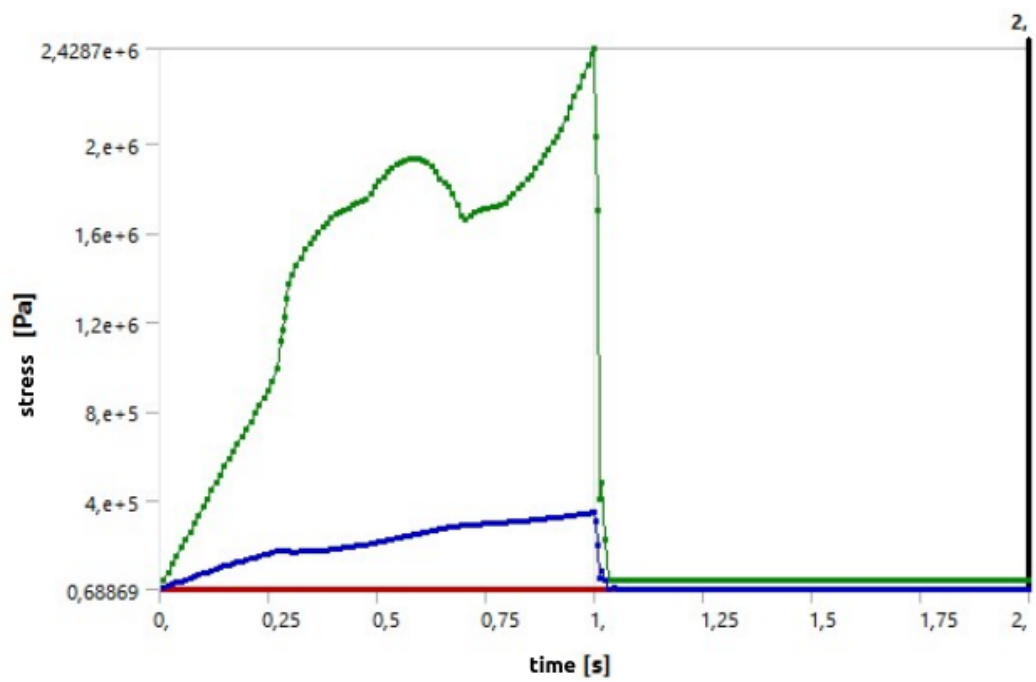
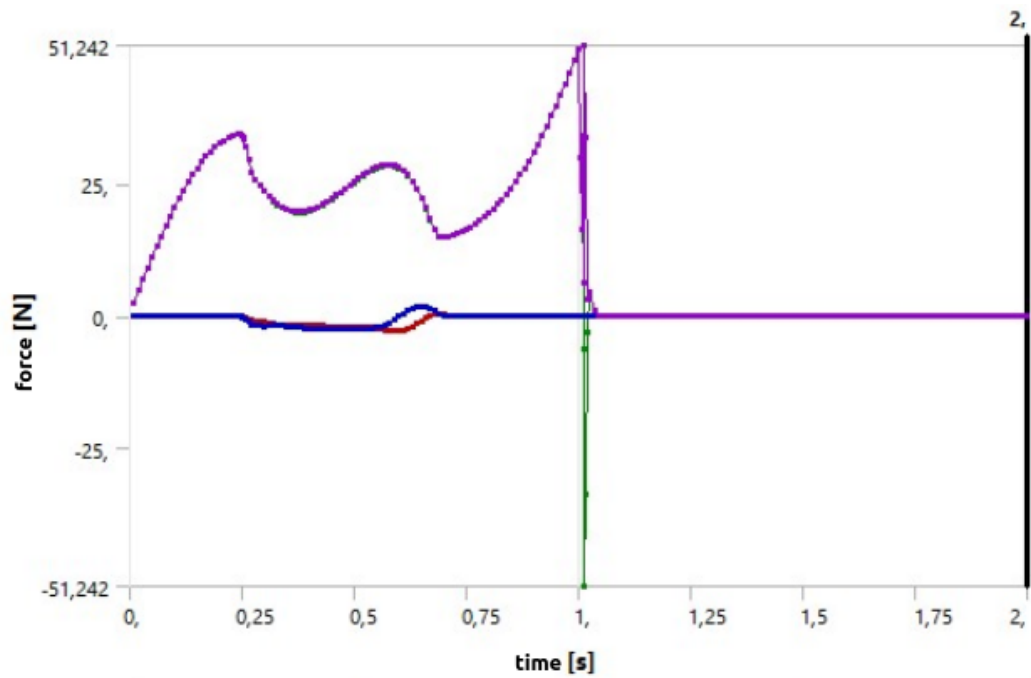FIGURE A.11: Equivalent stress structure B.
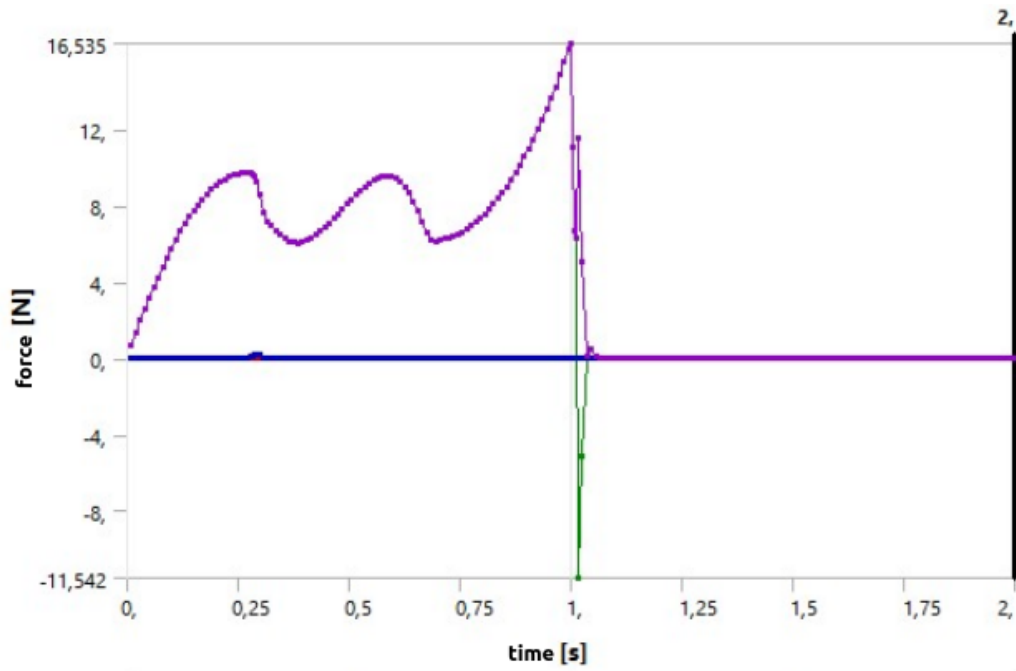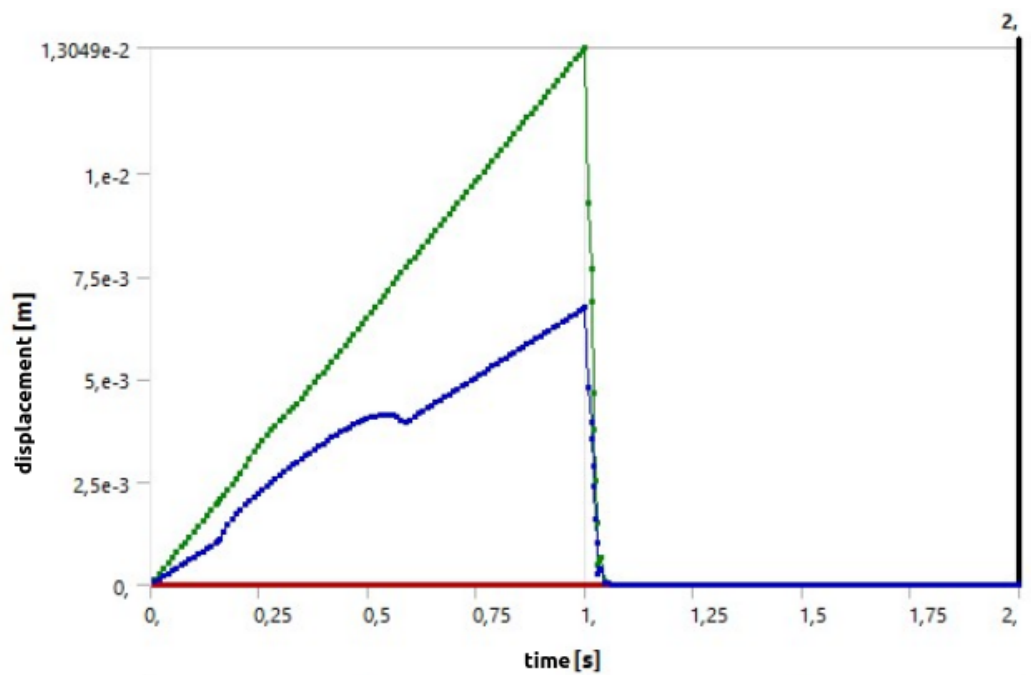
FIGURE A.12: Force reaction structure B.
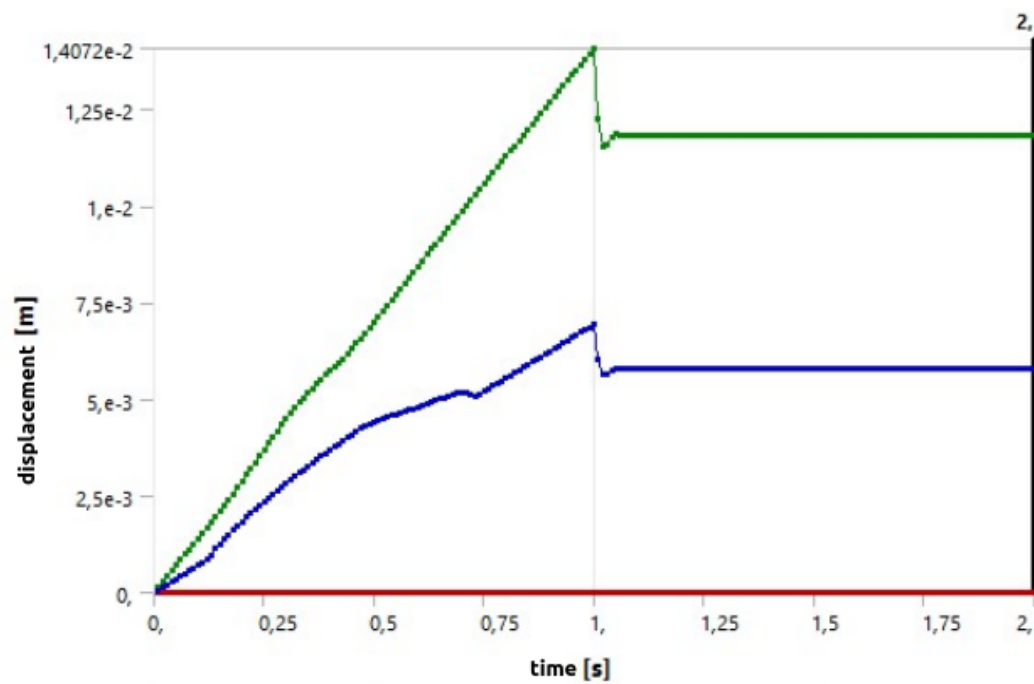
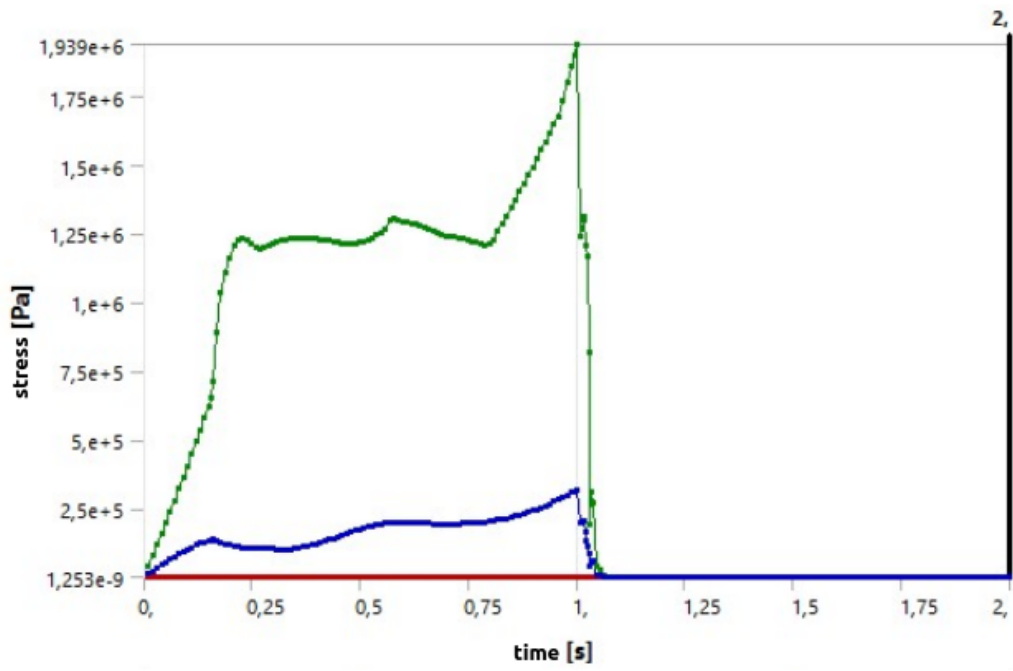FIGURE A.13: Displacement one element structure C.
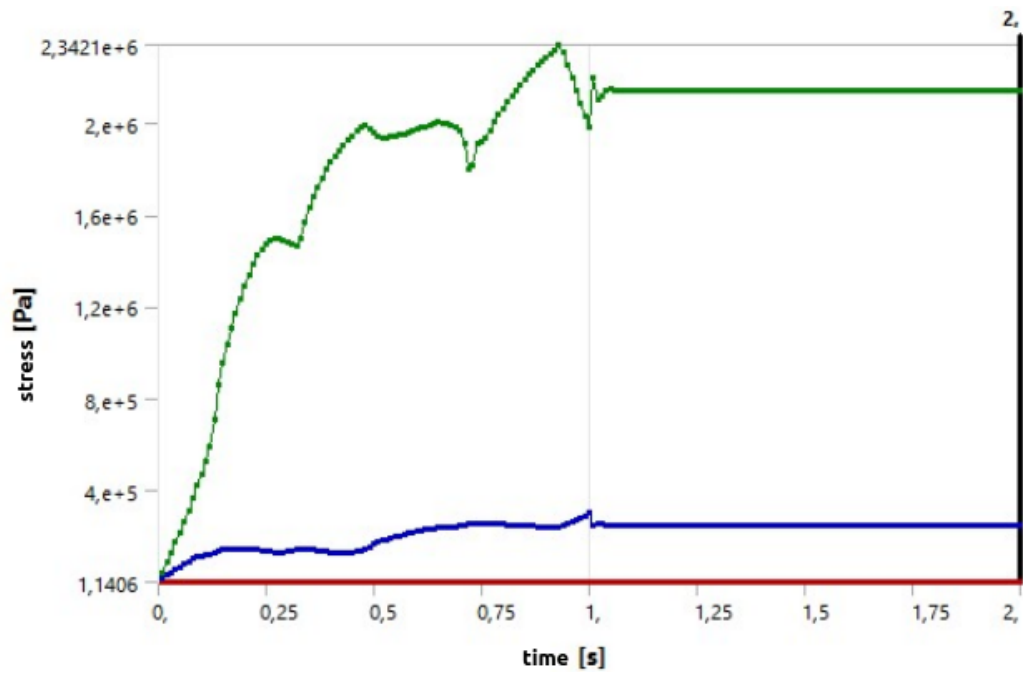
FIGURE A.14: Equivalent stress one element structure C.
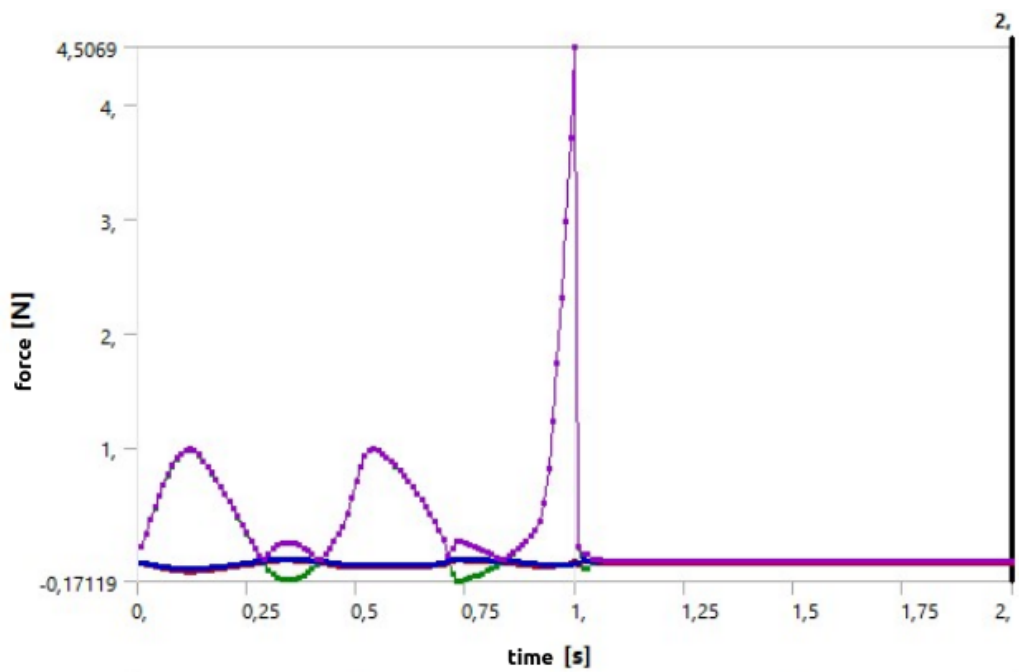
FIGURE A.15: Force reaction one element structure C.
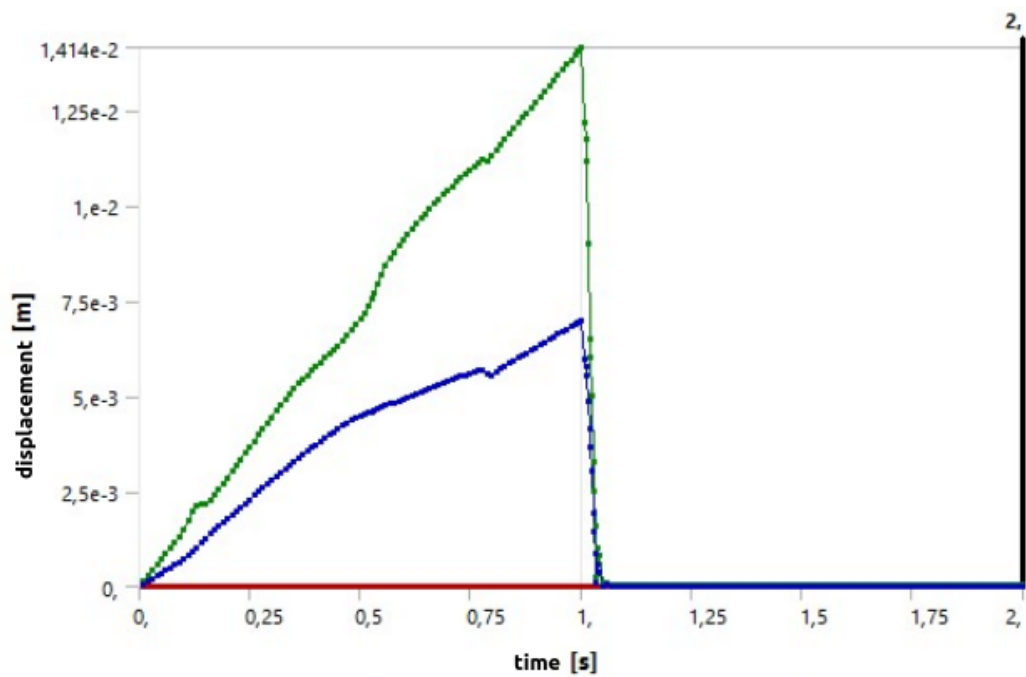
FIGURE A.16: Displacement structure C.
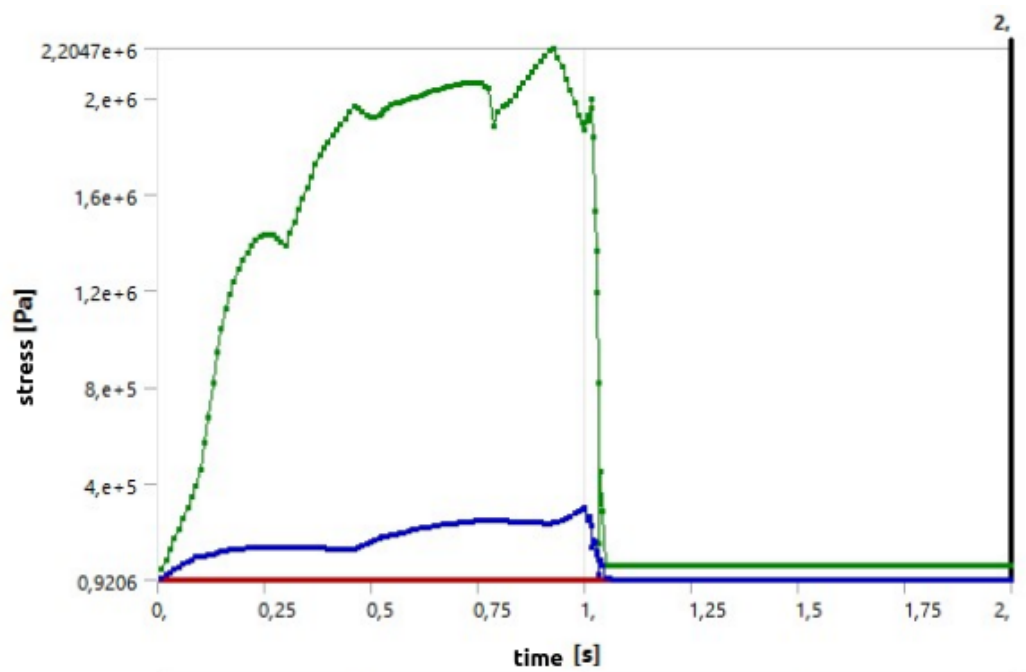
FIGURE A.17: Equivalent stress structure C.
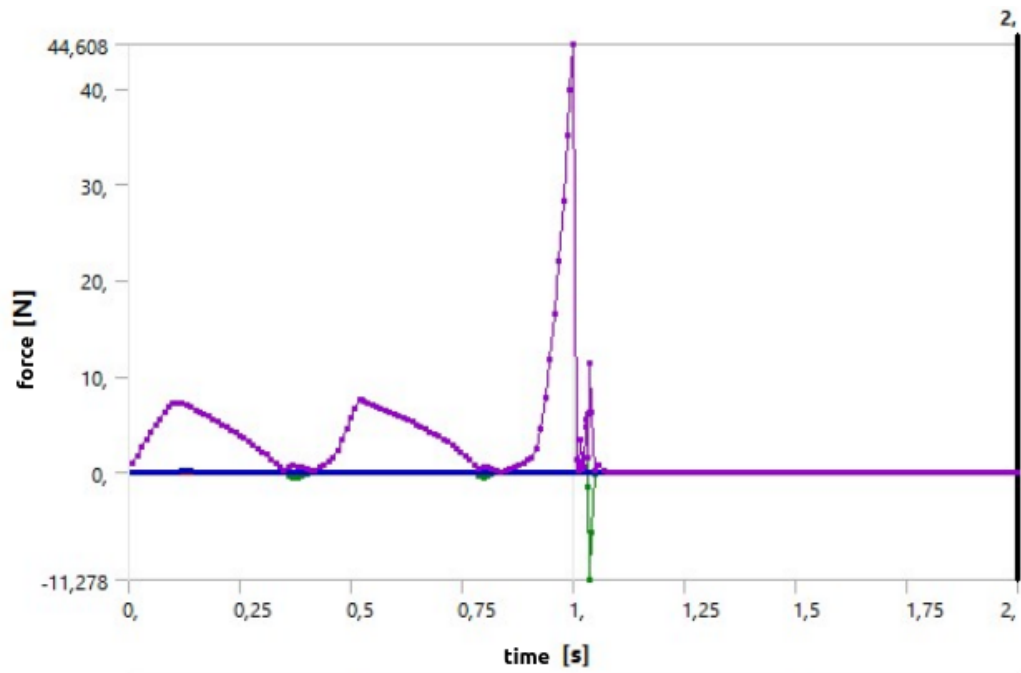
FIGURE A.18: Force reaction structure C.
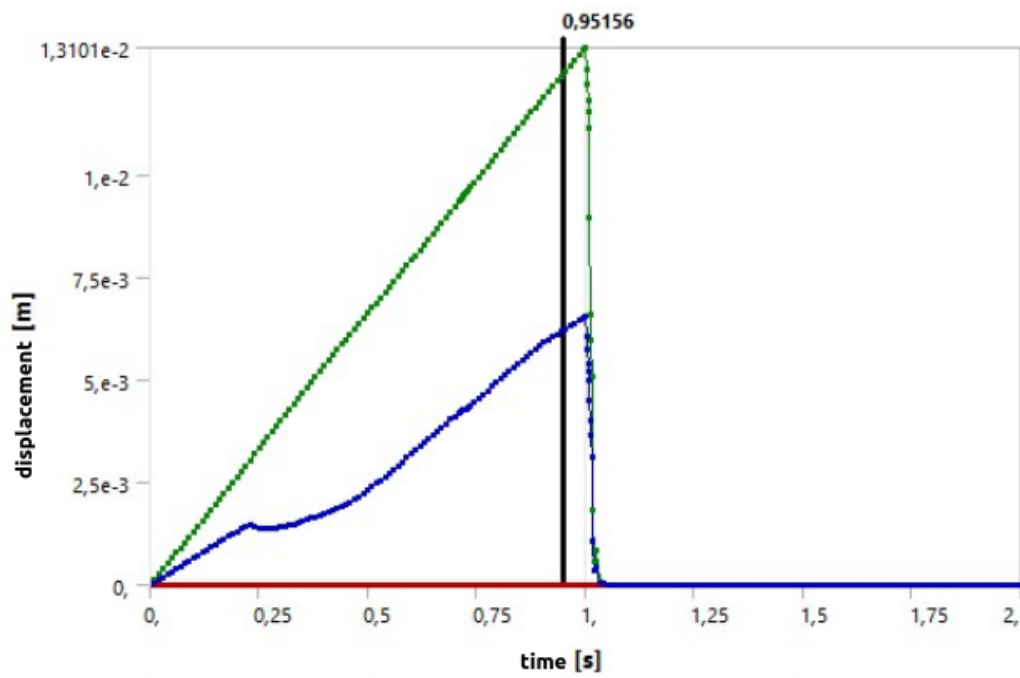
FIGURE A.19: Displacement one element structure D.
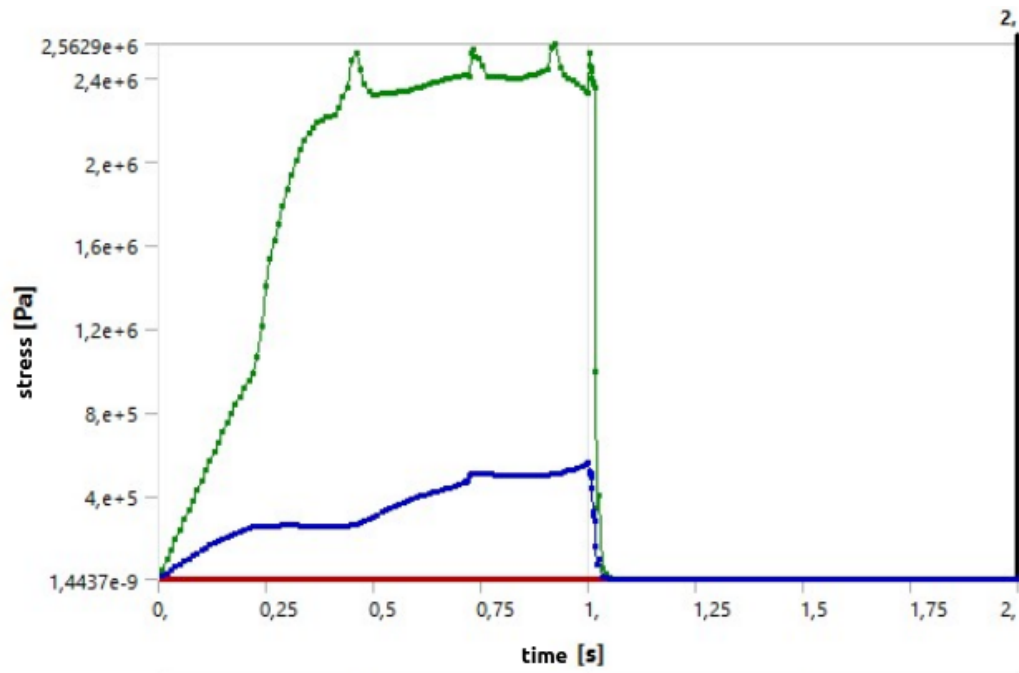
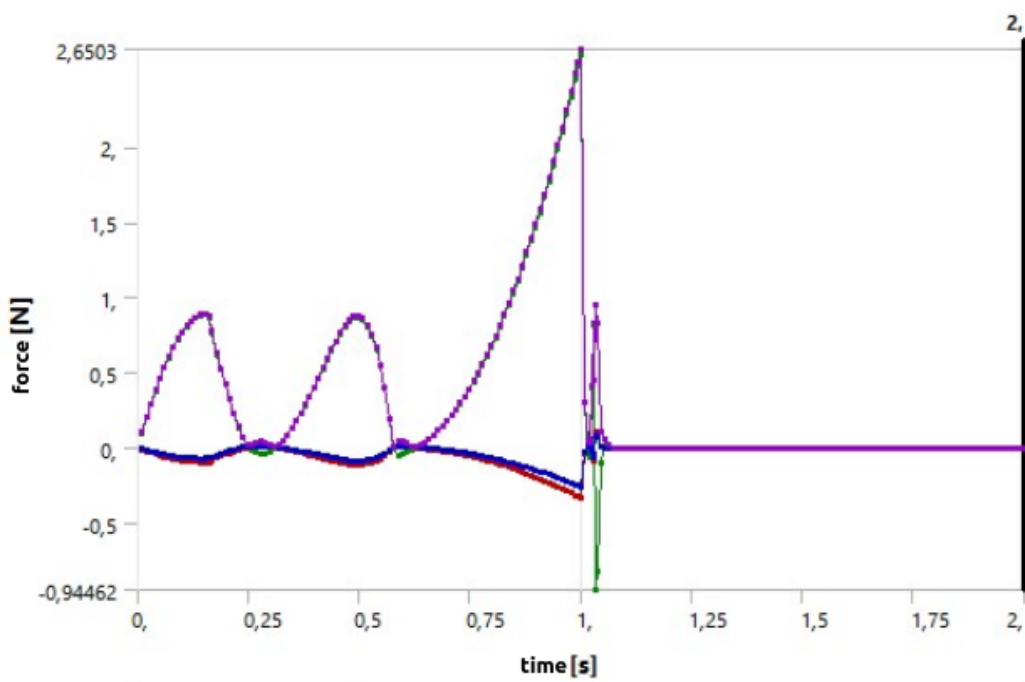FIGURE A.20: Equivalent stress one element structure D.
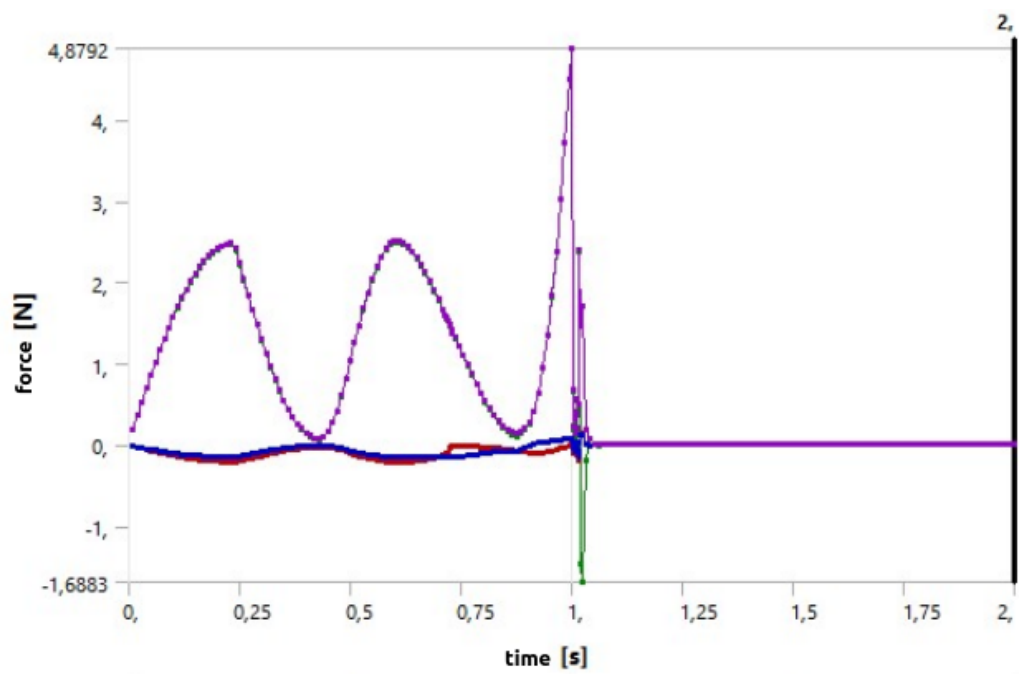
FIGURE A.21: Force reaction one element structure D.
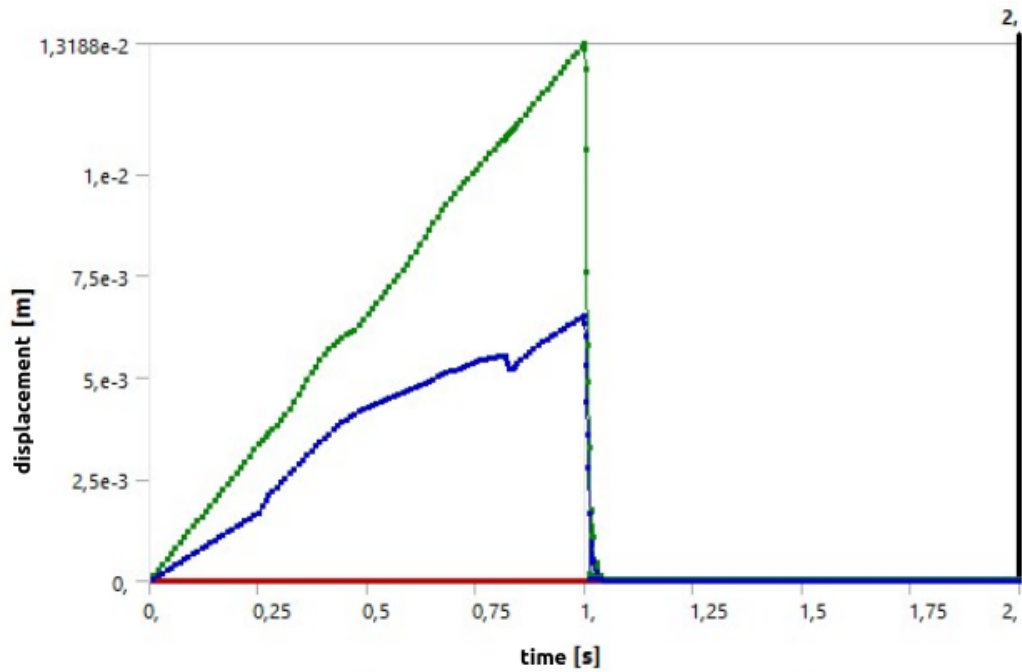
FIGURE A.22: Displacement structure D.
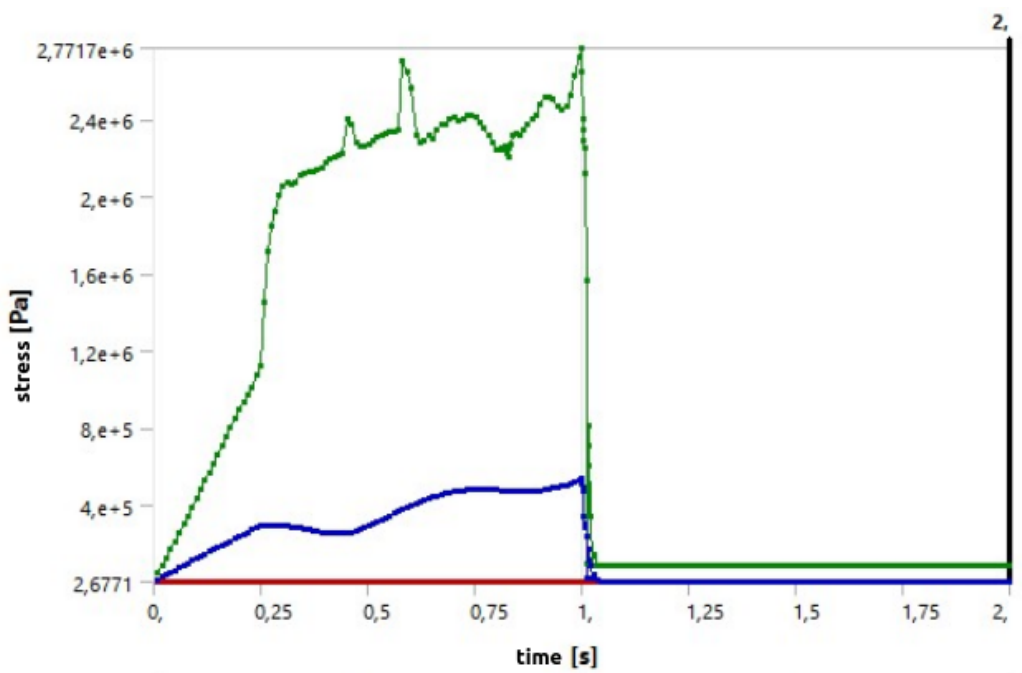
FIGURE A.23: Equivalent stress structure D.
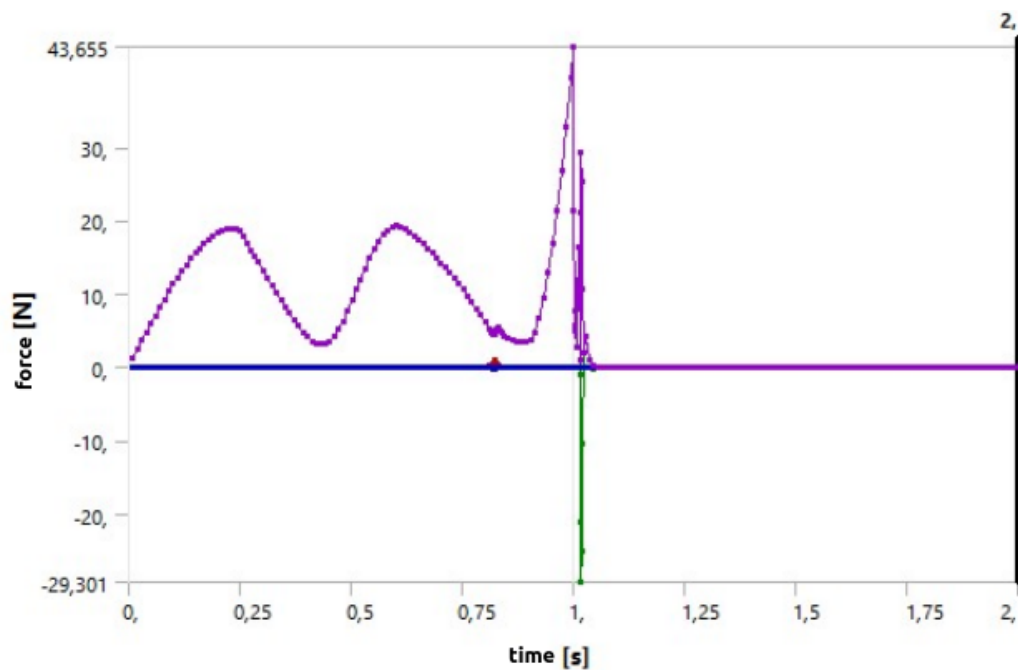
FIGURE A.24: Force reaction structure D.
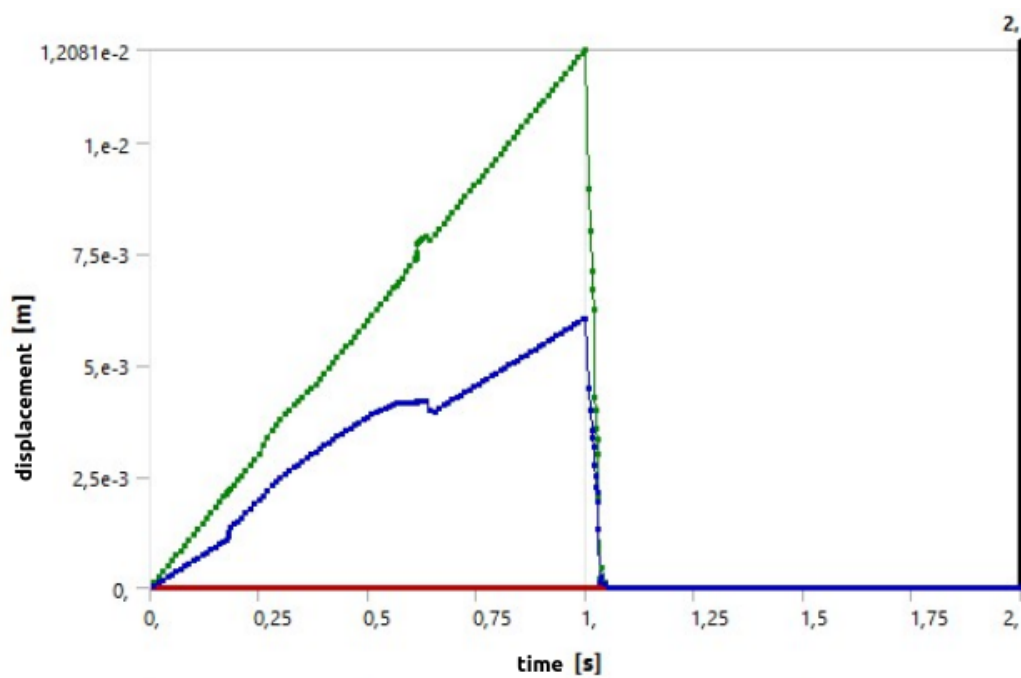
FIGURE A.25: Displacement one element structure E.
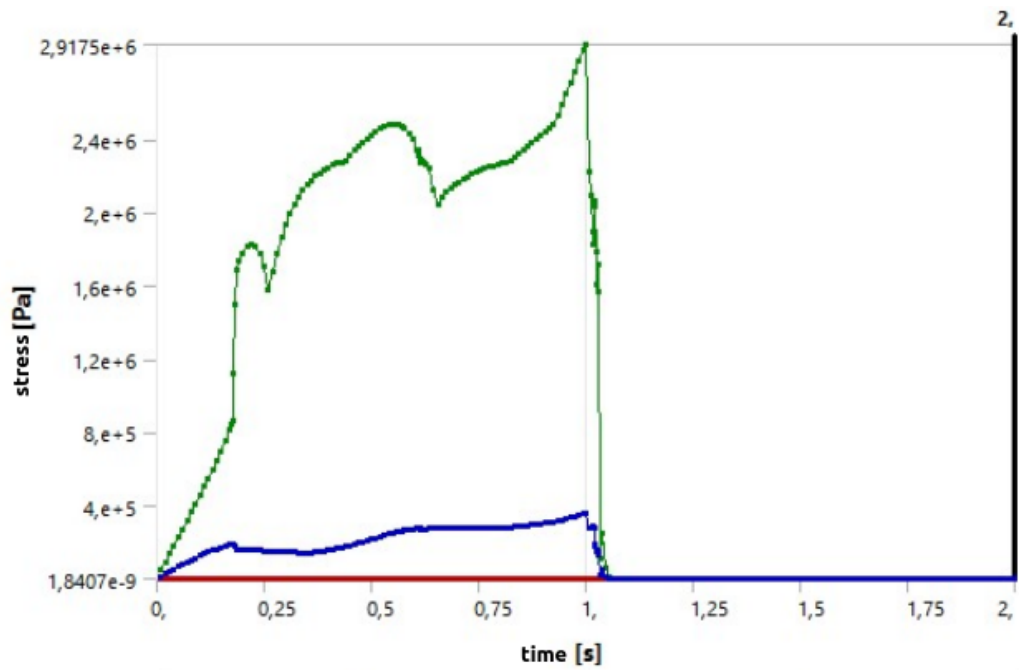
FIGURE A.26: Equivalent stress one element structure E.
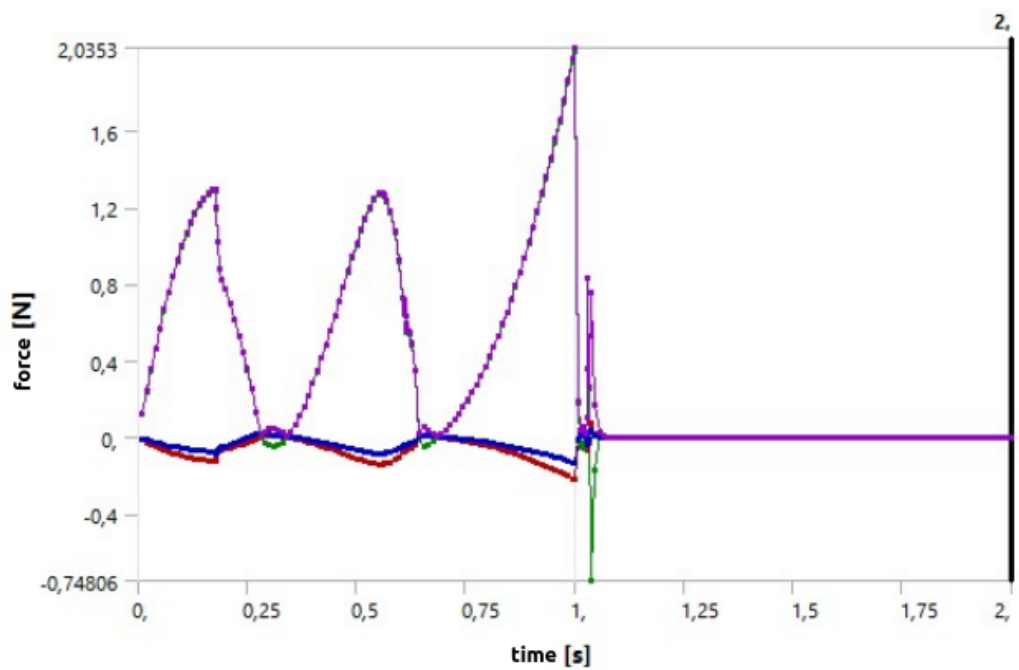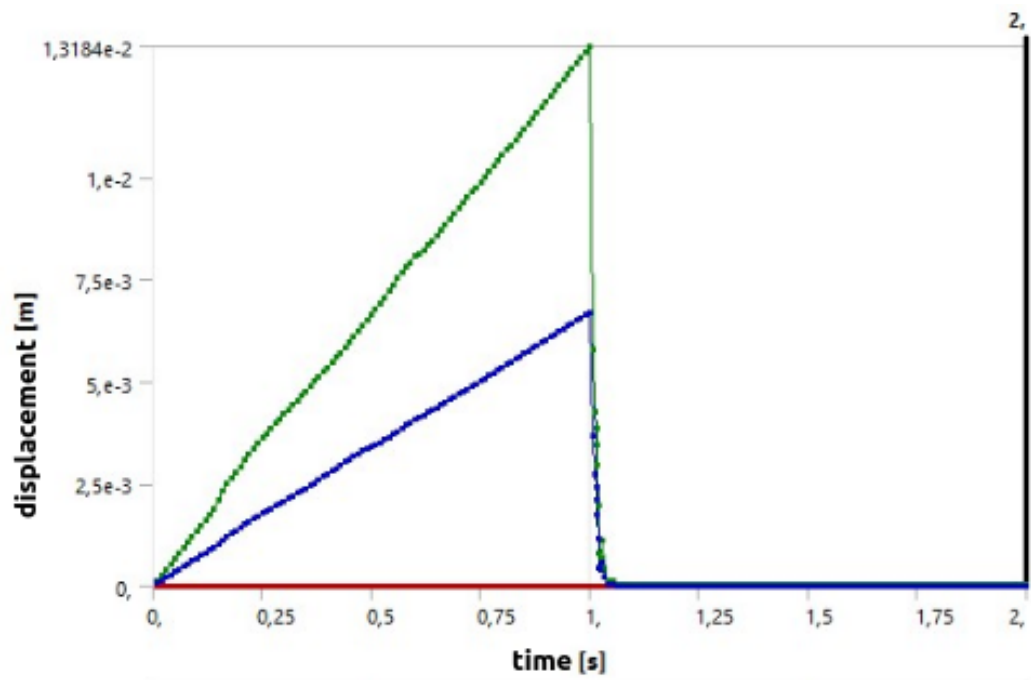

FIGURE A.27: Force reaction one element structure E.
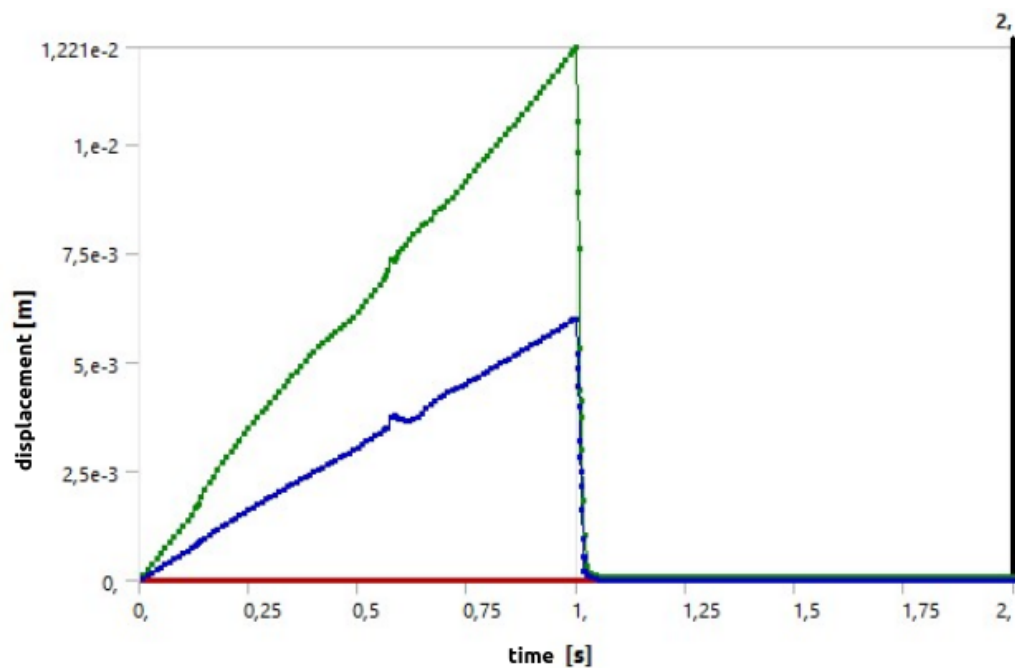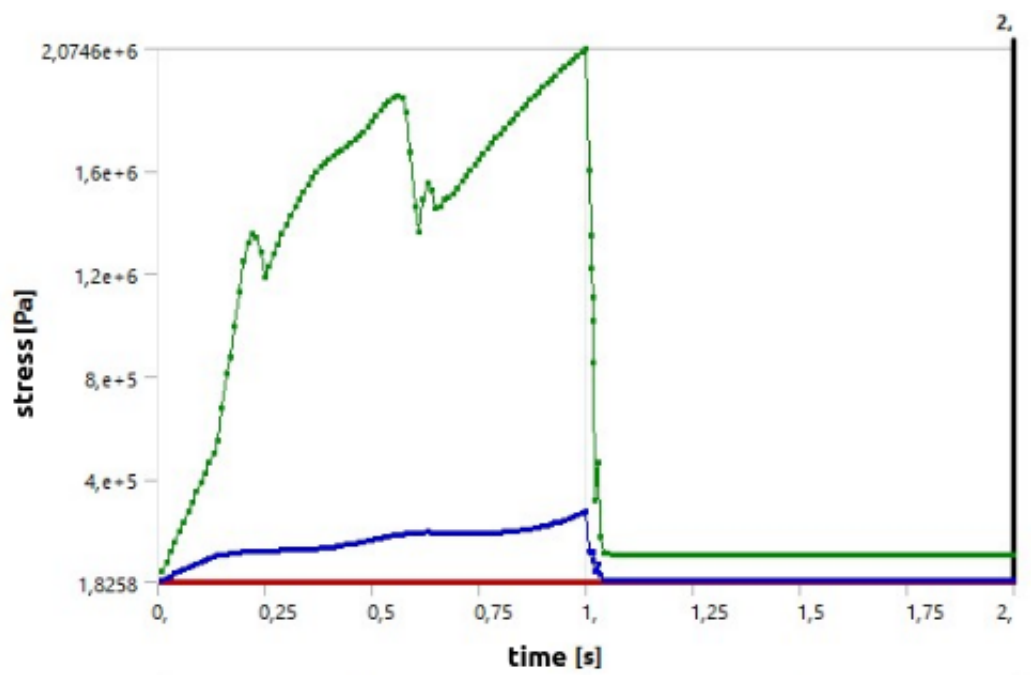
FIGURE A.28: Displacement structure E.
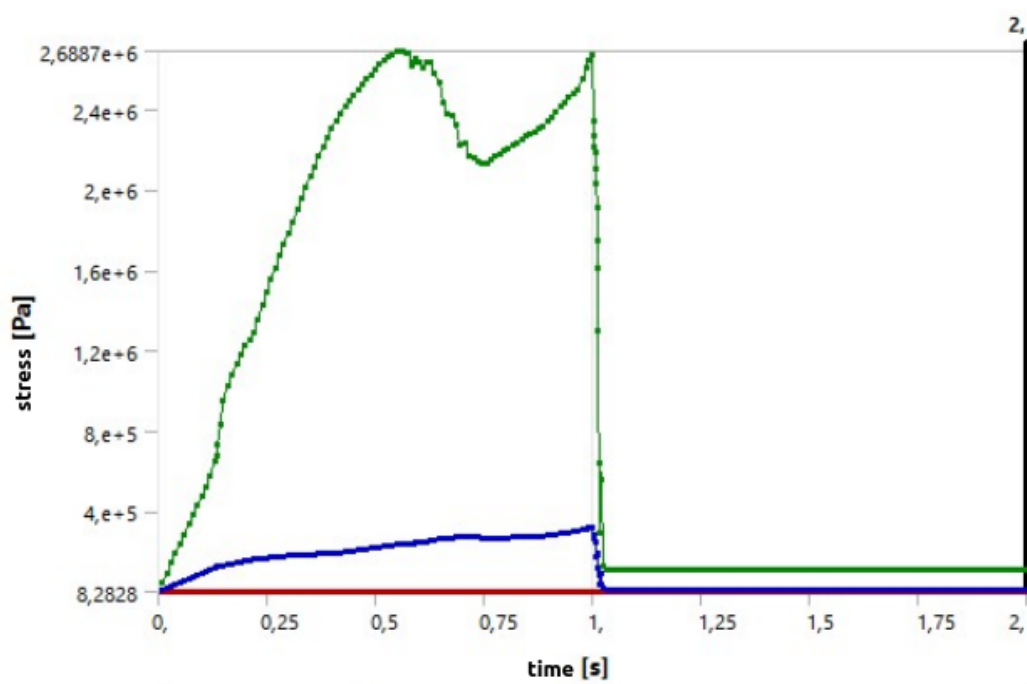
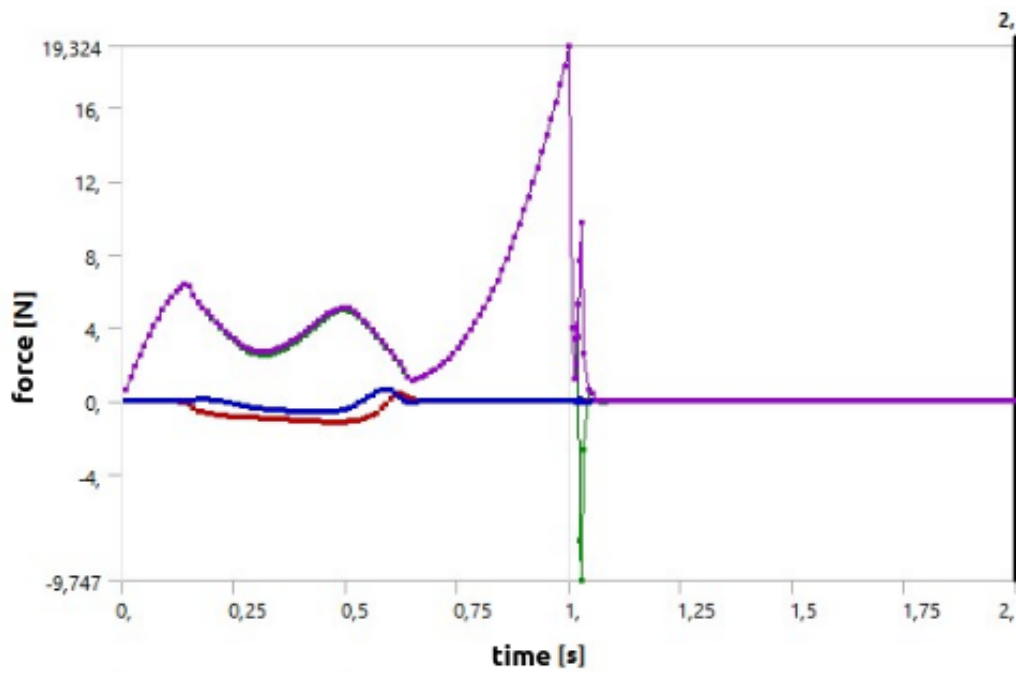FIGURE A.29: Equivalent stress structure E.
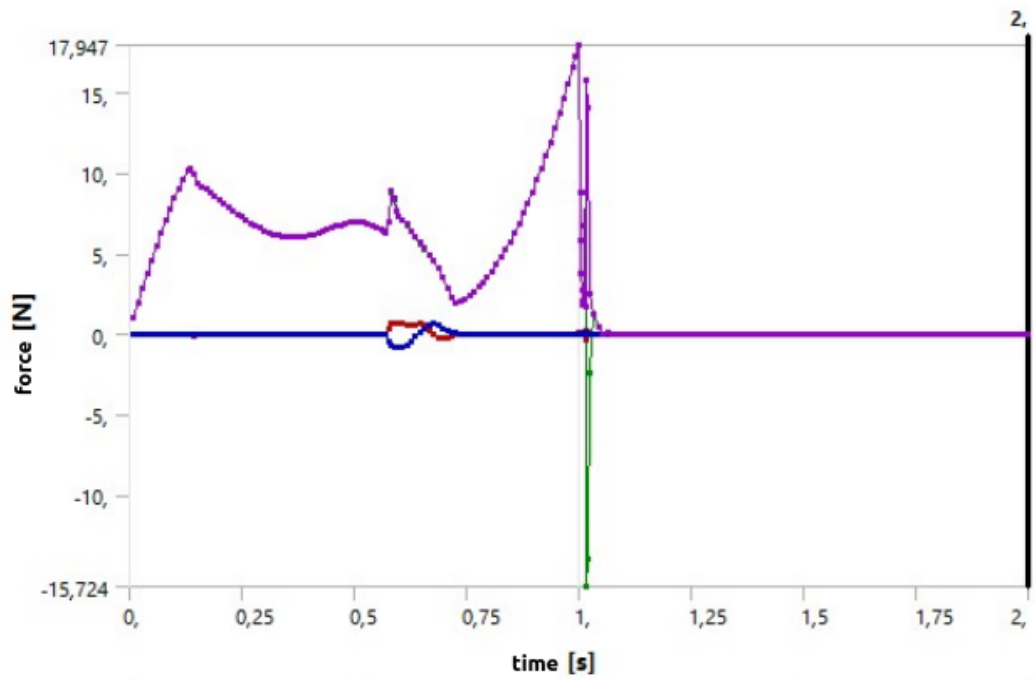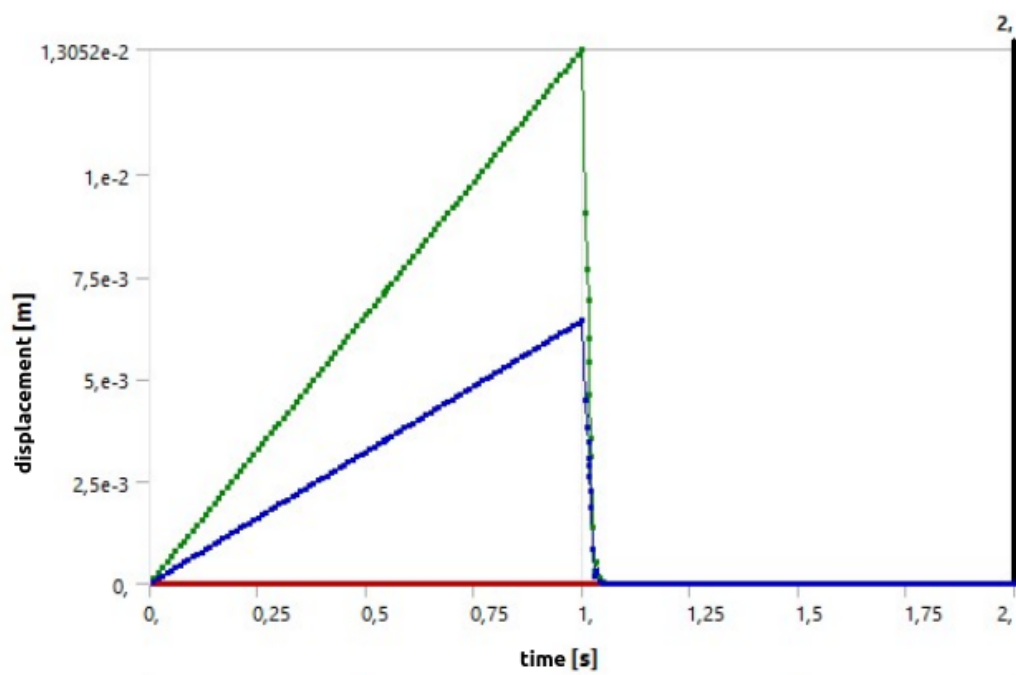
FIGURE A.30: Force reaction structure E.
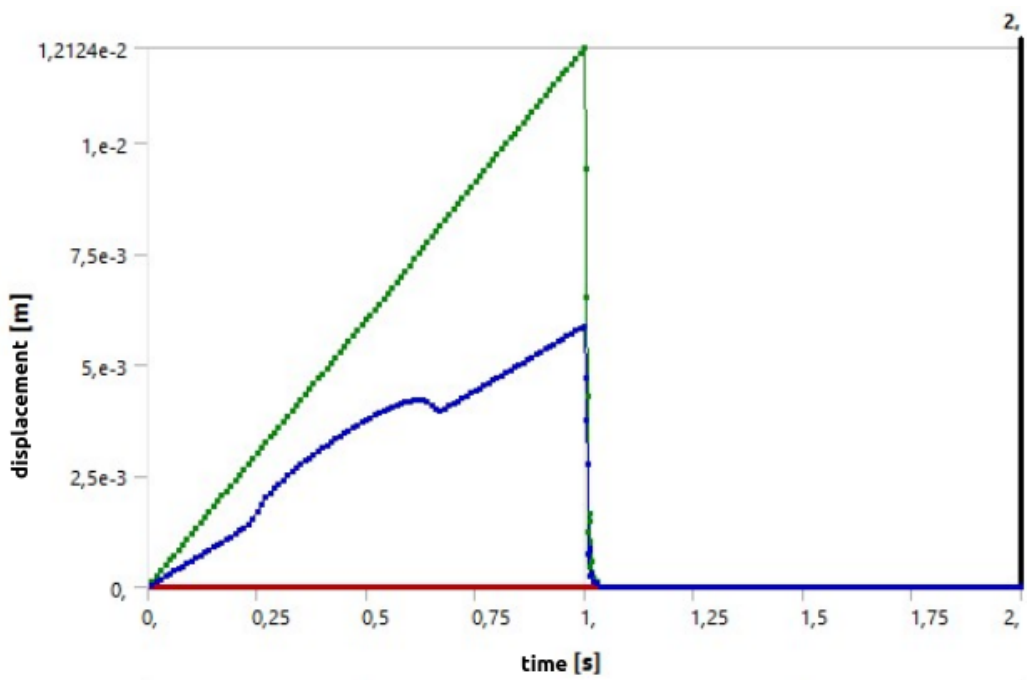
FIGURE A.31: Displacement one element structure F.
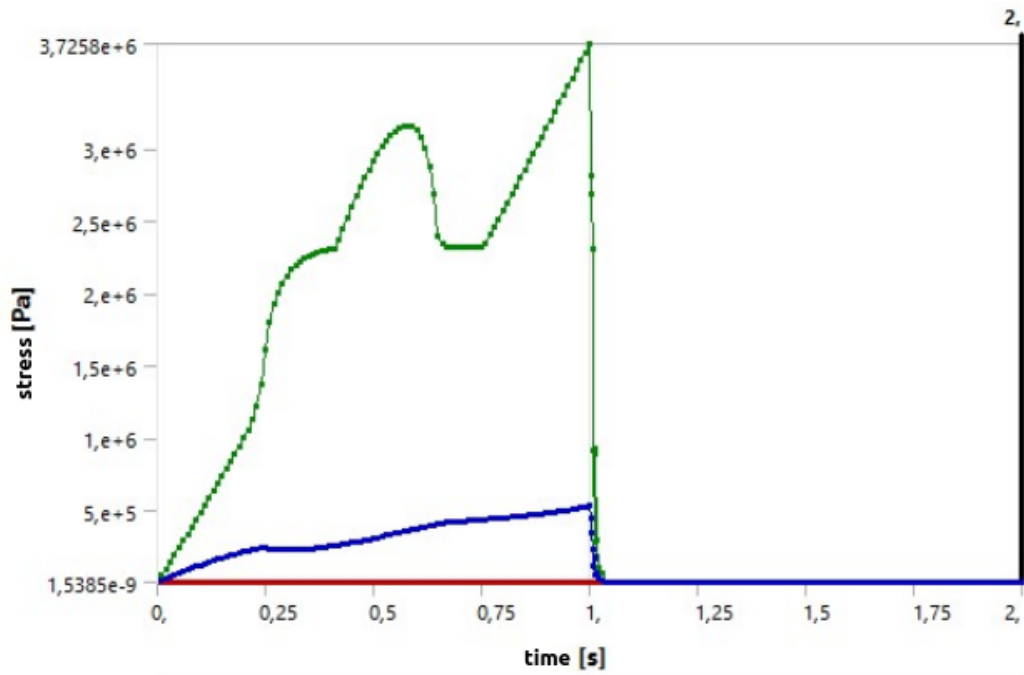
FIGURE A.32: Equivalent stress one element structure F.
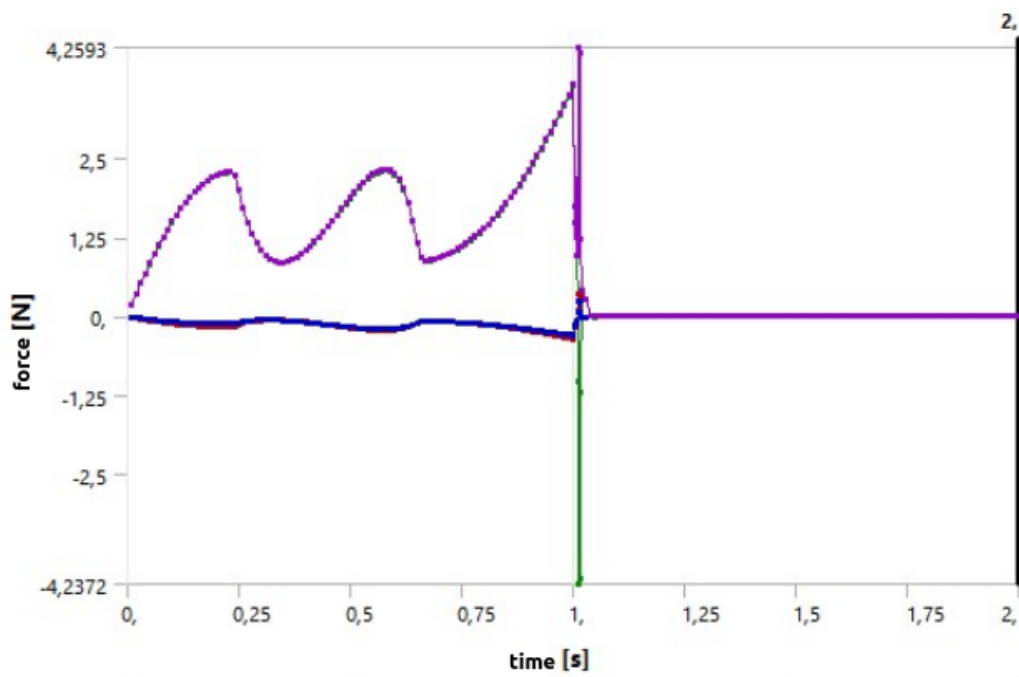
FIGURE A.33: Force reaction one element structure F.
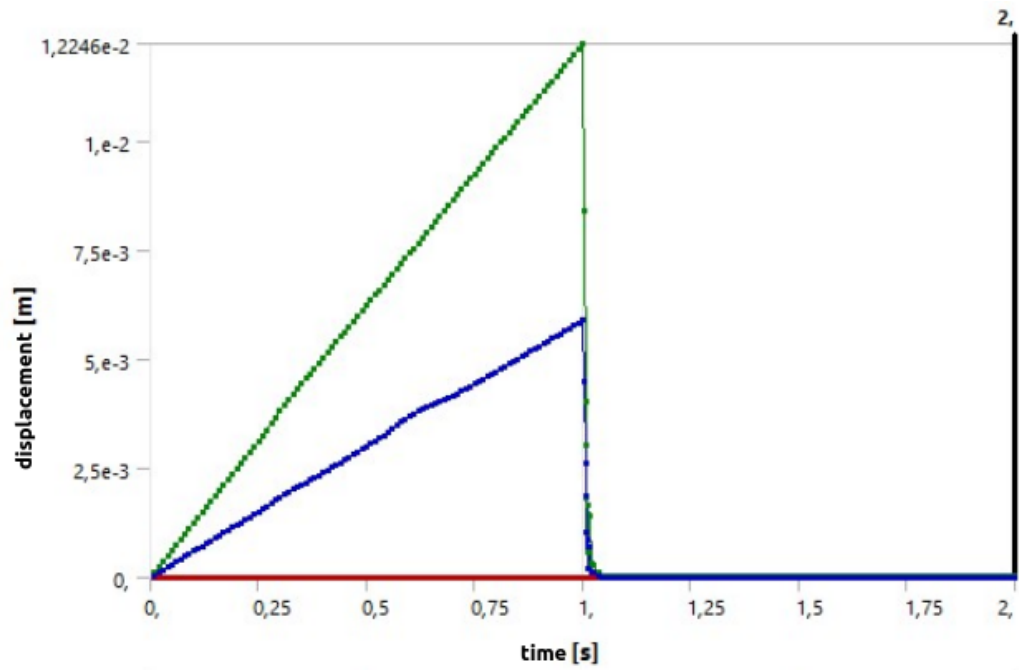
FIGURE A.34: Displacement structure F.
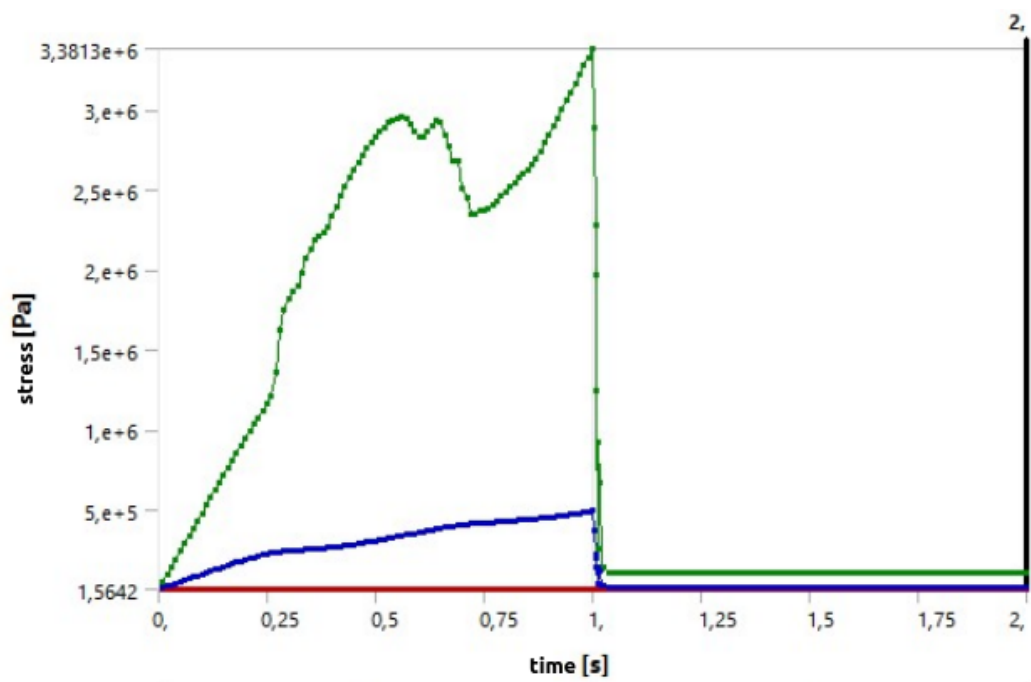
FIGURE A.35: Equivalent stress structure F.
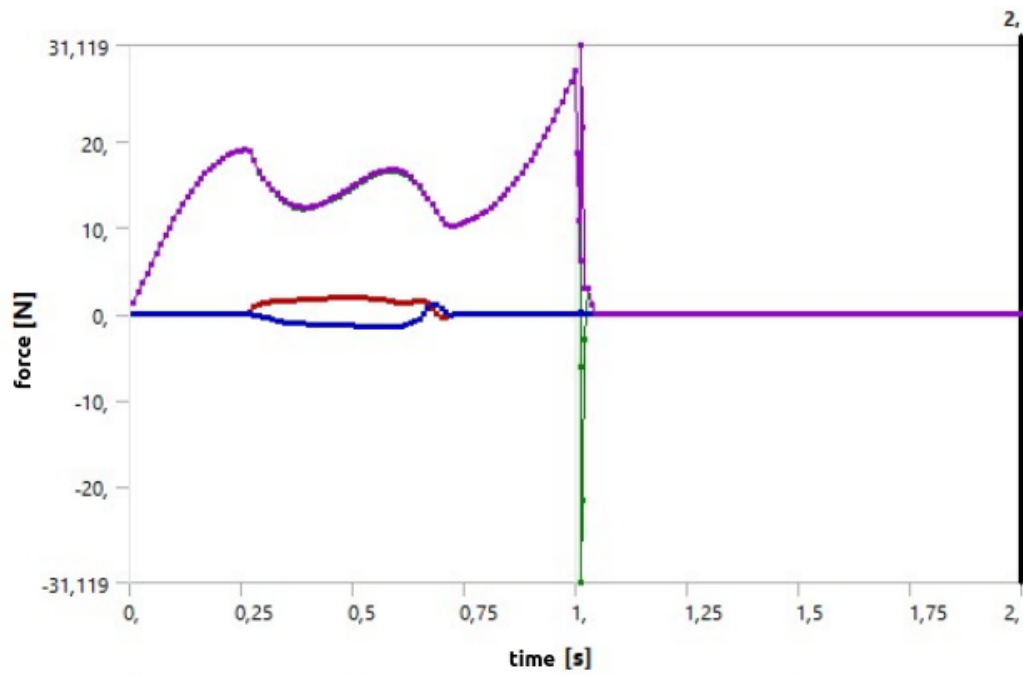
FIGURE A.36: Force reaction structure F.
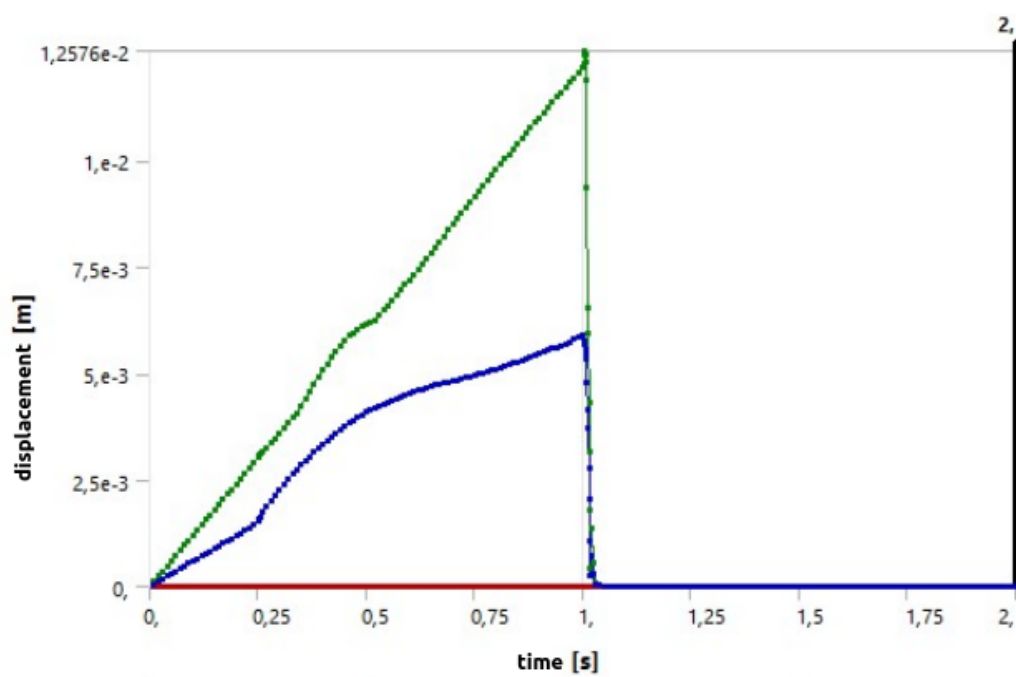
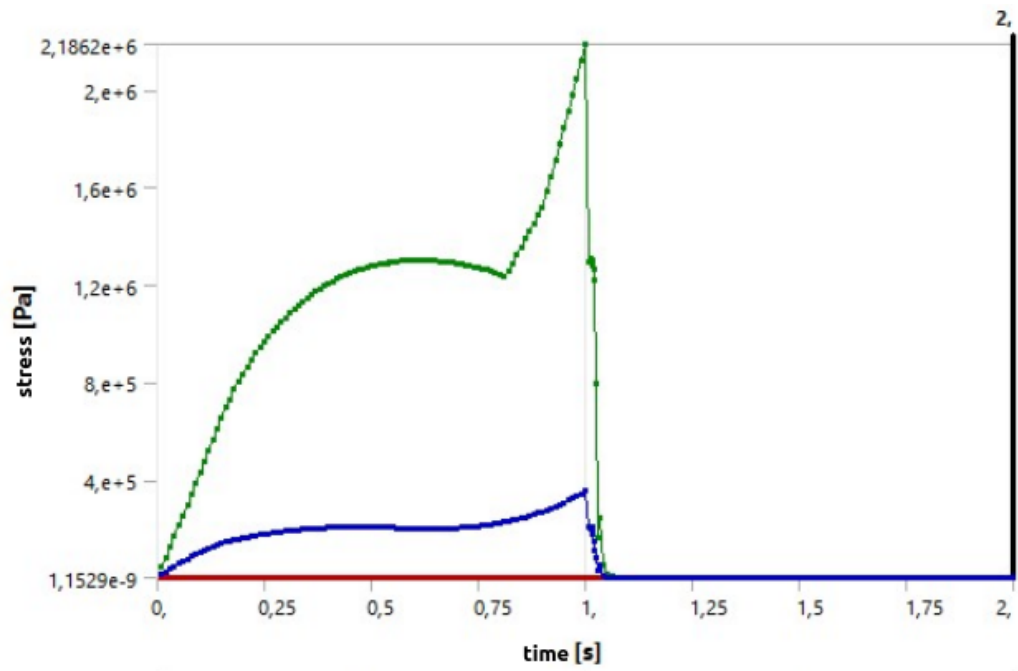FIGURE A.37: Displacement one element structure G.
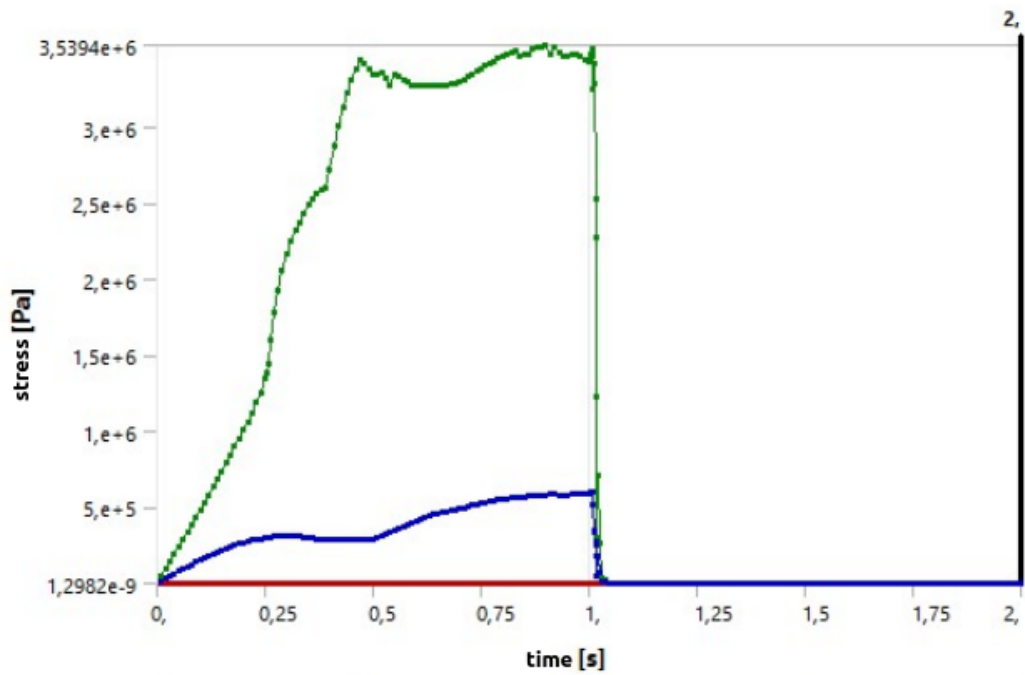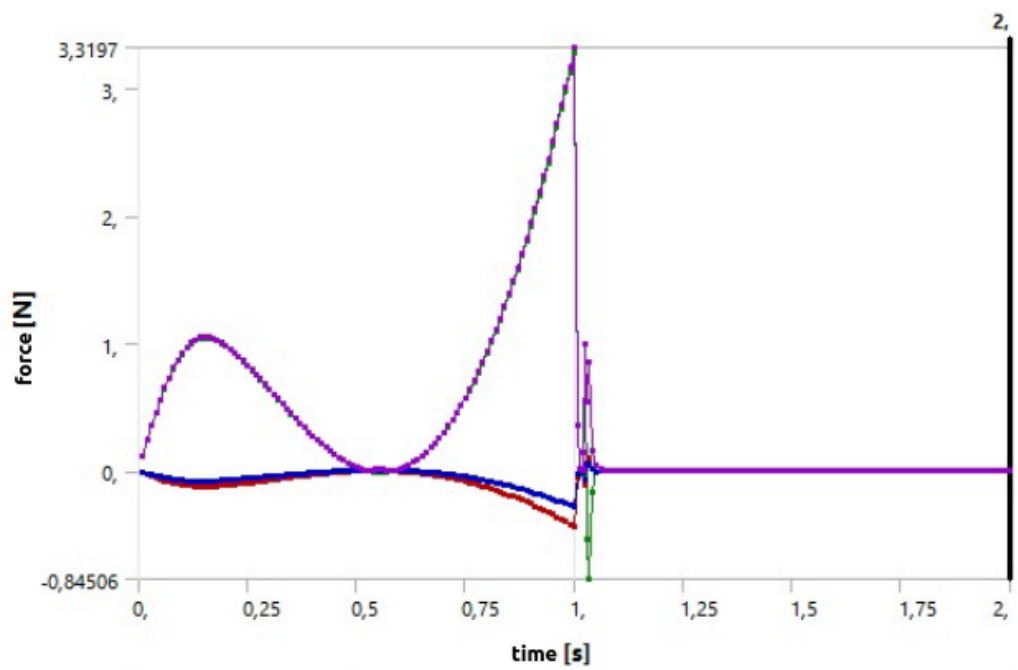
FIGURE A.38: Equivalent stress one element structure G.
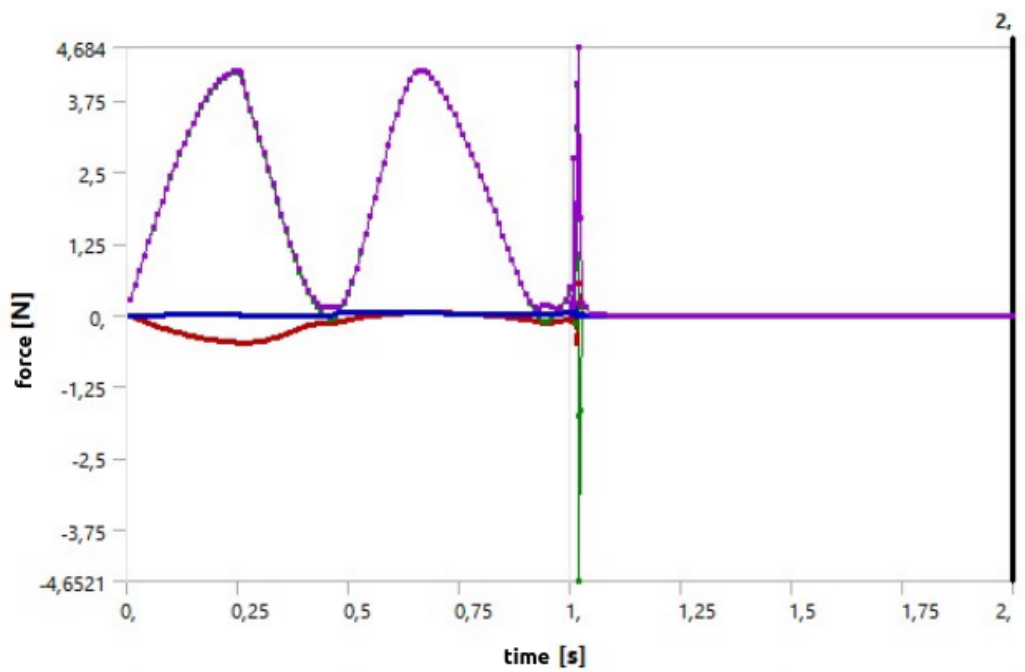
FIGURE A.39: Force reaction one element structure G.
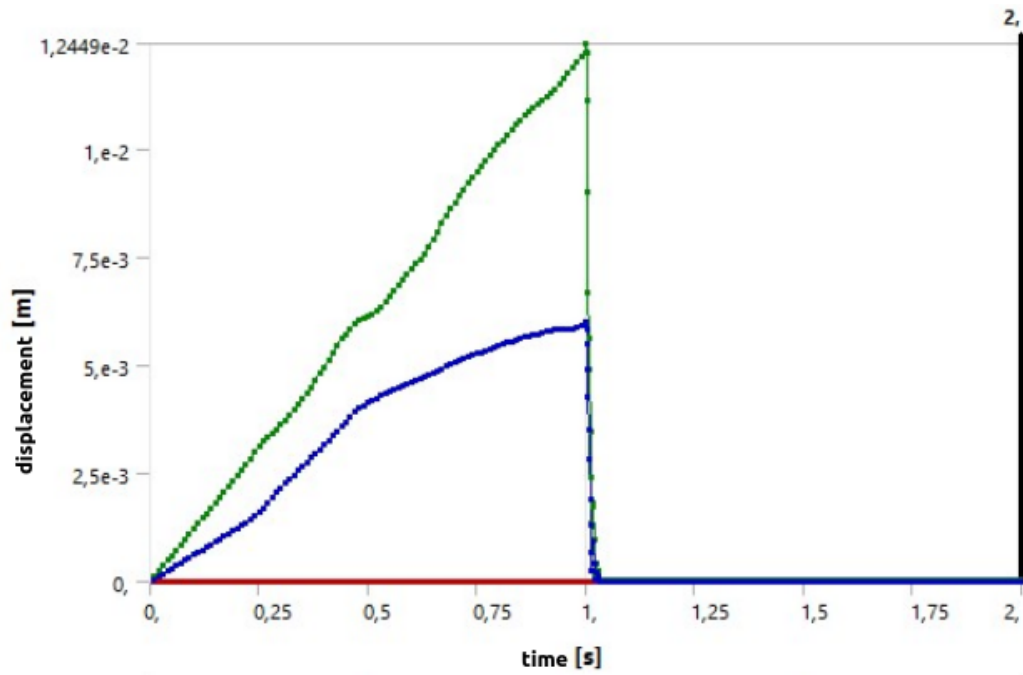
FIGURE A.40: Displacement structure G.
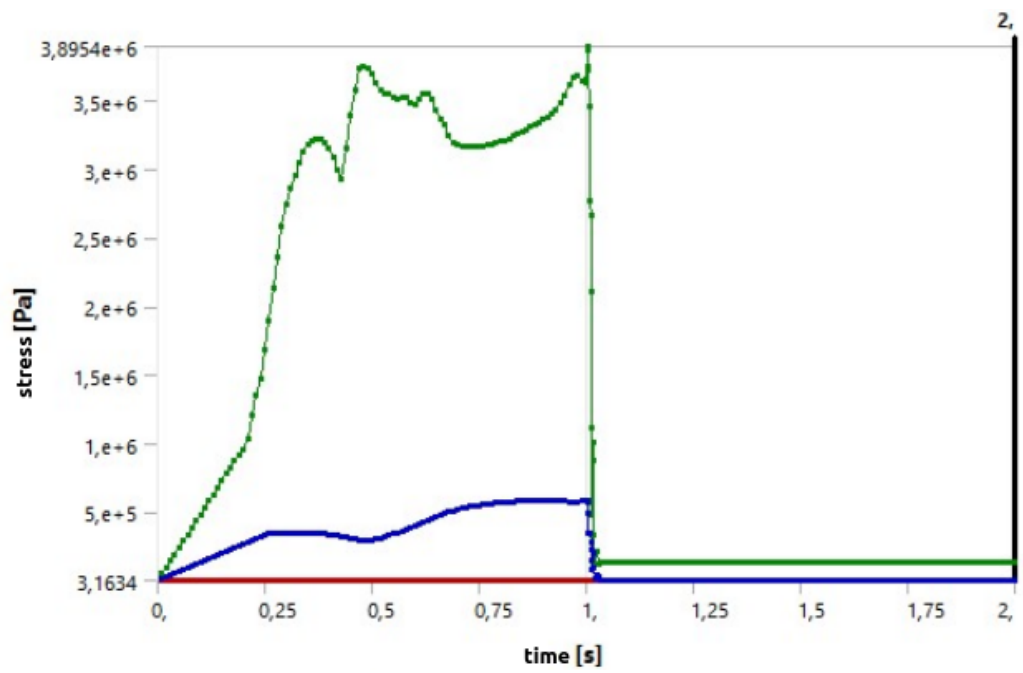
FIGURE A.41: Equivalent stress structure G.
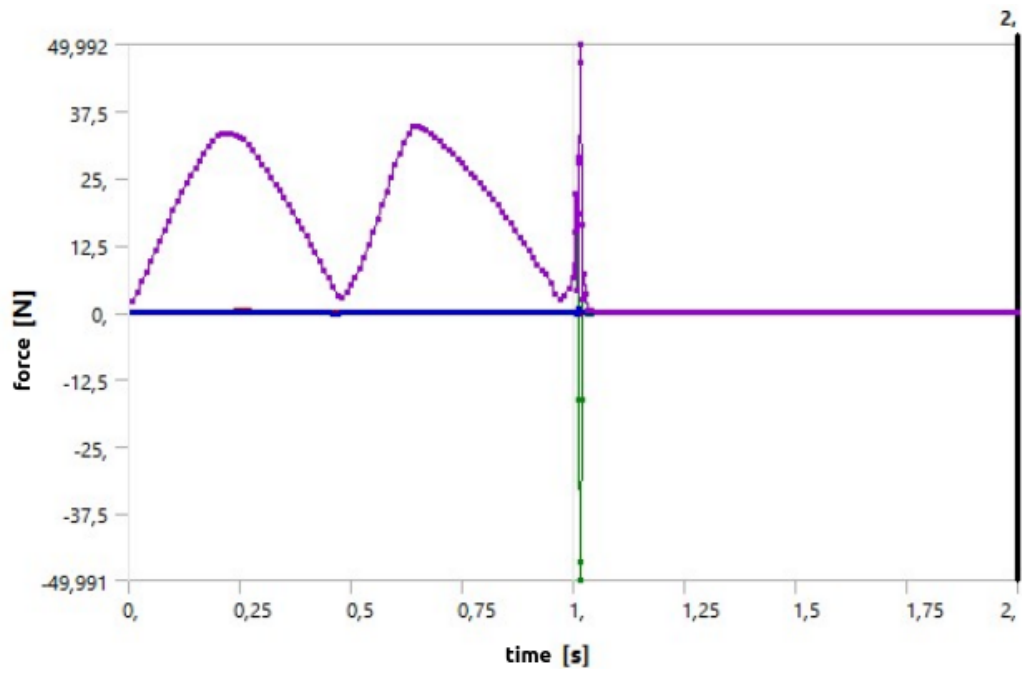
FIGURE A.42: Force reaction structure G.
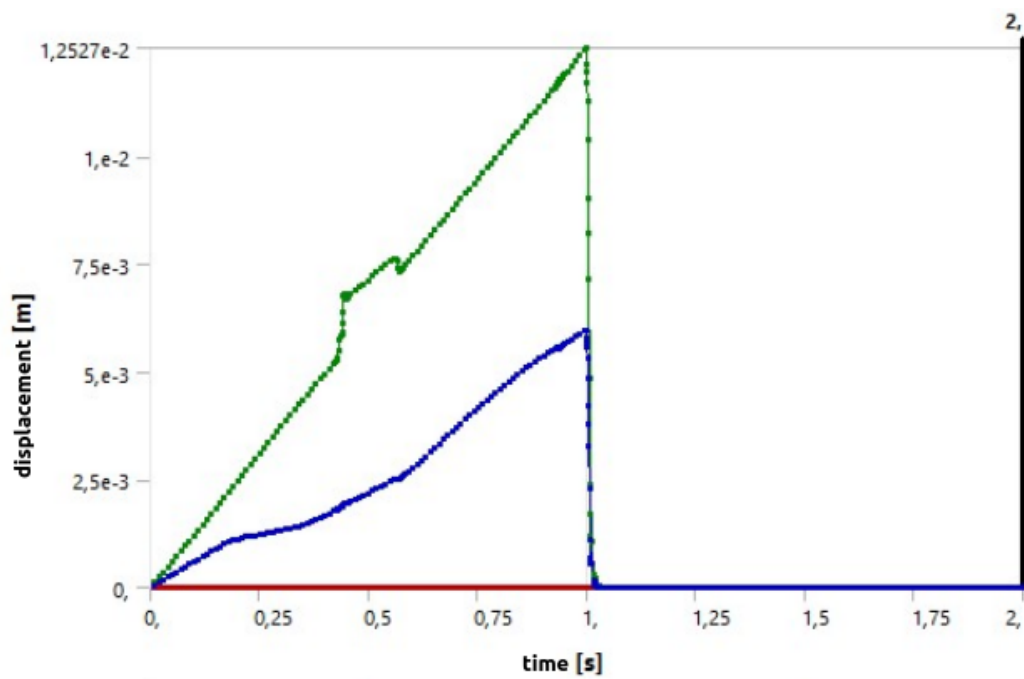
FIGURE A.43: Displacement one element structure H.
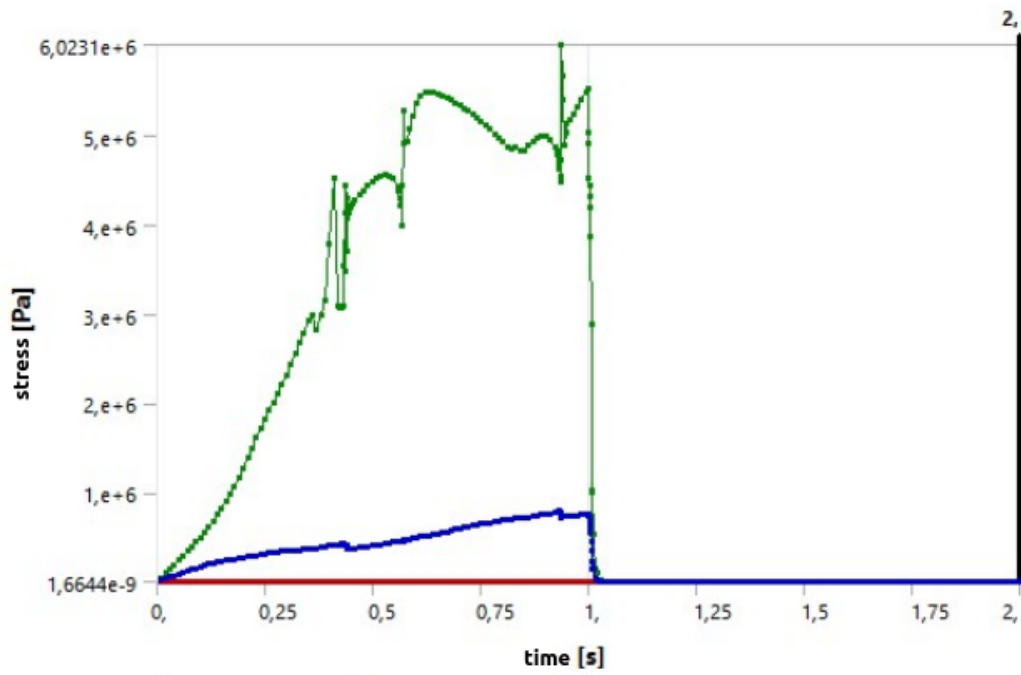
FIGURE A.44: Equivalent stress one element structure H.
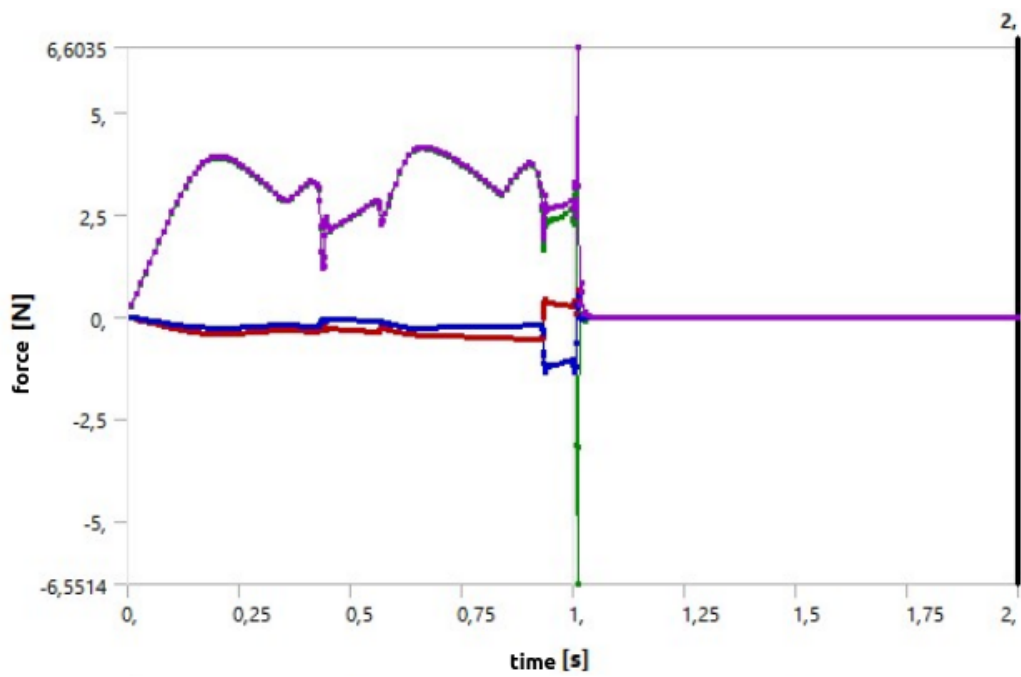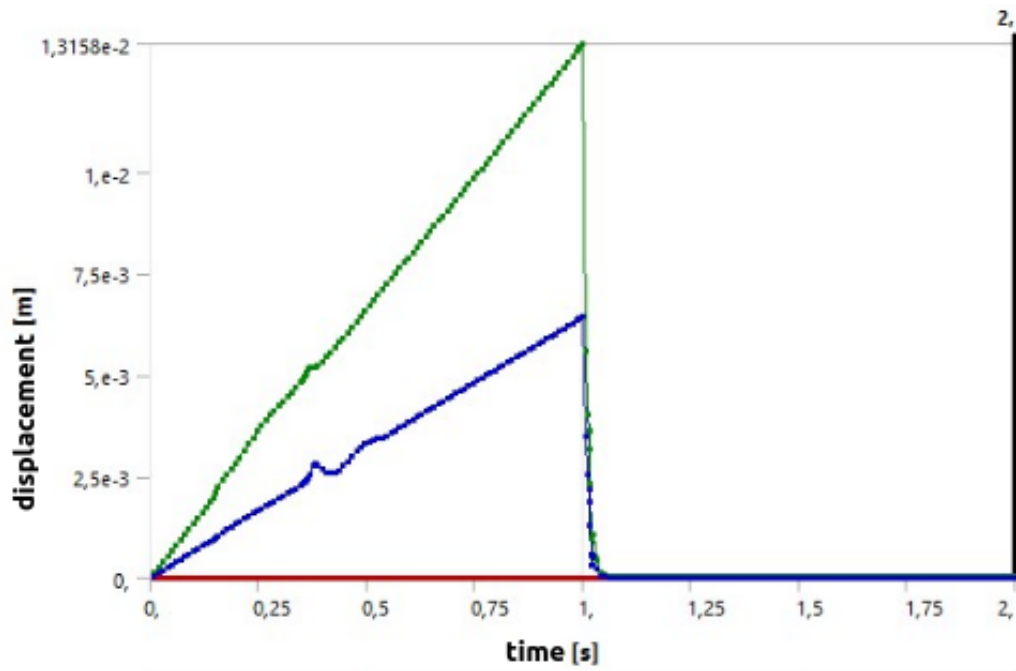

FIGURE A.45: Force reaction one element structure H.
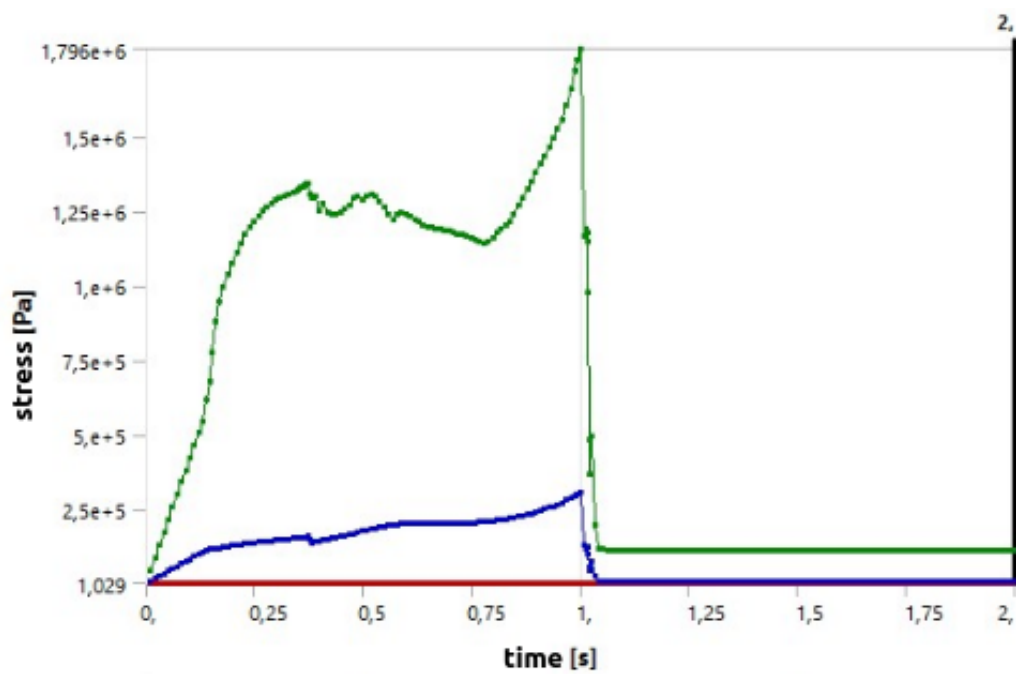
FIGURE A.46: Displacement structure H.
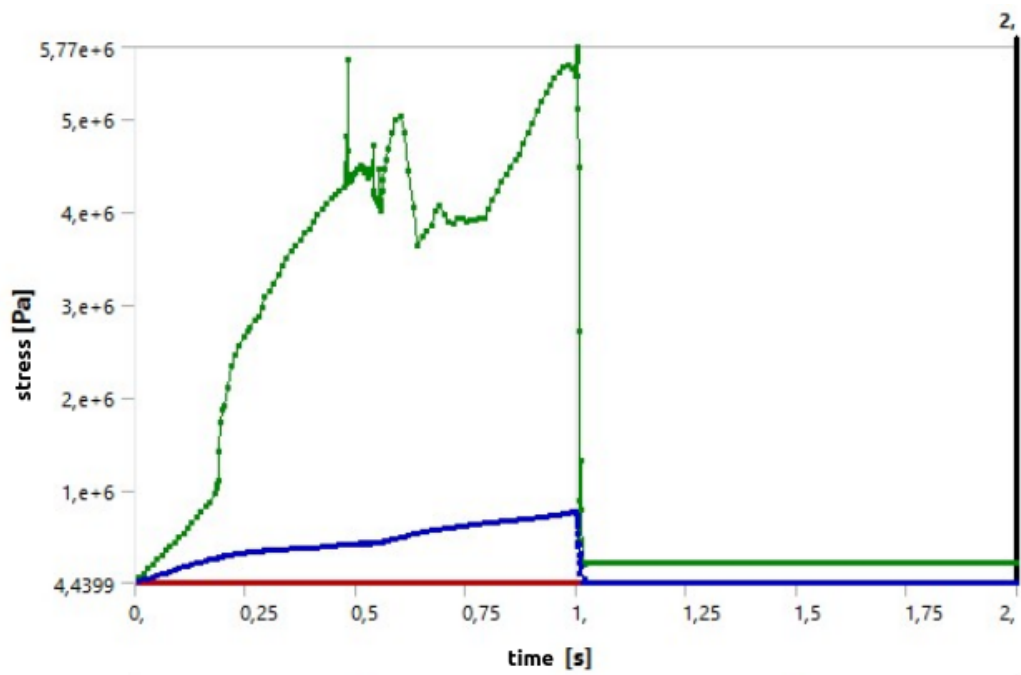
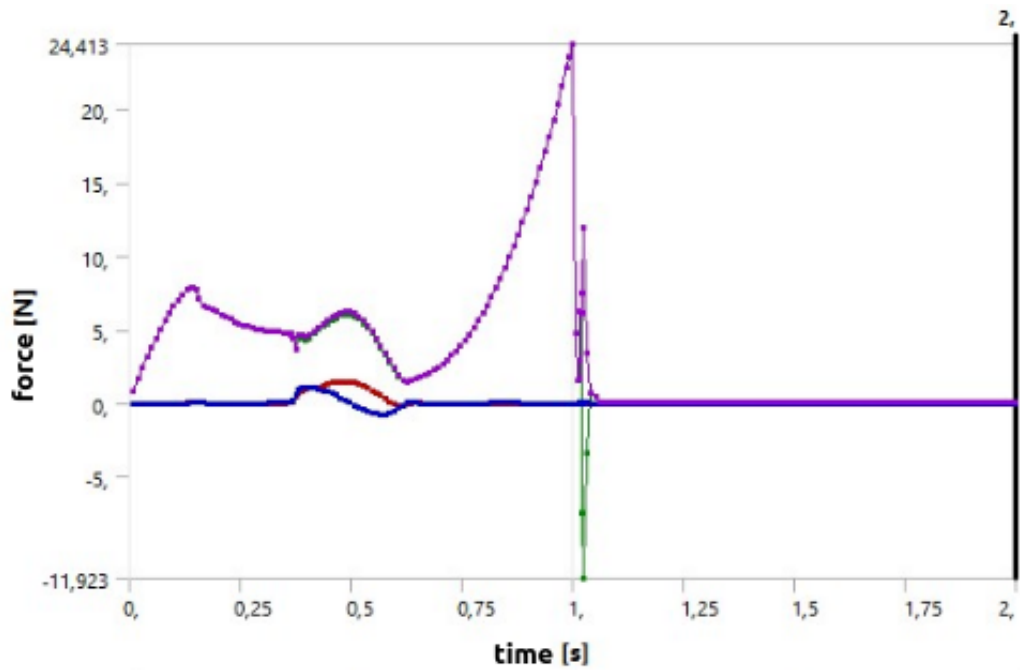FIGURE A.47: Equivalent stress structure H.
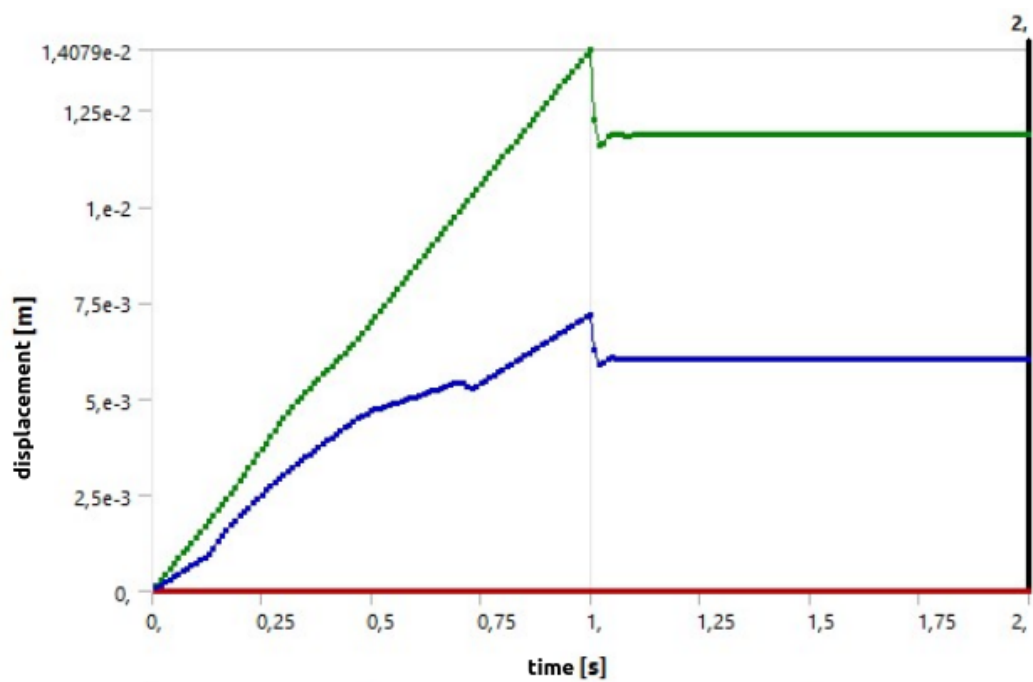
FIGURE A.48: Force reaction structure H.

FIGURE A.49: Displacement one element structure I.
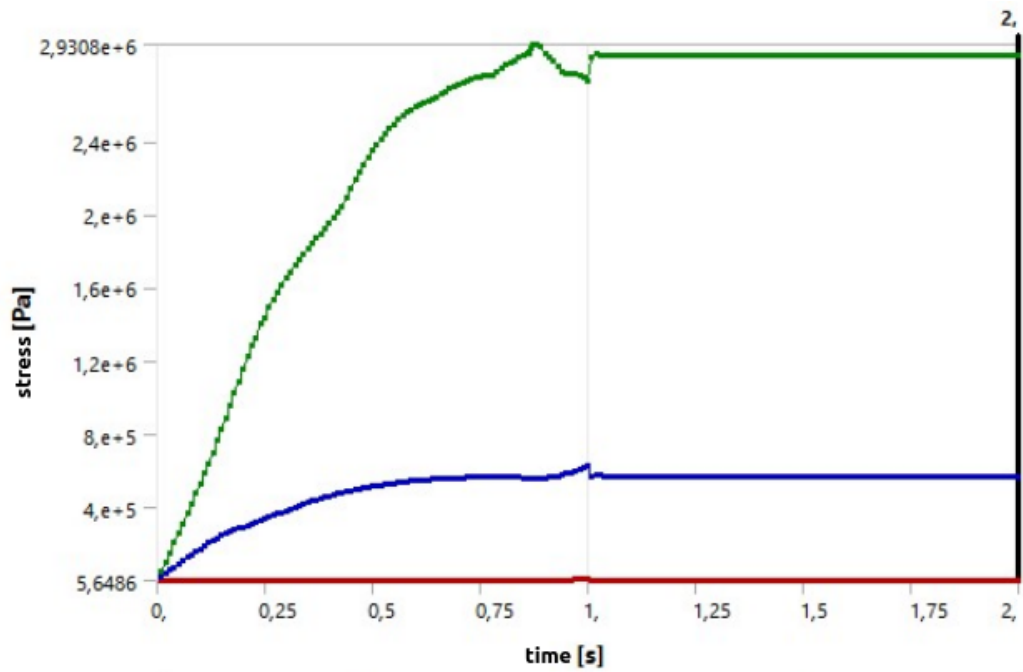
FIGURE A.50: Equivalent stress one element structure I.
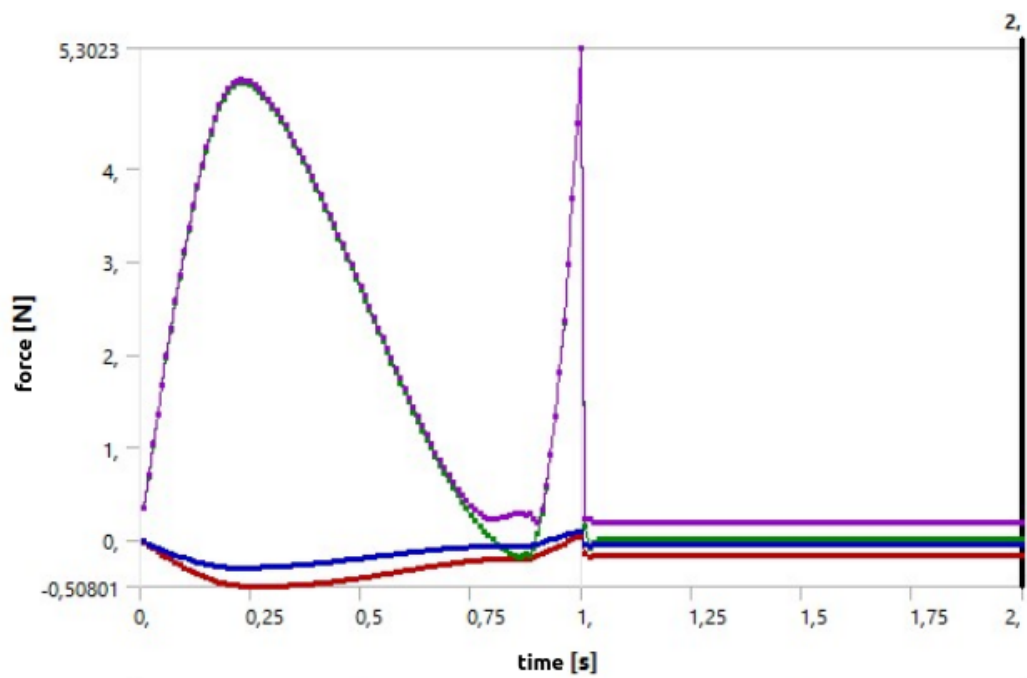
FIGURE A.51: Force reaction one element structure I.

FIGURE A.52: Displacement structure I.
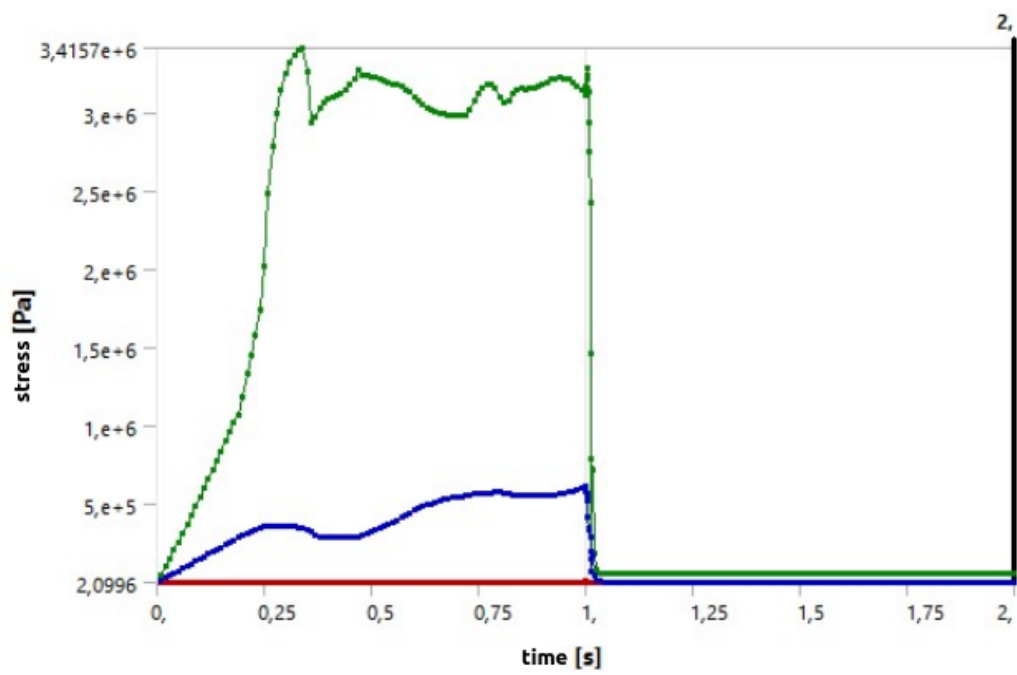
FIGURE A.53: Equivalent stress structure I.

FIGURE A.54: Force reaction structure I.

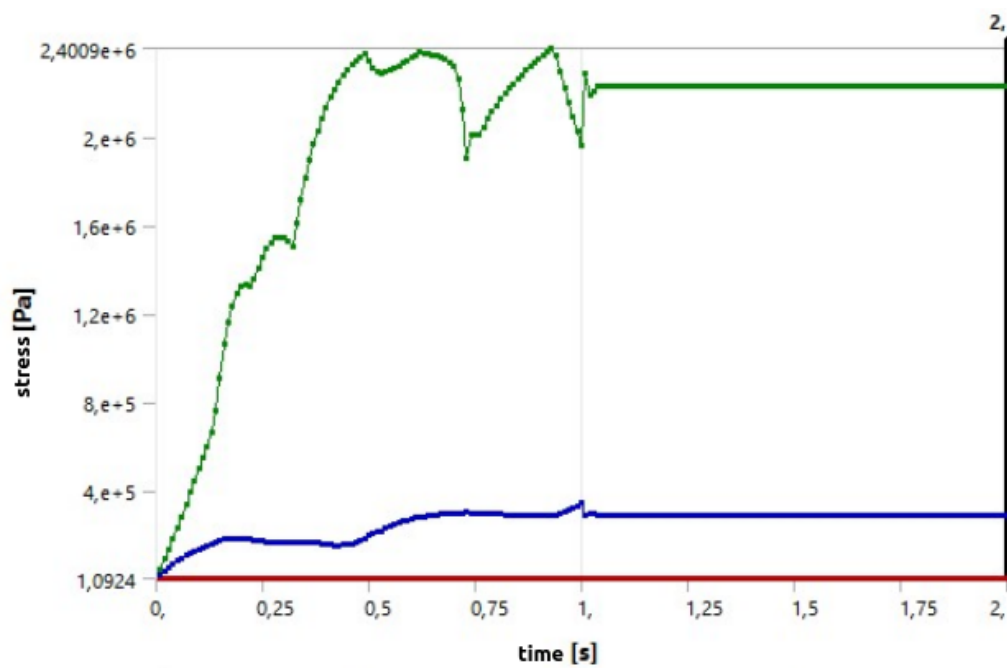FIGURE A.55: Displacement one element structure K.
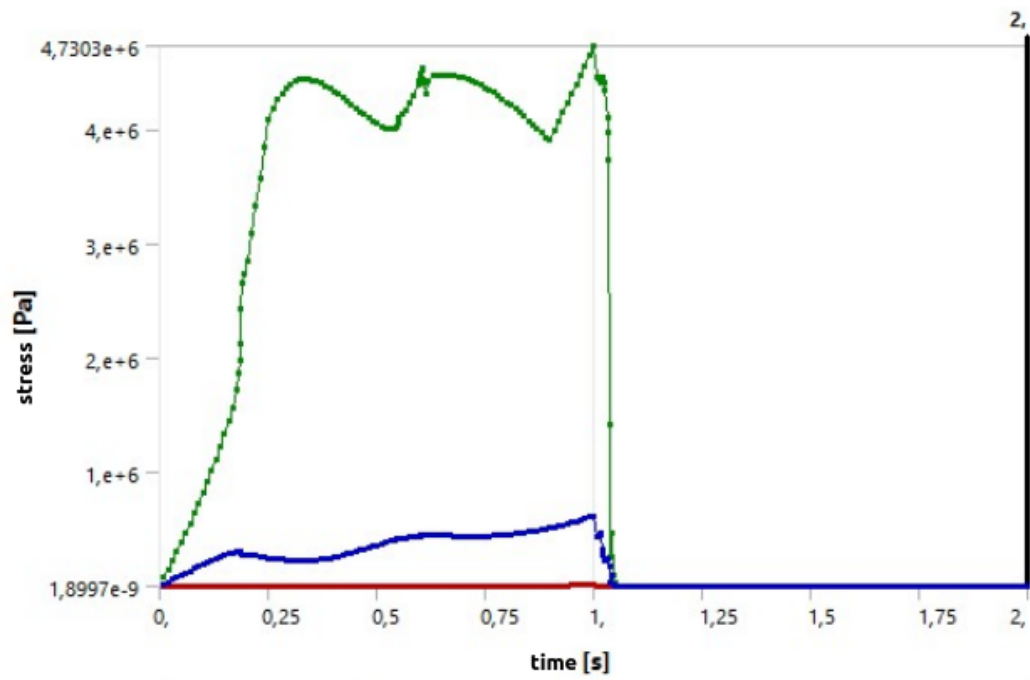
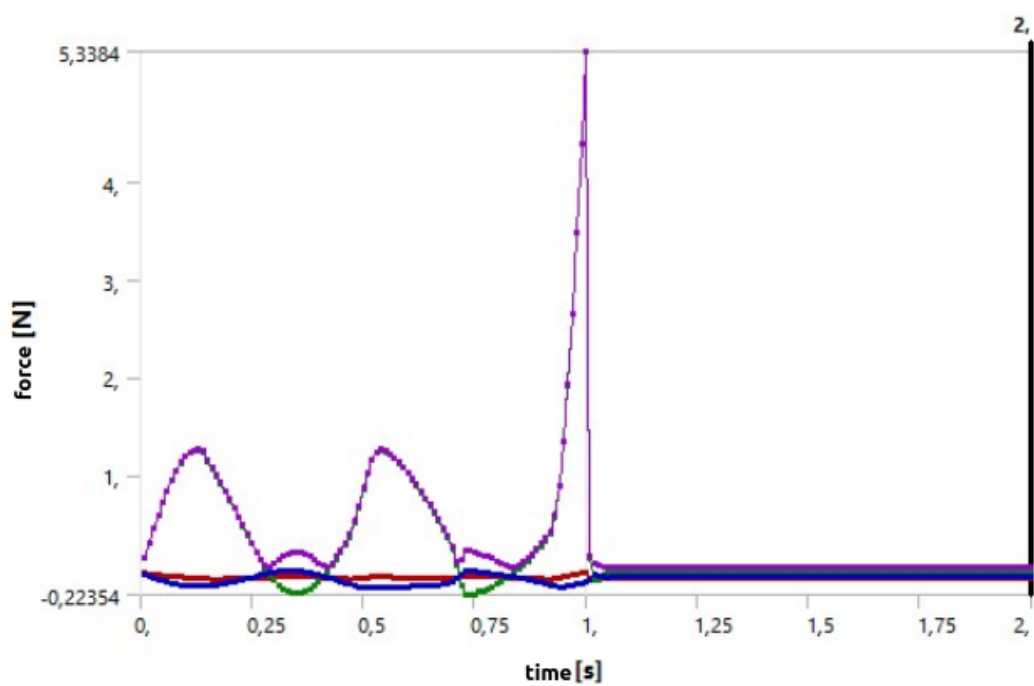FIGURE A.56: Equivalent stress one element structure K.
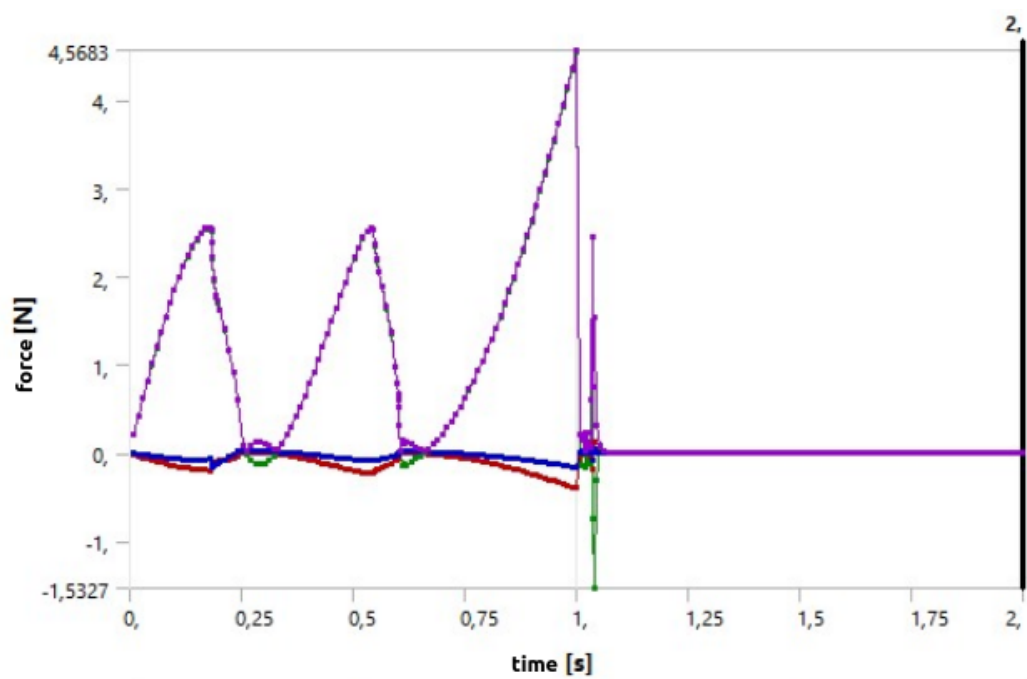
FIGURE A.57: Force reaction one element structure K.

FIGURE A.58: Displacement structure K.
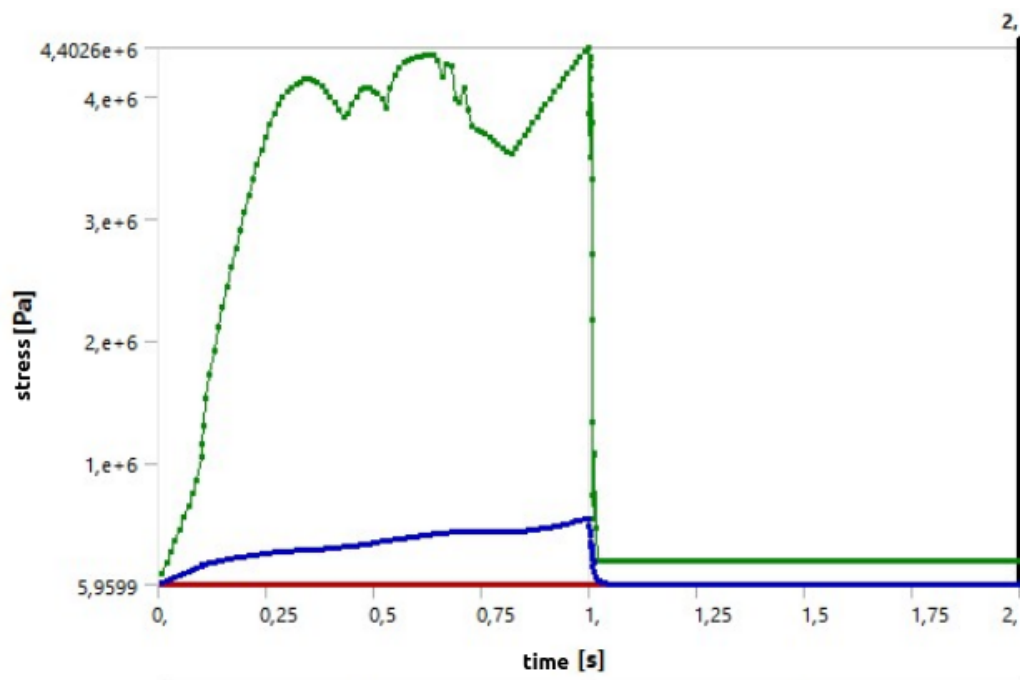
FIGURE A.59: Equivalent stress structure K.

FIGURE A.60: Force reaction structure K.

FIGURE A.61: Displacement one element structure L.

FIGURE A.62: Equivalent stress one element structure L.
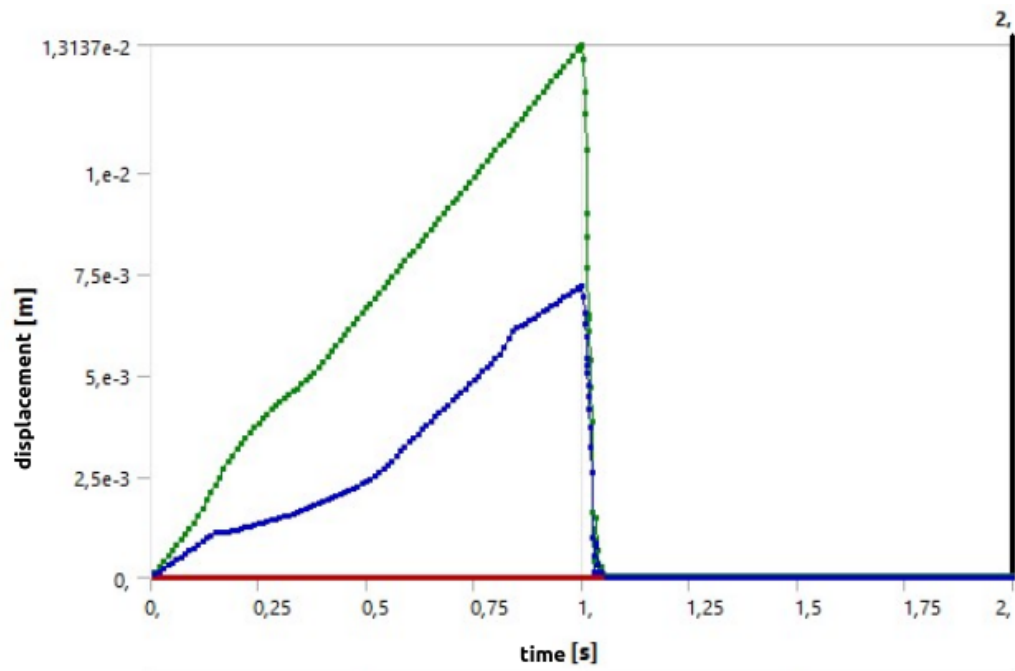

FIGURE A.63: Force reaction one element structure L.
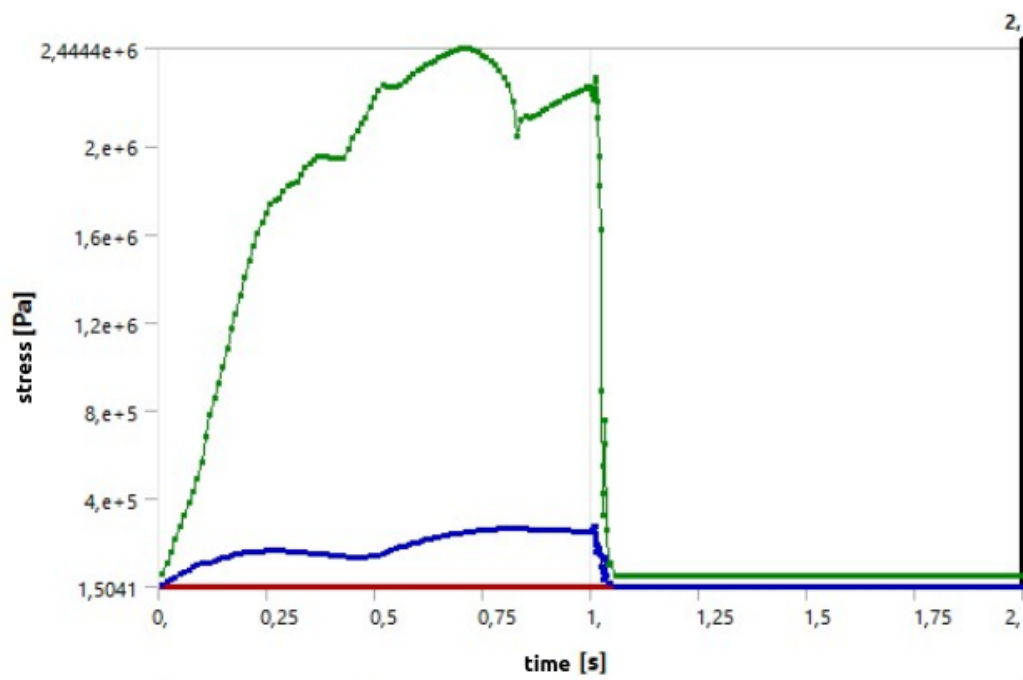
FIGURE A.64: Displacement structure L.

FIGURE A.65: Equivalent stress structure L.

FIGURE A.66: Force reaction structure L.

FIGURE A.67: Displacement one element structure M.

FIGURE A.68: Equivalent stress one element structure M.

FIGURE A.69: Force reaction one element structure M.

FIGURE A.70: Displacement structure M.
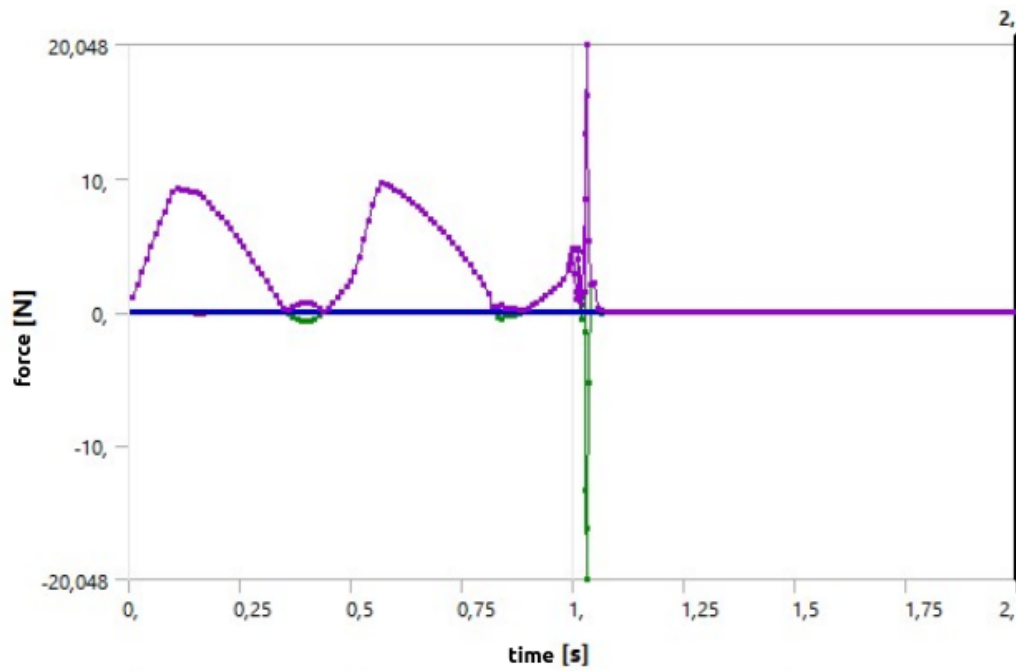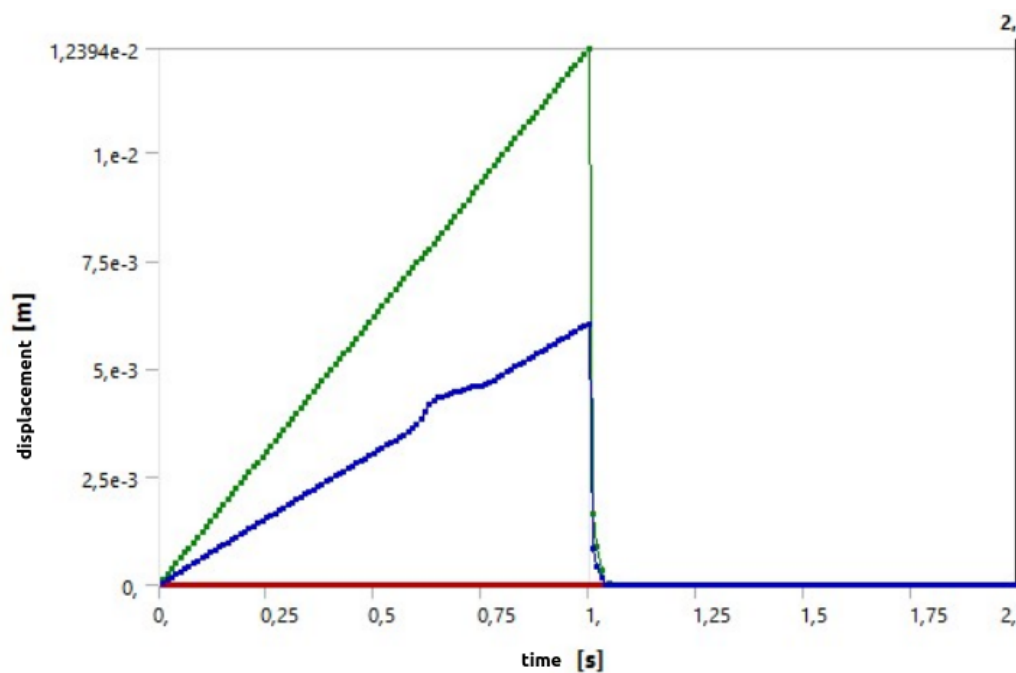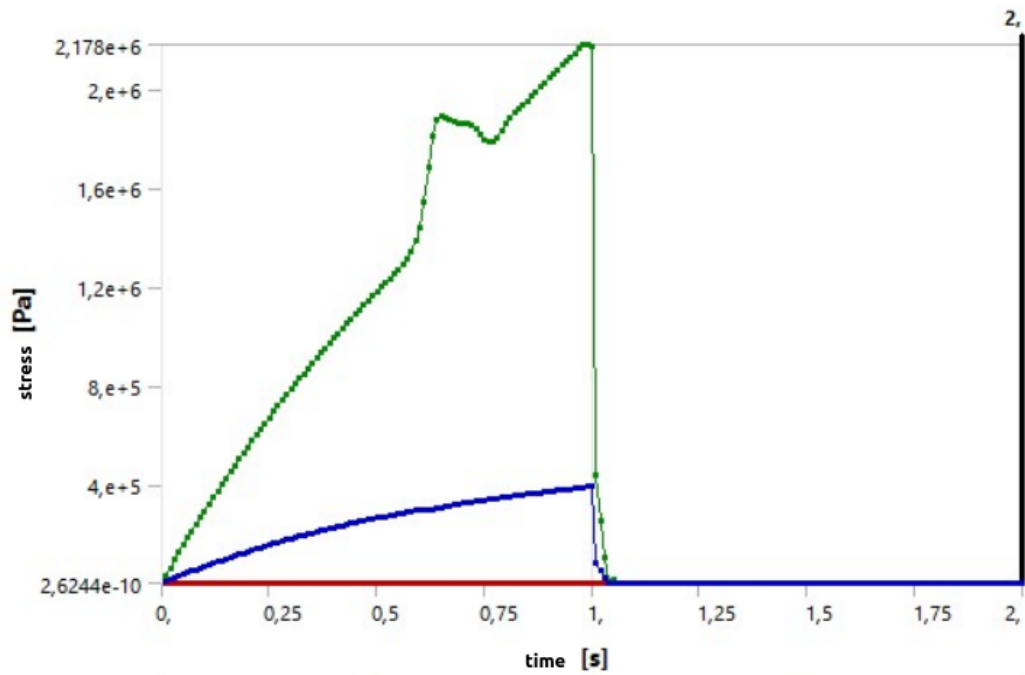

FIGURE A.71: Equivalent stress structure M.

FIGURE A.72: Force reaction structure M.

FIGURE A.73: Displacement one element structure N.

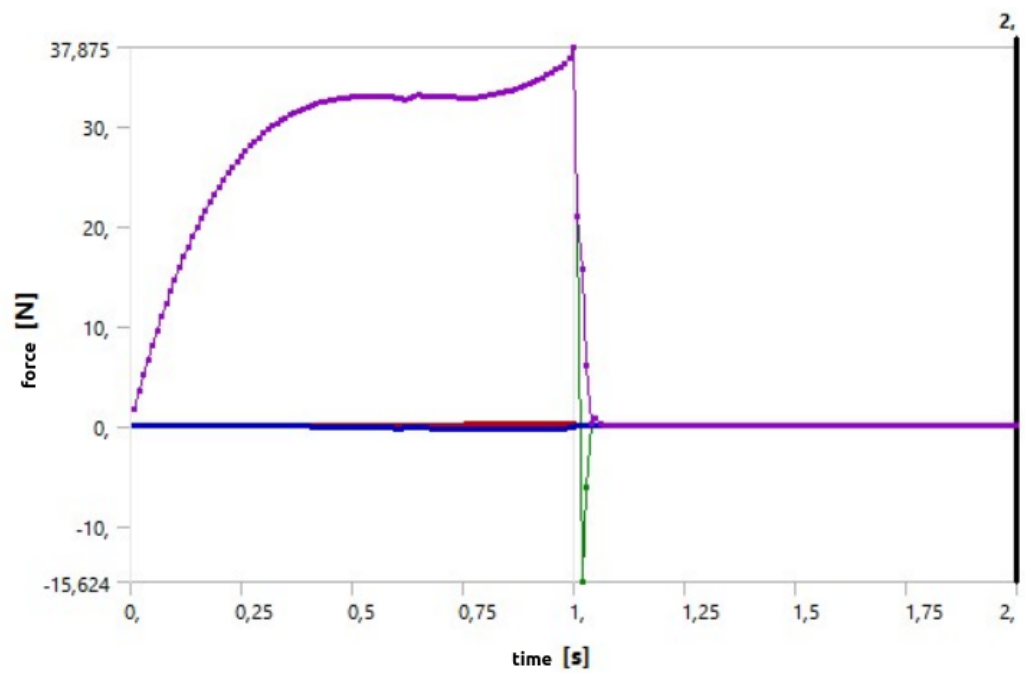FIGURE A.74: Equivalent stress one element structure N.

FIGURE A.75: Force reaction one element structure N.

FIGURE A.76: Displacement structure N.

FIGURE A.77: Equivalent stress structure N.

FIGURE A.78: Force reaction structure N.

FIGURE A.79: Displacement one element structure O.

FIGURE A.80: Equivalent stress one element structure O.

FIGURE A.81: Force reaction one element structure O.

FIGURE A.82: Displacement structure O.

FIGURE A.83: Equivalent stress structure O.

FIGURE A.84: Force reaction structure O.

A.0.2 Toroidal structure

FIGURE A.85: Displacement structure torA.

FIGURE A.86: Equivalent stress structure torA.
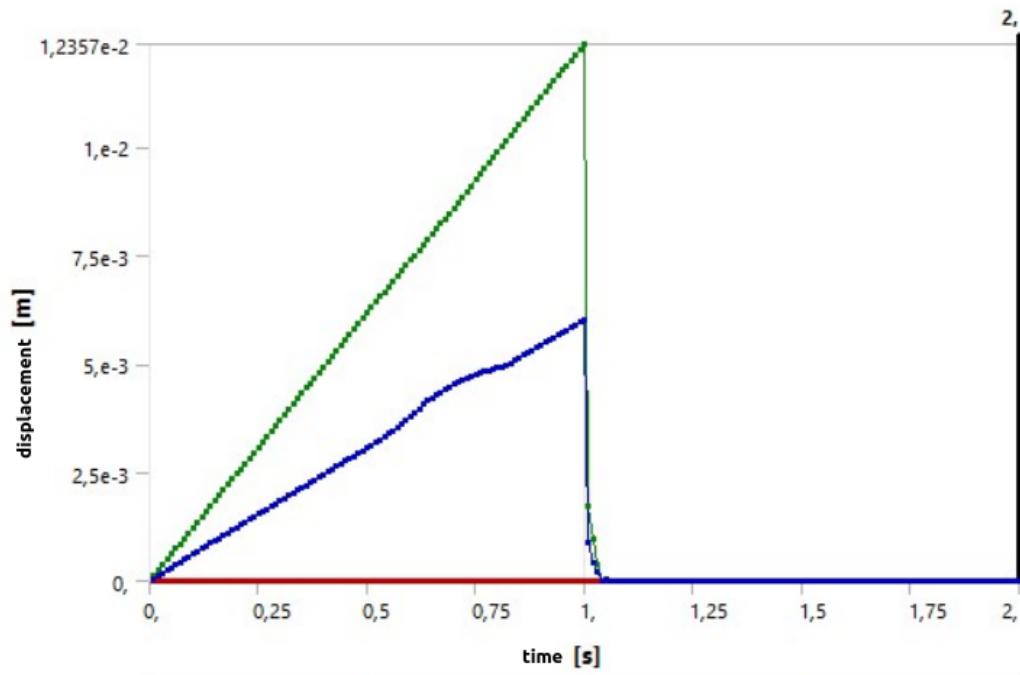

FIGURE A.87: Force reaction structure torA.

FIGURE A.88: Displacement structure torB.

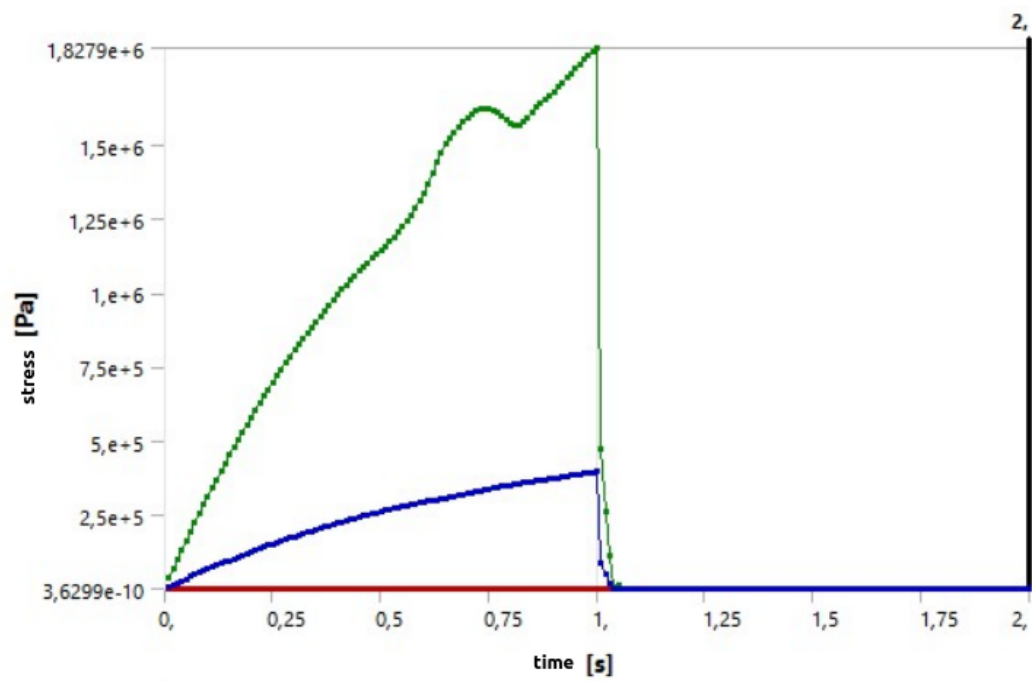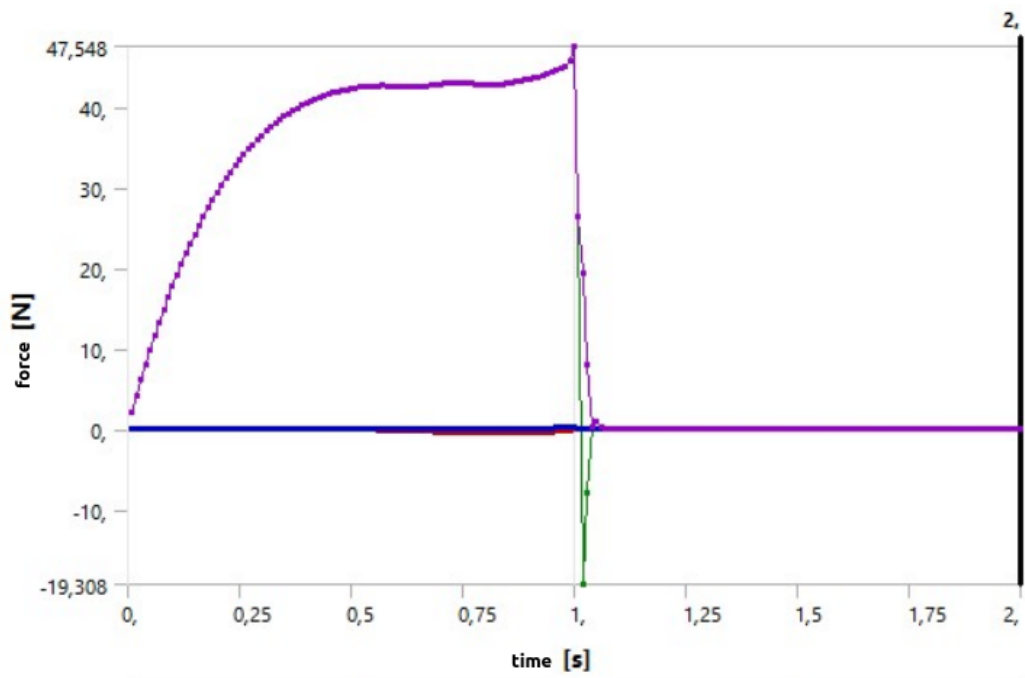FIGURE A.89: Equivalent stress structure torB.

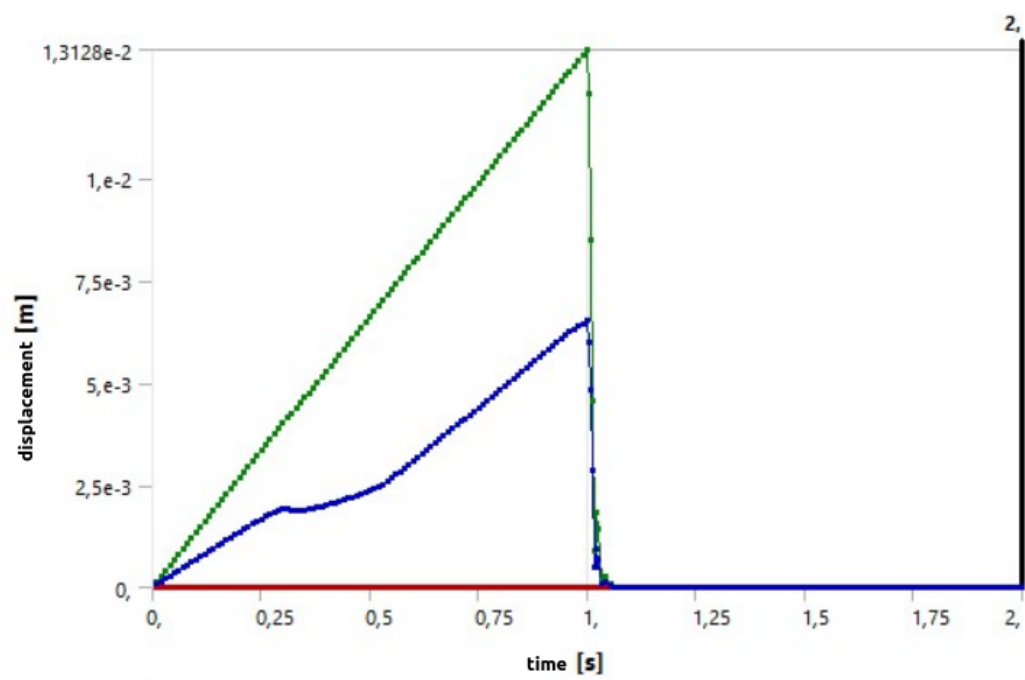FIGURE A.90: Force reaction structure torB.

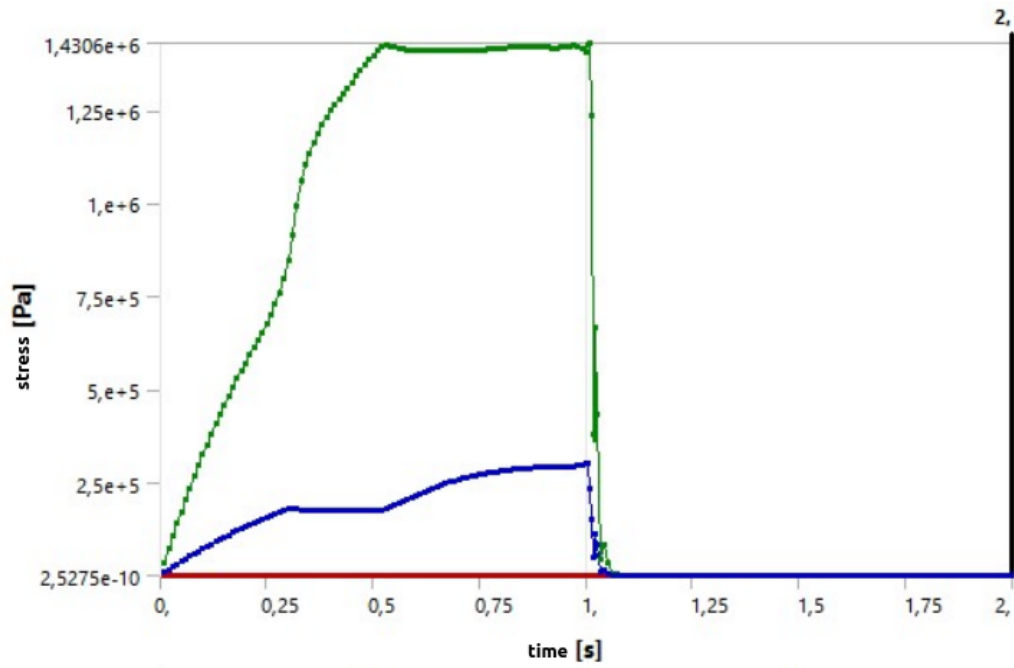FIGURE A.91: Displacement structure torC.
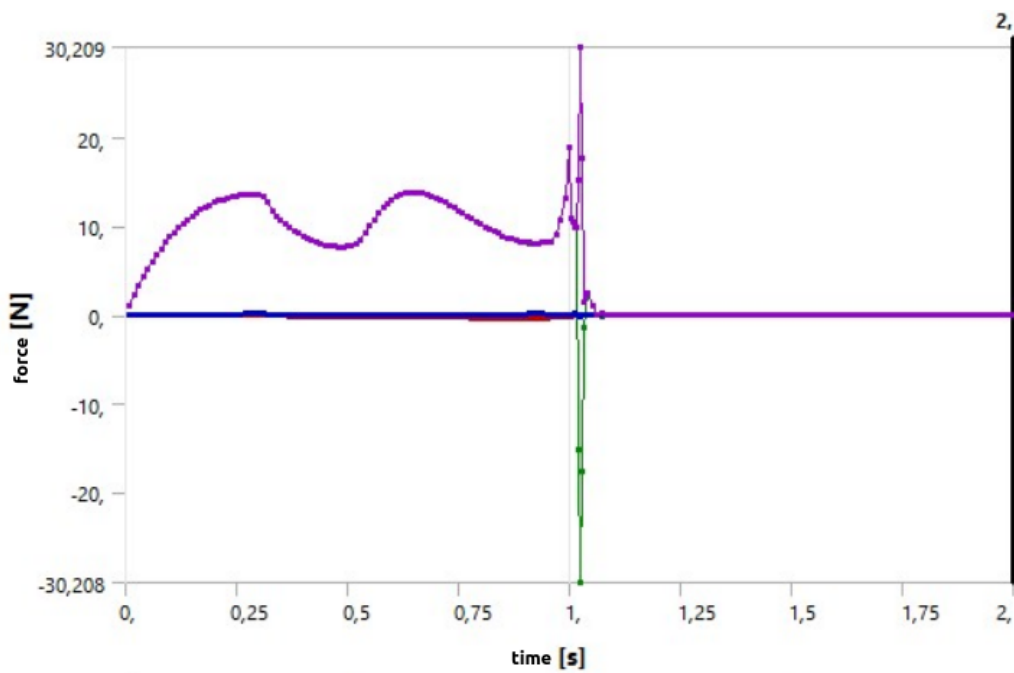
FIGURE A.92: Equivalent stress structure torC.

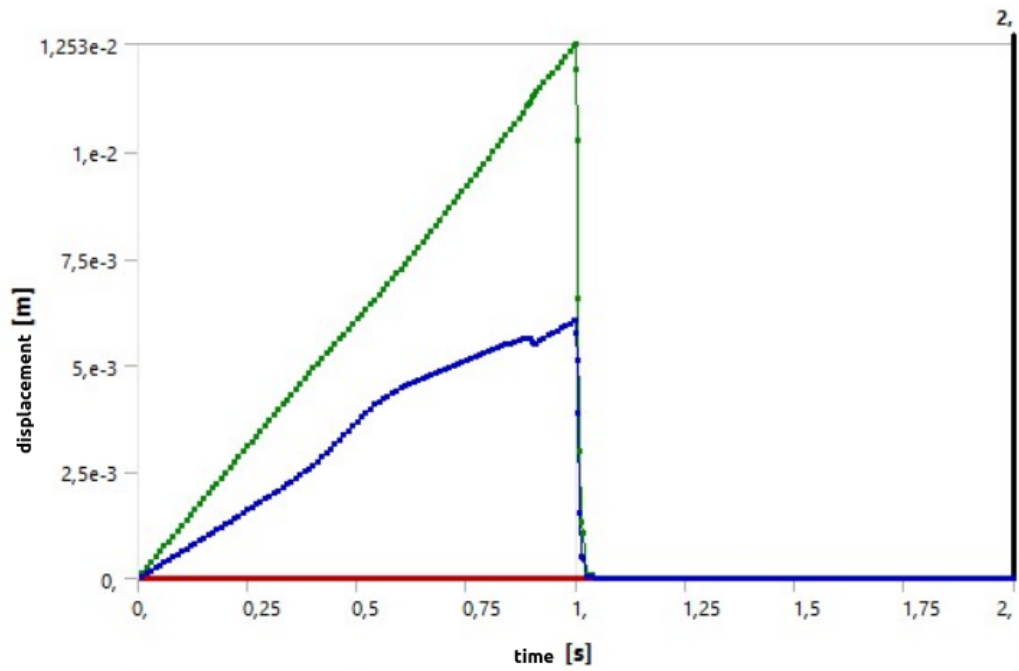FIGURE A.93: Force reaction structure torC.
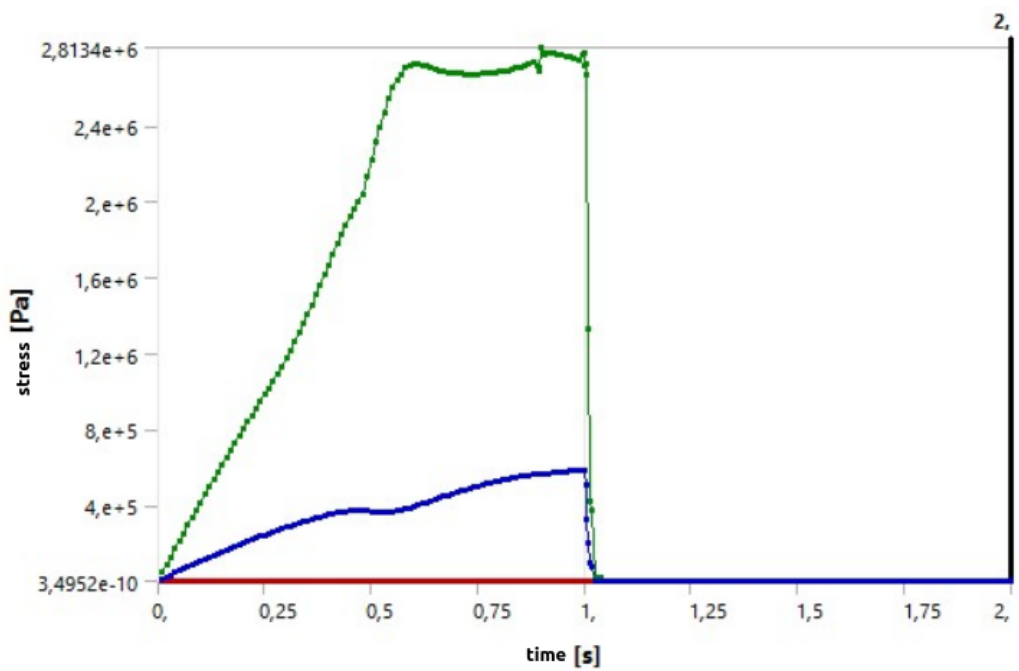
FIGURE A.94: Displacement structure torD.

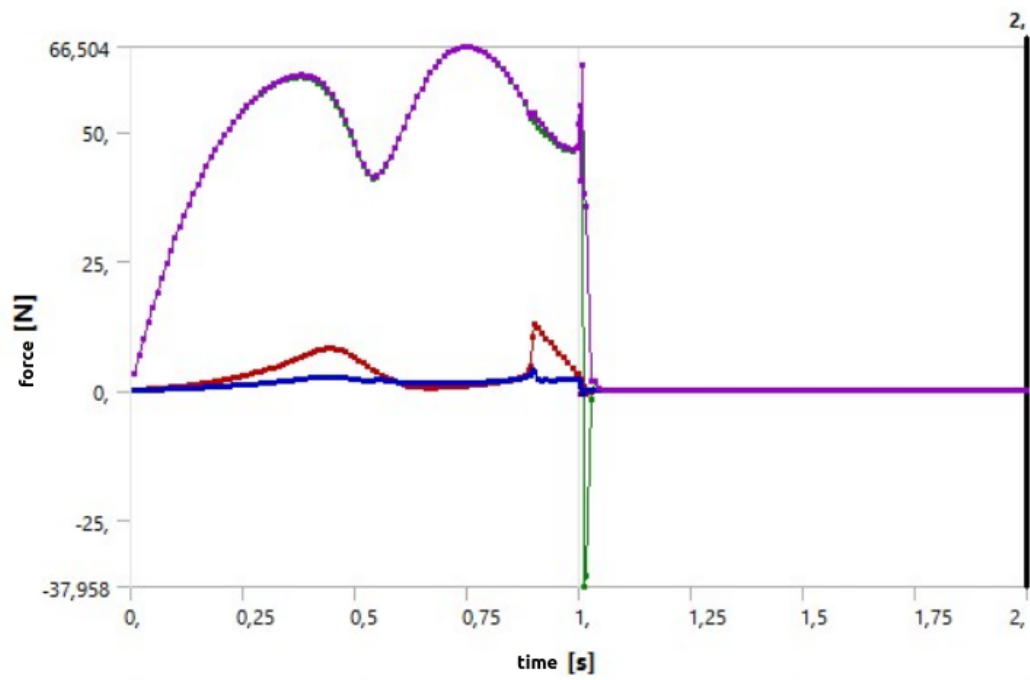FIGURE A.95: Equivalent stress structure torD.
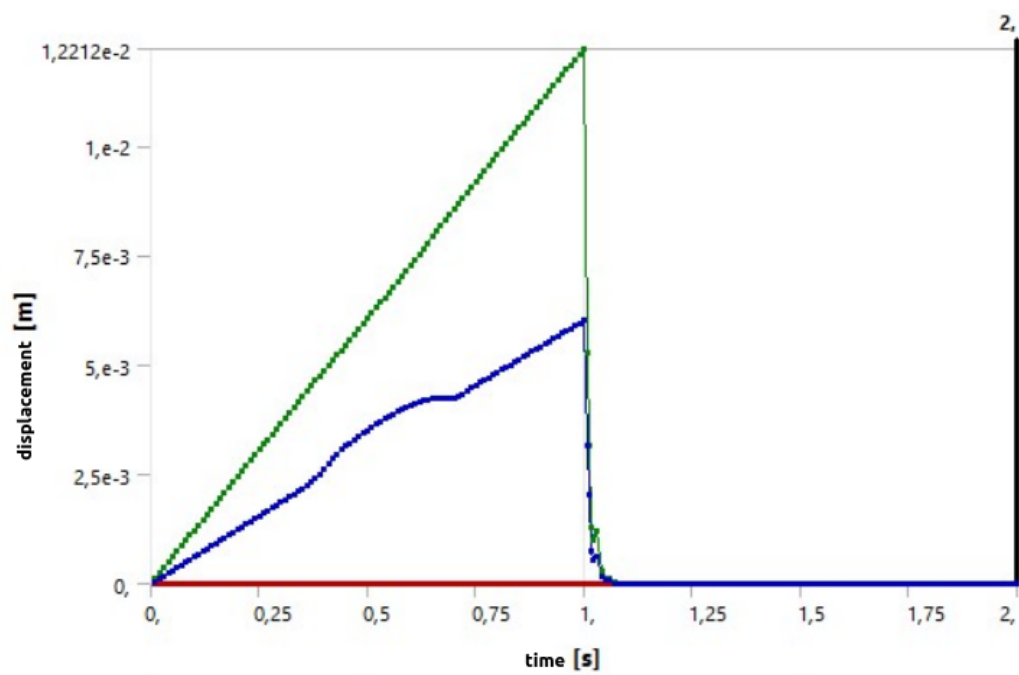
FIGURE A.96: Force reaction structure torD.

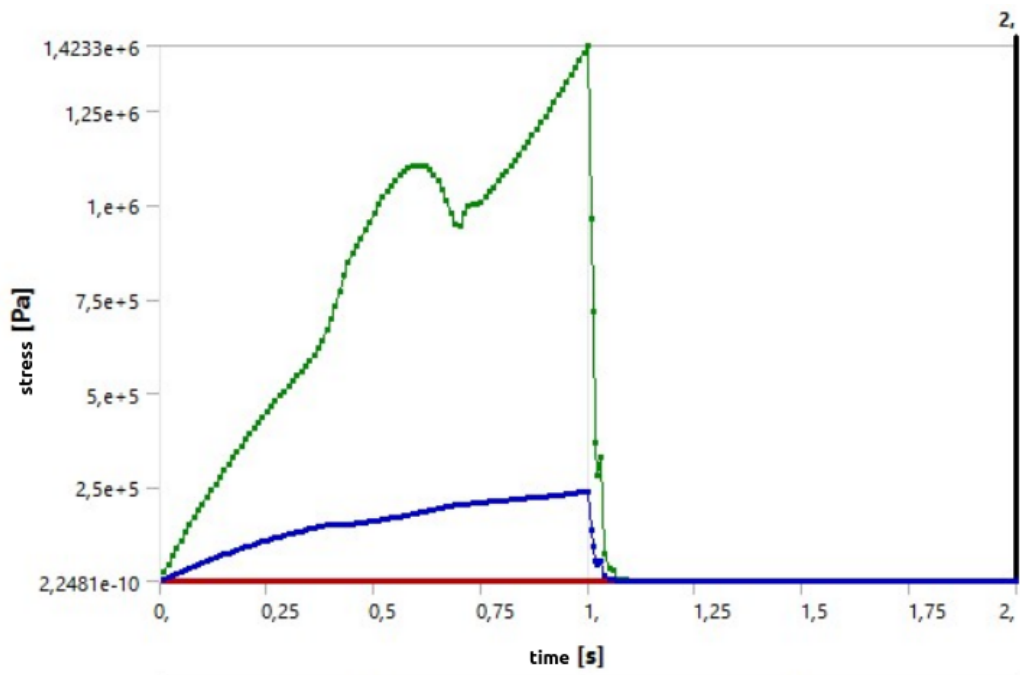FIGURE A.97: Displacement structure torE.
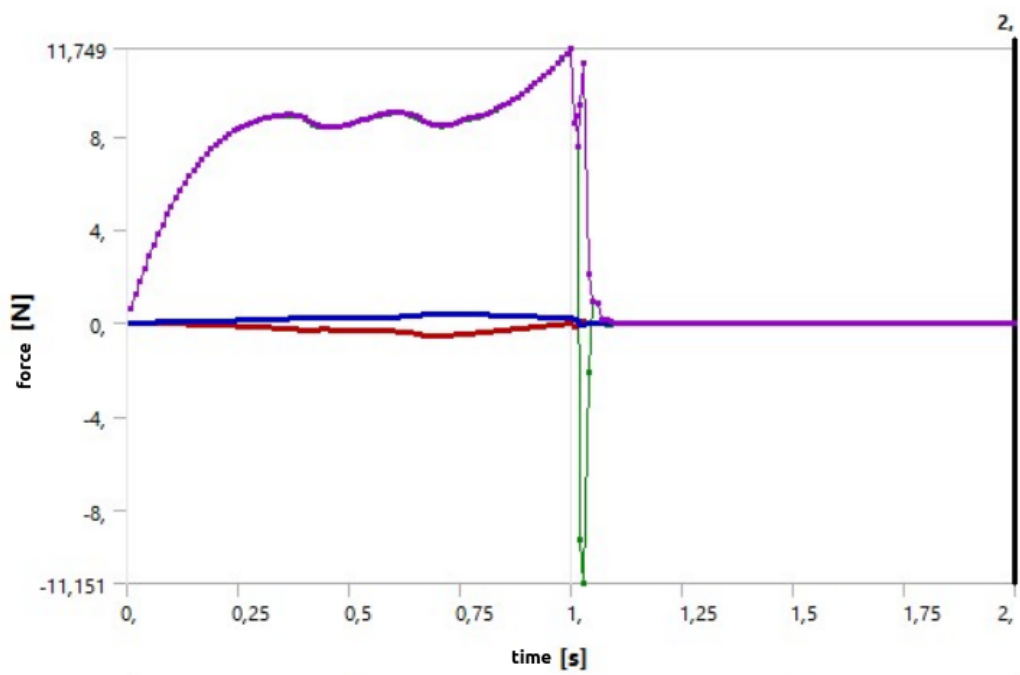
FIGURE A.98: Equivalent stress structure torE.

FIGURE A.99: Force reaction structure torE.

Bibliography

[1] Nan Hu and Rigoberto Burgueño. "Buckling-induced smart applications: recent advances and trends". In: *Smart Materials and Structures* (2015).

[2] C. Priyant Mark Surekha Kamath. "Review of Active Space Debris Removal Methods". In: *Space Policy* (2019).

[3] L. Anselmo M. Grassi D. Pavarin A. Francesconi F. Branz S. Chiesa N. Viola C. Bonnal V. Trushlyakov I. Belokonov L.T. DeLuca F. Bernelli F. Maggi P. Tadini C. Pardini. "Active space debris removal by a hybrid propulsion module". In: *Acta Astronautica* (2013).

[4] Bing Wang Xiaojun Tan Shaowei Zhu Shuai Chen Kaili Yao Peifei Xu Lianchao Wang Huaping Wu Yuguo Sun. "Cushion performance of cylindrical negative stiffness structures: Analysis and optimization". In: *Composite Structures* (2019).

[5] M. Corsi S. Bagassi M. C. Moruzzi F. Weigand. "Additively manufactured negative stiffness structures for shock absorber applications". In: *Mechanics of Advanced Materials and Structures* (2020).

[6] Xiaojun Tan Bing Wang Shuai Chen Shaowei Zhu Yuguo Sun. "A novel cylindrical negative stiffness structure for shock isolation". In: *Composite Structures* (2019).

[7] Li Ma Hang Yang. "Multi-stable mechanical metamaterials with shape-reconfiguration and zero Poisson's ratio". In: *Materials and Design* (2018).

[8] ASTM International. "ISO/ASTM 52900: Standard Terminology for Additive Manufacturing". In: (2015).

[9] S. Bagassi. "Additive Manufacturing Technologies and Applications". In: *Lecture notes* (2019).

[10] Robert M. Rivello. "Theory and analysis of flight structures". In: *McGraw-Hill* (1969).

[11] Michael Rackl. "Curve Fitting for Ogden, Yeoh and Polynomial Models". In: *Ostbayerische Technische Hochschule Regensburg Mechanical Engineering Department* (2015).

[12] Alessandro Freddi. "Imparare a progettare". In: *Pitagora editrice Bologna* (2004).

[13] ANSYS. "User's manual". In: (2018).

[14] ASTM International. "D695: Standard Test Method for Compressive Properties of Rigid Plastics". In: (2002).

[15] Stratasys. "Design for Additive Manufacturing with PolyJet". In: (2020).

[16] Stratasys. "Tango data sheet". In: (2018).

[17] ASTM International. "D638 14: Standard Test Method for Tensile Properties of Plastics". In: (2014).

[18] Michael W. Barclift and Christopher B. Williams. "Examining variability in the mechanical properties of parts manufactured via polyjet direct 3D printing". In: *Research Gate* (2012).

[19] Ana Pilipović Gorana Baršić Marko Katić and Maja Rujnić Havstad. "Repeatability and Reproducibility Assessment of a PolyJet Technology Using X-ray Computed Tomography". In: *Applied sciences* (2020).